

A hydrogeological study of the Kasteelberg Mountain Aquifer, Western Cape, South Africa

By

Bernardus Lambertus Pieters



Thesis presented in fulfilment of the requirements for the degree of
Master of Science in the Faculty of Science
in the Department of Earth Science
at Stellenbosch University

Supervisor: Dr WP de Clercq

Co-supervisor: Prof A Roychoudhury

March 2020

Declaration

By submitting this thesis electronically, I declare that the entirety of the work contained herein is my own original work, that I am the sole author thereof (save to the extent explicitly otherwise stated), that reproduction and publication thereof by Stellenbosch University will not infringe any third-party rights and that I have not previously in its entirety or in part submitted it for obtaining any qualification.

March 2020

Abstract

The availability of freshwater is one of the major factors that are limiting South Africa's development. With this in mind the area under investigation in this study forms part of the Sandspruit catchment, which is about 100 km north-east of Cape Town near the town of Riebeek Kasteel. The climate is semi-arid with a Mediterranean landscape.

This study forms part of multiple studies that were initiated to assist in alleviating the crisis brought about by the continuing drought in the Western Cape Province. This study investigated the possibility of utilising the Kasteelberg Mountain, located near the town of Riebeek Kasteel, as an additional source of freshwater.

The regionally fractured sandstone aquifer was the focus during the modelling, volume and porosity calculations in this hydrogeological research of the Kasteelberg Mountain Aquifer. This resulted in an estimated water reserve that can be sustainably extracted.

Sustainable development is needed to protect the sensitive ecosystems against anthropologic and climate-driven impacts. The study started with analysing the responses from water level loggers that were installed in boreholes in the study area to monitor the water fluctuations during the seasons so as to utilise this resource sustainably. During the study, the physical geology of the area was characterised. Geographic Information Systems (GISs) were used to generate maps and derive volumetric information needed to estimate water volumes, and this included the delineation of the watershed, elevation and the spatial maps of the boreholes that were monitored. A cascade model was created by using climate data collected from local weather stations and the physical character of the local sandstone to study the waterflow through the mountain. The cascade model was used to appraise its potential in runoff. Some common features between the proposed model and HYDRUS-1D runoff model are also discussed. Data was also used in the HYDRUS-1D model where the results generated were compared with the cascade model results and the measured results from fieldwork studies.

The study therefore reflected on the volume of water present in the mountain aquifer and despite the area experiencing its worst drought in a century, this excess water was available for extraction.

Opsomming

Die studie-area vorm deel van die Sandspruit-opvangsgebied. Die klimaat is semi-droog en kan beskryf word as 'n bedreiging vir ontwikkeling. 'n Studie is gedoen met die hoop om 'n addisionele varswaterbron te vind.

Hierdie studie vorm deel van 'n groter studie wat ten doel het om die droogtegeteisterde Wes-Kaap se druk te verlig deur addisionele varswaterbronne te vind. Die studie fokus op die Kasteelberg, wat net buite die dorp Riebeeck Kasteel geleë is.

Tydens hierdie hidrologiese ondersoek is daar gevind dat die akwifer hoofsaaklik bestaan uit sandsteen wat deel van die Tafelberg Groep vorm. Nate en krake is ook volop in hierdie poreuse sandsteenrotse. Vir die doeleindes van hierdie studie is die akwifer as homogeen met betrekking tot sy geologiese samestelling beskou.

Die studie het grondwatervlakregistreerders geïnstalleer in bestaande boorgate om die seisoenale waterfluktuering te meet. Die fisiese karakterisering van die geologie is onderneem waar die totale porositeit en samestelling eerstens vasgestel is. Geografiese Inligtingstelsels (GIS)- sagteware is gebruik om die berg te karteer, asook die waterskeidings af te lei, oppervlaktes te bepaal, metings van die berg te doen en die verspreiding van die toetsboorgate te karteer. Plaaslike weerstasiedata is bekom en deur middel van die opstel van 'n kaskade-model in MS Excel is die geofisiese inligting ingespan om meer te ontdek van die water wat deur die berg vloei. Excel is dus ook gebruik om die volume van die akwifer te bepaal en die model kon die waterdra vermoë van die akwifer benader. Excel-resultate is gevolglik vergelyk met die HYDRUS-1D-model se resultate en die model het die Excel-resultate bevestig en met fisiese waarnemings ooreengestem wat in die veld gemaak was. Die studie het daarin geslaag om te bewys dat hoewel die Wes-Kaap tans deur die ergste droogte in 100 jaar geteister word, die Kasteelberg Akwifer steeds genoeg neerslag ontvang om as waterbron vir plaaslike ontginning te dien, wat sodoende die druk op die bestaande waterinfrastruktuur sal kan verlig.

Table of contents

Chapter 1 INTRODUCTION	13
1.1. Motivation.....	15
1.2. Hypothesis.....	16
1.3. Aims and objectives of the study.....	16
1.4. Approach and methodology	17
Chapter 2 LITERATURE REVIEW	19
2.1 Introduction	19
2.2 Geological background.....	20
2.2.1 Introduction	20
2.2.1 Malmesbury Group	21
2.2.2 Tygerberg Terrane.....	23
2.2.3 Swartland Terrane.....	23
2.2.4 Boland Subgroup.....	23
2.2.5 Table Mountain Group (TMG).....	24
2.2.6 Piekenierskloof Formation	25
2.2.7 Graafwater Formation	25
2.2.8 Peninsula Formation	25
2.2.9 Structural features	26
2.3 Geomorphology	27
2.4 Study area	29
2.4.1 Local dam levels and water availability	32
2.4.2 Water security.....	34
2.5 Groundwater and hydrology.....	34
2.5.1 Groundwater monitoring and modelling.....	38
2.5.2 Hydrological modelling	39
2.6 Concluding remarks	41
Chapter 3 METHODOLOGY	43
3.1 Introduction	43
3.2 Lithology and hydrology.....	45
3.1 Monitoring of boreholes.....	46
3.2 Atmospheric data.....	48
3.3 GIS	48

3.4 Spatial and temporal rainfall variability and associated trends in the Kasteelberg area – precipitation and evapotranspiration.....	51
3.5 Land cover.....	52
3.6 Aquifer volume calculations.....	52
3.7 Porosity calculations	53
3.7.1 Porosity	53
3.7.2 Permeability.....	55
3.8 Water table and factors that influence recharge	55
3.9 Cascade model.....	56
3.10 Water storage	62
3.10.1 Local studies in the past.....	62
3.10.2 Groundwater.....	63
3.10.3 Soil.....	63
3.11 Hydrus model.....	63
3.11.1 Model setup.....	64
3.12 Specifics of the model setup in HYDRUS-1D.....	65
3.1 Conclusion.....	67
Chapter 4 RESULTS AND DISCUSSION.....	69
4.1 Introduction	69
4.2 The role of DEM's in the study.....	69
4.3 Climate and borehole response data.....	74
4.4 Implications of the Excel model.....	80
4.5 The Hydrus model and the Excel model in comparison	81
4.6 Conclusion.....	84
Chapter 5 CONCLUSION.....	85
5.1.1 Recommendations for future research.....	88

List of figures

Figure 1 Illustrates the moving of a period rainfall pattern over the last 100 years, observed during the months of April and May in the Western Cape, South Africa (Du Plessis & Schloms 2017)	14
Figure 2 Land use in the Boland mountains (WWF, 2013).....	20
Figure 3 Local geological map of south-western Western Cape, from Belcher (2003) who adapted it from Rabie et al. (1974).	22
Figure 4 DEM of the study area.....	28
Figure 5 The location of the study area, which is part of the Sandspruit, Western Cape, South Africa	32
Figure 6 Actual (a) and idealised (b) dual-porosity reservoir model (Warren & Root 1963) used in the HYDRUS-1D model.....	35
Figure 7 Estimated potential transpiration PT for renosterveld and wheat field with Hydrus (Vermeulen, 2010)	37
Figure 8 Characterisation of the climate variation through a comparison between (a) Franschhoek, (b) HLS Boland, and (c) Langebaanweg in terms of evapotranspiration (ET), average temperature (TM) and rainfall (R/d) (De Clercq et al. 2009).....	38
Figure 9 Geological cross section of the Kasteelberg region, with the SW fault possibly causing a permeable barrier to impede free flow of water (SRK, 2007)	39
Figure 10 The modelled results in salt movement from the Sandspruit catchment linked to water movement, (De Clercq 2015).....	40
Figure 11 A graphic representation of the dynamic in groundwater occurrence in the Kasteelberg to Berg River landscape (De Clercq 2015).....	41
Figure 12 Conceptual flow model of the Sandspruit catchment area (Jovanovic et al. 2011a)	45
Figure 13 Locations of boreholes monitored during the study are indicated in purple. Those that are numbered are the property of PPC and have the longest continual datasets, 4 June 2013 to 4 April 2016.....	48
Figure 14 DEM of the study area and surrounding area.....	50

Figure 15 Watershed model created with GIS software	51
Figure 16 Illustrates the change in the water table before and after recharge for the Kasteelberg Mountain. A) shows the rough estimated water table in the Kasteelberg Mountain during the summer when recharge is at its lowest due to limited precipitation during the summer months. It can thus be regarded as the minimum level of the water table. The three rectangles represent the blocks into which the mountain was divided for modelling purposes. B) shows the surface area receiving precipitation with the rectangles illustrating how the surface recharge was calculated. C) This figure should also be viewed along with the cascade model calculations in Excel. It also illustrates the reason why the volume of the aquifer was first calculated to later be used in the cascade system.	53
Figure 17 Surface of the Kasteelberg Mountain Aquifer, showing elevation starting at 200 m with 100 m increments.....	71
Figure 18 BH1 (Foot slope) – Water level from 11 August 2015 to 25 April 2016, this is indicated by the red line. The blue line indicates temperature during this time (generated by Solinst software).	72
Figure 19 BH2 (Mid slope) – Water level from 4 October to 25 April 2017, left to right, this is indicated by the red line. The blue line indicates temperature during this time.	73
Figure 20 Rainfall in the study area, 2010 to 2017 (Hortec, 2018)	74
Figure 21 Ground water levels in the boreholes, BH1 is located closest to the Kasteelberg Mountain, with BH2 and BH3 both located further east, but BH2 being near a local open mine (data from 4 June 2013 to 4 April 2016).....	75
Figure 22 Weekly rainfall in the study area, used in HYDRUS-1D modelling. Day 1 is 25 June 2015 to 22 December 2017; high precipitation is indicative of winter due to predominant winter rainfall in the study area (Hortec, 2018).....	77
Figure 23 Daily precipitation and borehole water level.....	78
Figure 24 HYDRUS-1D results, A) Actual Surface Flux, B) Potential Surface Flux.....	82
Figure 25 HYDRUS-1D model results, A) Surface Run-Off, B) Evaporation	83

List of tables

Table 1 Lithology specific to the study area, adapted from (SRK, 2007)	25
Table 2 Local geological sequences in the study area (adapted from Jovanovic et al. 2011b; Belcher 2003; Demlie et al. 2011; Gresse et al. 2006)	27
Table 3 Water Source Areas (WSAs) are grouped into 21 areas in South Africa, water source areas in bold are classified as the country's strategic water source areas (WWF 2013)	31
Table 4 Dam levels in the Western Cape, for the years 2016 and 2017 (Head 2017).....	33
Table 5 Geological characteristics of the local lithology (Lin 2007)	39
Table 6 Shows the minimum, maximum, mean and standard deviation with regard to borehole yields (l/s) linked to geological units, adapted from Demlie et al. 2011).....	46
Table 7 Locations of the borehole monitored during the study	47
Table 8 Screenshot from Excel, showing the division of the aquifer into eight layers, as well as density and porosity values that are used during modelling.....	54
Table 9 Screenshot from Excel, showing the division of the aquifer into eight layers, illustrating the values used in modelling, fractured sandstone, density and porosity and percentage infiltration rate	57
Table 10 Screenshot from Excel, showing the division of the aquifer into eight layers, and the input data to the left, rain and evapotranspiration.....	60
Table 11 Screenshot from Excel, showing the division of the aquifer into eight layers, and the input data in the left, rain and evapotranspiration and the calculations used to calculate the excess water in the system	61
Table 12 Water Flow and rock hydraulic parameters where θ_r is the residual soil water content, θ_s the saturated soil water content, α the parameter α in the soil water retention function [L^{-1}], n the parameter n in the soil water retention function, K_s the saturated hydraulic conductivity, K_s [LT^{-1}], l tortuosity parameter in the conductivity function [-], w_2 the parameter w for material M [-]. Relative weighting factor for the sub curve of the second overlapping sub-region, α_2 the parameter a for material M [L^{-1}], for the second overlapping sub-region and n_2 the parameter n for material M [-], for the second overlapping sub-region.	66

Table 13 Root water uptake where P0 is the value of the pressure head below which roots start to extract water from the soil, POpt the value of the pressure head below which roots extract water at the maximum possible rate, P2H the value of the limiting pressure head, below which roots cannot longer extract water at the maximum rate (assuming a potential transpiration rate of r_{2H}), P2L as above, but for a potential transpiration rate of r_{2L} , P3 the value of the pressure head, below which root water uptake ceases (usually taken at the wilting point), r2H the potential transpiration rate [LT^{-1}] (currently set at 0.5 cm/day) and r2L the potential transpiration rate [LT^{-1}] (currently set at 0.1 cm/day).	67
Table 14 The regional water table is shown with measurements at the start of the rainy season and at the end of the rainy season. The last two columns are calculated by subtracting the measured water level in the borehole from the Z value, height of the borehole, as indicated on the DEM, shown in Figure 15 . Table 14 shows the results of the regional water table before and after the main rainfall period for 2015.	70
Table 15 Total monthly precipitation and average water level responses	79
Table 16 Summary of the eight layers used in the Excel calculations, Table 11	80
Table 17 Altered division of the Excel summary used in HYDRUS-1D modelling	81

Abbreviations

Agis	Agricultural Geo-Referenced Information Systems
CMA	Catchment Management Agencies
CMB	Chloride Mass Balance
CSIR	Council for Scientific and Industrial Research
DEM	Digital Elevation Models
DTM	Digital Terrain Model
DWAF	Department of Water Affairs and Forestry
EC	Electrical Conductivities
GDP	Gross Domestic Product
GPS	Global Positioning System
HRU	Hydrological Response Unit
LiDAR	Light Detection and Ranging
Mamsl	Metres above mean sea level
MAR	Mean annual runoff
NFEPS	National Freshwater Ecosystem Priority Areas
NGA	National Groundwater Archive
NIMA	National Imagery and Mapping Agency
NLC	National Land-Cover Project
NPS	Nominal Pulse Spacing
NWA	National Water Act
RDM	Resource Directed Measures
SDR	Source Directed Controls
SRTM	Shuttle Radar Topographical Mission
SWAT	Soil and Water Assessment Tool
TauDEM	Terrain Analysis Using Digital Elevation Models

TMG	Table Mountain Group
USDA	United States Department of Agriculture
USGS	U.S. Geological Survey
WEF	World Economic Forum
WRC	Water Research Commission
WRM	Water Resource Management
WSA	Water Source Areas
WWF	World Wildlife Foundation

Acknowledgements

I dedicate this work to my Creator, Lord God Almighty, without whom I would not have been able to complete this study.

I would like to thank the following people:

Dr De Clercq, for the excellent guidance, encouragements and patience during the years I worked on this research project.

My wife, Petro Pieters, for her continued support, encouragement and assistance with grammar and spell checking of this document. With Are van Schalkwyk also reviewing the document thereafter.

Michael Beukes, for repairing my computer the day before the hand-in date and saving those last-minute edits.

Hendrik van der Merwe, who helped with some of the fieldwork at PPC.

My family and friends, you are my support system – thank you for your prayers, and words of encouragement.

If there is anyone I left out, I really appreciate your contribution towards my project.

Chapter 1 INTRODUCTION

In recent years, numerous advances have been made both at a national and international level in the field of water quality monitoring and management. With the recent increased interest in water resources management and security, more resources are being allocated to water resource management research and development globally. The first widespread assessment of South Africa's water resources was done in the 1950s, coinciding with the start of modern hydrology (Midgley *et al.* 1952). Other national studies later followed in 1969, 1981, 1994 (WR90), 2008 (WR2005) and 2013 (NWRS2) (Pitman 2011). These studies have both shaped and changed our understanding of climate cycles, rainfall and water resources in South Africa. This has led to the National Water Act 36 of 1998, which made the Department of Water Affairs and Forestry (DWAF) the custodian of water resources in South Africa.

The area of interest in this study is the Sandspruit catchment, a tributary of the Berg River, which is located near the agricultural town of Riebeeck West. The Sandspruit catchment covers an area of 155 km² roughly 50 km north of Cape Town, South Africa. Rainfall occurs predominantly in the winter months of May to October (Du Plessis & Schloms, 2017). The study area receives a mean annual rainfall of 400 mm, with temperatures ranging between a maximum of 24 to 31°C and minimum of 8 to 11°C (Bugan 2014). The climate of the study area is classified as semi-arid and the mean annual evaporation is estimated at 2 200 mm annually (Bugan 2014).

An additional water source is needed to help with the sustainable management of the area as groundwater is extracted for both agricultural and municipal purposes. This has led to numerous studies by the Department of Water Affairs and Forestry and other interest groups that investigated and continue to investigate and monitor the groundwater salinity in the area so as to determine the impact on sustainable use (De Villiers 2007; Fey & De Clercq 2004b; Fourie 1976; Gorgens & De Clercq 2006; Greef 1990; Van Rensburg *et al.* 2011; Bugan 2014). This widespread use of groundwater in the area gave rise to the question of how much is available to sustainable extraction. The model estimating the groundwater reserve is shown in the Results chapter and is discussed in later chapters.

Water users in the study area need to be informed about the potential damages of over-extraction and its associated environmental repercussions. To better interpret and display the situation in the study area, geographical information systems (GISs) will be used. A GIS is a very powerful tool to display spatial and temporal information visually.

In Chapter 2, previous studies and reports will be discussed. The studies and reports include hydraulic density of populations and its effects and strain on water. The Department of Water and Sanitation has also stated that the Western Cape is experiencing the worst drought in 400 years and has have still not recovered (DWS 2019). In **Figure 23**, it can clearly be seen that seasonal rainfall pattern shifts occur in the Western Cape. The paper by Du Plessis and Schloms (2017) shows a projected recovery period during which both groundwater and conventional water storage methods (dams) are recharged during the 20- to 40-year cycles. This study will thus attempt to ascertain the possibility of utilising groundwater to act as a buffer during the “dryer” years, as shown in this study. Due to the study area being used predominantly for agricultural practices, the availability of water is crucial for the local economy.

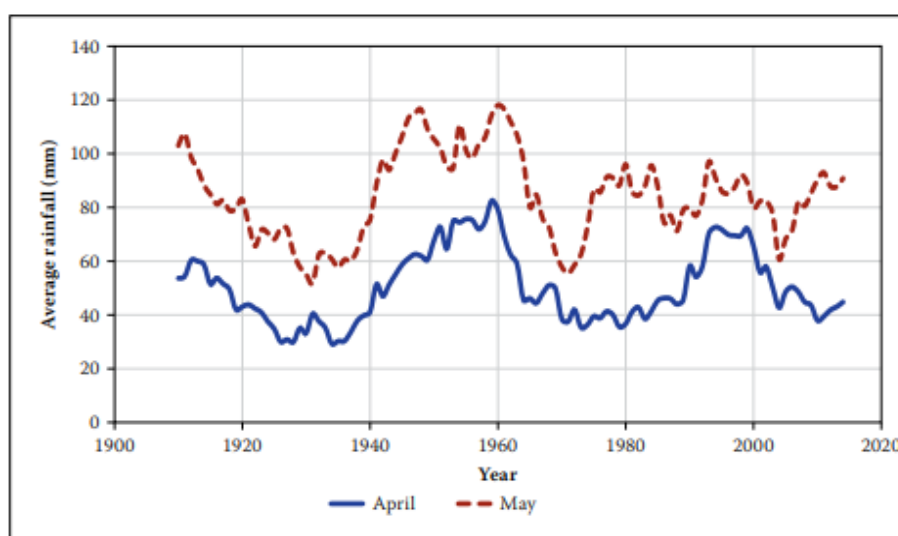


Figure 1 Illustrates the moving of a period rainfall pattern over the last 100 years, observed during the months of April and May in the Western Cape, South Africa (Du Plessis & Schloms 2017)

Official statistics are used to describe the current state of dams in the Western Cape (see **Table 3**). With the background stated in both the current situation and the discussion on past studies, mention will be made to the water security and growth concerns that influence the future of the province.

The Kasteelberg Mountain in the Sandspruit catchment was identified as it has been functioning as a “sustainable” water supply for over a century. GIS data such as DEMs and contour maps will first be created to later adapt and calculate the surface and volume of the mountain.

Borehole and weather station data will be used in Excel to model a cascade model and prepare the data for later modelling in HYDRUS-1D.

Upon completion of these tasks, the results are displayed in Chapter 4 and discussed in Chapter 5. In the concluding Chapter 6, fulfilment of the objective set in this study and the results are discussed. The hypothesis is re-evaluated and altered to incorporate findings and lessons learned during the study.

It is necessary to first investigate the methods and assumption associated with this study in the Aims and Objective Chapter. The final aim of this thesis is therefore to monitor groundwater changes and ultimately to calculate the volume and water-carrying capacity of the Kasteelberg Mountain Aquifer.

1.1. Motivation

Demand for clean water overtook storage capacity and is placing South Africa in a position where the buffering capacity of rivers is reduced due to a lack of said resource (Turton 2009) and subsequently compromising national water supply security and sustainable development.

The study area has been identified to be a potential new source of freshwater for the City of Cape Town. Previous work has been done in the area to determine the possibility of utilising this water resource. Yet the resource potential has not yet been estimated. This study will use previous studies along with newly collected and acquired data to achieve this objective. Given that the West Coast of South Africa is characterised as a Mediterranean climate with infrequent winter rainfall and is a semi-arid region with high summer evapotranspiration, freshwater is a scarce resource – even more so in the Western Cape. The Atlantic Ocean can be found directly to the west and the cold Benguela current flows along the coast, generating the Mediterranean climate with mainly winter rainfalls. This leads to a large demand for agricultural water during the seasons with high evapotranspiration, which puts a strain on existing water resources. Vegetation in the area includes fynbos, succulents, bushes and some sedges.

There is increased pressure globally on freshwater resources and in South Africa, specifically in the Western Cape Province, a new water source is needed. The implementation of modern, more water-effective agricultural methods and industry will have to be implemented by policy to compensate for water scarcity in the country. Other anthropogenic impacts, such as agriculture, industry, habitat destruction, increasing population and the pollution of these natural resources, pose a clear and imminent danger if not correctly managed. An immediate response to the preservation and protection of these freshwater resources is vital to sustainable economic growth and development. To achieve this goal, a clearer understanding of the local Kasteelberg Mountain aquifer is needed. This will also be one of the outcomes of this study.

Climate change is also expected to play a significant role in the future of the western/south-western regions of South Africa (Bugan 2014; WWF 2012), adding to the already stretched reserves.

1.2. Hypothesis

Kasteelberg is a high-rainfall area and is surrounded by large-scale agricultural and mining activity, which makes it ideal to clearly show the groundwater variation during summer and winter months. From these datasets two models will be created: HYDRUS and a cascade model in Excel. The cascade model will be used to estimate the water-carrying potential of the aquifer and the HYDRUS model will be compared to the cascade model to see to what degree the two approaches differ in their results.

1.3. Aims and objectives of the study

The aim of this study is to review available data and to supplement it with newly collected data, to calculate the capacity of the Kasteelberg Mountain Aquifer, to measure groundwater changes during seasonal change, to determine the reserve potential of the aquifer and to discuss the possible utilisation of the aquifer by the local municipalities.

To calculate the capacity of the Kasteelberg Mountain Aquifer

The area plays host to numerous parties utilising the aquifer for agricultural and municipal uses. Investigating links between the surface and groundwater may give insight into the health of the aquifer system and the current management thereof. A case can then be made for the

utilisation of the water resource and whether the current ecological protective measures are satisfactory.

To measure groundwater changes during seasonal change

By using local boreholes, the changes in water levels were measured over the span of multiple seasons to study the correlation between groundwater level, rainfall and the consequent lag before recharge occurs.

To determine the reserve potential of the Kasteelberg Mountain Aquifer

This will be achieved using GIS software, local geology and geological maps to help calculate the water retention and carry capacity of the aquifer.

To discuss the possible utilisation of the Kasteelberg Mountain Aquifer

This will be accomplished by comparing the groundwater table during the summer and winter seasons, monitoring rainfall and calculating the recharge and water absorption potential of the aquifer. These measurements will be used in combination with the volume calculations of the aquifer in GIS software. The results will be used to speculate as to the feasibility of utilising the aquifer for freshwater in the surrounding area.

1.4. Approach and methodology

A comprehensive approach to understanding the hydrological response to the Kasteelberg Mountain Aquifer was taken in this study. The research includes archival and collected temporal, spatial, hydrological and meteorological data sets.

The study involved the following steps:

- Literature review
- Data collection
- Fieldwork
- Interpretation of hydrological and climate data
- Calculating the Kasteelberg's dimensions using Qgis
- Cascade model
- Hydrus model

The closest weather station is located on the slope of the mountain and was used during this study. Other known weather stations in the surrounding area include stations in Moorreesburg

(South African Weather Service), De Hoek (South African Weather Service), Laggewens (Department of Agriculture and South African Weather Services) and Goedertrou (WRC – currently inactive).

Weather (meteorological) data is necessary for rainfall and evaporation estimations that represent the driving force of water fluxes in the catchment. Rainfall data is used to calculate the surface water and groundwater flow.

In a study that was conducted in November 2008 (Jovanovic *et al.* 2011b) it was decided to divide the Sandspruit catchment area into three sections, based on geology. The upper reaches are defined by sandstone and Malmesbury shale. The mid-reaches are defined by the undulating Malmesbury shales. The lower reaches are defined by Malmesbury shales in conjunction with alluvial sandy soils.

Chapter 2 LITERATURE REVIEW

2.1 Introduction

South Africa is a water-scarce country with an average annual rainfall of 465 mm, with 860 mm being the world average (NWRS2 2013a). In the past, South Africa has invested heavily in water infrastructure (1930s, 1970s, and 1980s) and monitoring water quality (NWRS2 2013b). Water supply cannot simply be solved by building more dams and new infrastructure. There are currently 4 395 dams of which 350 are controlled by the Department of Water Affairs (DWA) (NWRS2, 2013a). Addressing the water security issue (discussed in full later in this chapter) will include upgrading of existing infrastructure with modern technologies and rehabilitating South Africa's "water banks", namely catchment areas that feed both surface and subsurface water reserves. The general conception that dams are our only water resource is wrong and people need to be educated about this. They need to understand that the current water infrastructure depends on the natural "infrastructure" that supplies and sustains a healthy ecosystem, of which society may utilise the excess water. Annually, 10 000 million m³ surface water and 2 000 million m³ groundwater is allocated in South Africa (NWRS2 2013a) for anthropogenic uses. Figure 2 shows the main water sources and uses for the Boland district. This is a water-scarce area and a large part of the local economy is agricultural in nature. Multiple businesses also rely on the agricultural sector for products or for employment. This study will attempt to indicate if the Kasteelberg Aquifer is a viable additional source of water in the area.

The World Wildlife Fund (WWF) recently stated that the climate change models predict a grim future for South Africa's already stressed water reserves, stating that changes in both rainfall and temperature will negatively impact South Africa's water storage capabilities. While South Africa is a water-scarce country, it boasts as the country with the third highest level of freshwater biodiversity, with 223 river ecosystems and 792 types of wetland ecosystems.



Figure 2 Land use in the Boland mountains (WWF, 2013)

1.4.1. Hydraulic density of population

Researchers have been warning about this impending humanitarian crisis for more than a decade (Ferreira 2017), yet little was done to prepare for this crisis. Despite these warnings by researchers, the local government expanded free housing, which increased the strain on water resources.

With a still growing population and limited water resources it has been reported that South Africa has an annual water deficit of 38 billion m³ (Cowan 2017).

2.2 Geological background

2.2.1 Introduction

The Cape Super Group (CSG) is composed of sediments that were deposited in a shallow marine environment with evidence of tidal waves (Rust 1967). Also present are non-marine braided-fluvial environments that date back to the early Ordovician to early Carboniferous period. Outcrops are found along the entire length of the Cape Fold Belt (CFB) and are

predominantly siliclastic in nature. The succession of quartz arenites, shale, siltstone, conglomerates and a thin diamictite unit are subdivided into the Table Mountain, Bokkeveld and Witteberg groups respectively (Broquet 1992; Du Toit 1954; Rust 1967; Theron & Loock 1988; Theron 1962).

The regional geology (see Figure 3) of the study area is generally composed of the Malmesbury Group and the Table Mountain Group (TMG). The catchment area is within the limits of the Swartland and Tygerberg “terranes” as described by Von Venh (1983). Regionally the lithology of the area is characterised by low-grade-metamorphosed volcanic sedimentary succession, intruded by syn- to post-orogenic granitoids (Gresse *et al.* 2006). Poor exposure in the area has resulted in extrapolation in the regional geology and should be included in uncertainty studies.

2.2.1 Malmesbury Group

The Malmesbury Group is currently divided into three subgroups (see **Figure 10**), referred to as the south-western Tygerberg formation, central Swartland Subgroup and the north-eastern Boland Subgroup (Gresse *et al.* 2006). The Malmesbury Group overlies the Swartland Group, but is locally separated by an unconformity.

The formation of the Malmesbury Group is currently interpreted as a marine depositional environment (Rozendaal & Scheepers 1995; Belcher 2003) with the interlayered intermediate to mafic volcanic rocks probably representing oceanic crust. The origin of the Malmesbury Group is thought to be linked to a passive continental margin setting and the resulting filling of a basin with marine and flyschoid (a syn-orogenic sediment) deposits, within the passive continental margin (Rozendaal & Scheepers 1995; Belcher 2003). Shale layers from the Precambrian era are deeply weathered and were submerged in an oceanic environment till the late tertiary (Verwoerd *et al.* 1974). The Malmesbury Group have been subjected to low to medium-grade metamorphism as well as polyphase plastic and brittle deformation (Rozendaal & Scheepers 1995).

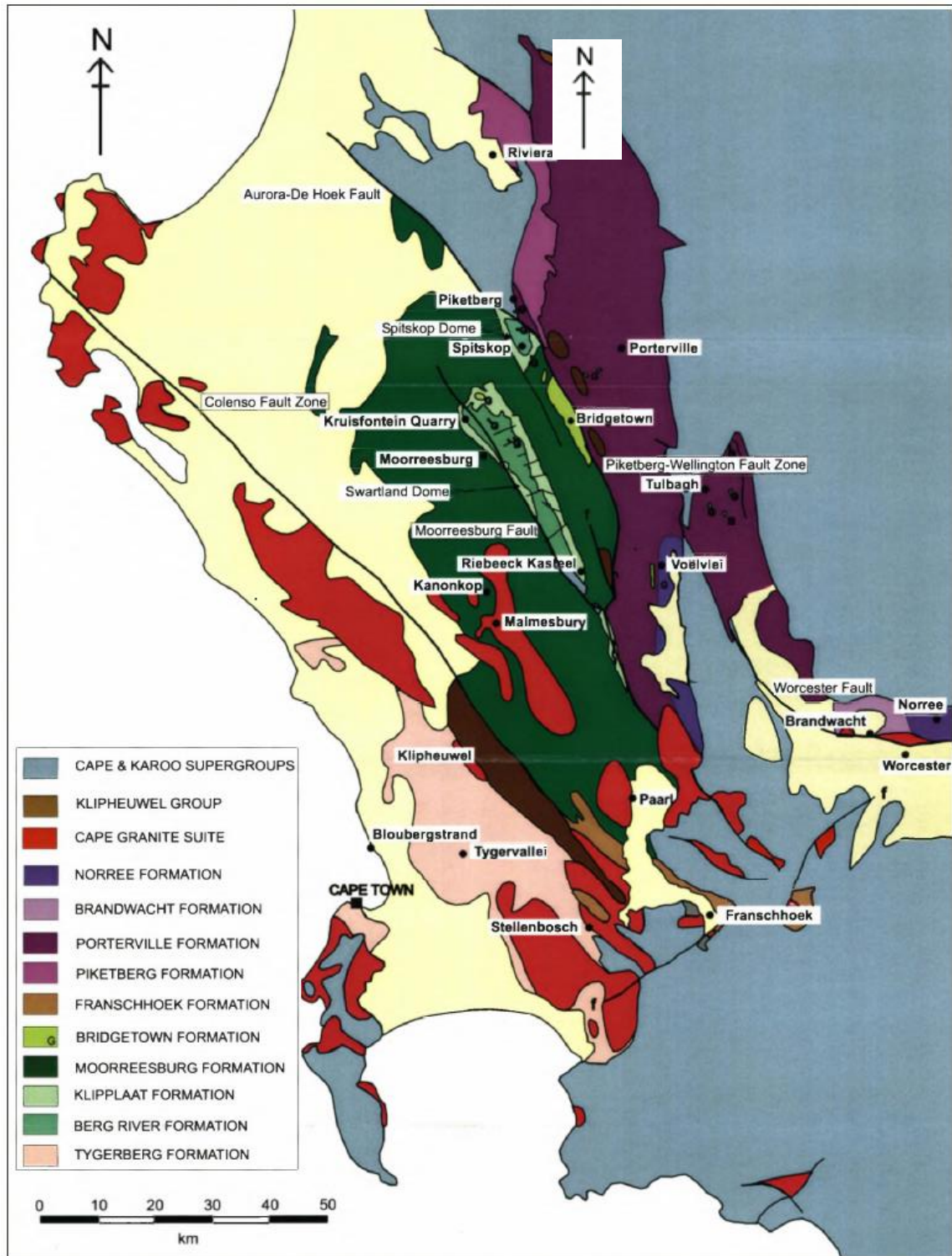


Figure 3 Local geological map of south-western Western Cape, from Belcher (2003) who adapted it from Rabie et al. (1974).

The Malmesbury Group is often difficult to study due to limited outcrops and the argillaceous nature of the group's lithological units that make up the bulk of the group (Demlie *et al.* 2011).

2.2.2 Tygerberg Terrane

The Tygerberg Terrane is overlain by the Malmesbury Group and is currently interpreted as a turbidite sequence. Its deposition as a turbidite deposit would have been located on the edge of an oceanic basin shown by the greywackes and phyllites (Rozendaal & Scheepers 1995). This feature is exposed for 3 km between Sea Point and Cape Town, which also exhibits sedimentary structures such as cross-bedding, ripple marks, ripple cross-lamination graded bedding and slumping channelling (Gresse *et al.* 2006). Interlayered rocks ranging from intermediate to mafic volcanic are currently thought to represent oceanic rocks (Rozendaal & Scheepers 1995).

The Bloubergstrand member exposed 15 km north of Cape Town, exhibits a local volcanic succession with a tuff, agglomerate and altered amygdaloidal andesite make-up.

2.2.3 Swartland Terrane

The Swartland Terrane consists of the Swartland Group and the Franschoek and Bridgetown Formations, with the Moorreesburg, Klipplaat and Berg River Formations grouped to form the Swartland Group.

These formations that make up the Swartland Subgroup are considered tectonostratigraphic units that are exposed in the form of the Swartland and Spitskop domes (Gresse *et al.* 2006). Sediment deposition is thought to be associated with the deformation of an accretionary prism/fore-arc (Belcher 2003).

The Swartland Terrane is an ancient shelf deposit due to the occurrence of mica schists, fine-grained quartzites and quartz schists, limestone and dolomite lenses (Rozendaal & Scheepers 1995).

The Berg River Formation is the lowermost formation and is made up of chlorite schist and greywacke (impure limestone lenses and quartz schist are found towards the top) (Gresse *et al.* 2006).

2.2.4 Boland Subgroup

The Boland Terrane is representative of a nearshore depositional environment, indicated by coarse-grained quartzites, quartz schists and psammites (sandstone or arenite) with conglomerate and phyllite bands present (Rozendaal & Scheepers 1995).

2.2.5 Table Mountain Group (TMG)

The Table Mountain Group (TMG) can be found in the Western and Eastern Cape Provinces of South Africa. The genesis for the TMG are thought to be sedimentary deposits that were deposited during the Ordovician to Silurian age, in an east-trending basin on a stable continental shelf (Rust 1973). The TMG has been influenced by two major tectonic events, Permo-Triassic Cape Orogeny and by the fragmentation of Gondwana in the Mesozoic.

Outcrops can be found from Nieuwoudtville to Cape Agulhas and stretching east towards Algoa Bay. The TMG also diminishes in thickness, from 4 400 m in the south to merely 900 m at its northern limit. Major sections of the TMG in the study area are quartzitic sandstones (Rozendaal & Scheepers 1995; Bagan 2014; Jovanovic *et al.* 2011b; Verwoerd *et al.* 1974). The Cape Orogeny had the effect of tectonically thickening the sequences in the Southern Cape where strain was higher.

In the study area, the TMG can be divided into three distinct units, as summarised in **Figure 9**.

Table 1 Lithology specific to the study area, adapted from (SRK, 2007)

Formation	Major lithological units	Maximum thickness in study area (m)
Piekenierskloof	Quartzitic sandstone & conglomerate	10
Graafwater Peninsula	Impure sandstone & shale Quartzite	55 500

2.2.6 Piekenierskloof Formation

The Piekenierskloof Formation, contrary to the group it forms part of, thins towards the south. As in **Table 1**, the Formation is only 10 m thin in the study area. The unit comprises basal conglomerates overlain by coarse grained sandstone.

2.2.7 Graafwater Formation

The Graafwater Formation follows conformably on the Piekenierskloof Formation and is only 55 m thick near the Kasteelberg, see **Table 5**. The unit as a whole is 440 m thick in Graafwater and thinning in the east and north (Rust 1967).

2.2.8 Peninsula Formation

The Kasteelberg mostly consists of the Peninsula Formation, as seen in Figure 10. The figure also shows that the Formation in this area is ~500 m thick, see **Table 5**. Characteristic of the unit are successions of medium to coarse grained, thickly bedded, grey sandstone which weathers to a greyish colour (Rust 1967).

The CFB is located 33 S and is east-west striking, which predominantly consists of sedimentary and metamorphic rocks. The entire geological succession with each respective sub-division, thickness and lithology is summarised in **Table 2**.

The geology of the Sandspruit catchment is dominated by the Table Mountain Group (TMG) in the elevated areas and the Malmesbury shales dominating the mid to lower elevated areas (Jovanovic *et al.* 2011b). Granite in the area also contributes to the surrounding clay soils, being derived from the weathered granite (Jovanovic *et al.* 2011b).

Semi-weathered rocks originating from the Malmesbury Group also cause a low hydraulic conductivity, with hydraulic conductivity decreasing with decrease in elevation (Jovanovic *et al.* 2011b).

2.2.9 Structural features

The Malmesbury Group acts as both a stratigraphic and tectonic link that incorporate the three terrains or domains, namely the Tygerberg, Swartland and the Boland subgroups (Gresse *et al.* 2006). Further structural features include the Colenso- and Piketberg-Wellington fault. The Colenso fault (Saldanha-Stellenbosch) acts as the physical divide between the south-western Tygerberg and central Swartland subgroup (Gresse *et al.* 2006). Tygerberg Terrane features S-type granite that is separated by the Colenso Fault from the younger I-type granitoids in the Swartland Terrane (Gresse *et al.* 2006), while the Piketberg-Wellington fault zone divides the central Swartland and north-eastern Boland subgroup (Gresse *et al.* 2006; SRK 2007). Both the Colenso and Piketberg-Wellington fault zones display reactivation in a sinistral strike-slip and vertical displacement (Gresse *et al.* 2006; SRK 2007).

Table 2 Local geological sequences in the study area (adapted from Jovanovic *et al.* 2011b; Belcher 2003; Demlie *et al.* 2011; Gresse *et al.* 2006)

Period	Group	Formation	Lithology
Quaternary	-	-	Silcrete/Ferricrete
		-	Loam and sandy loam soil
		Springfontein	Light grey to pale red sandy soil
Paleozoic	Table Mountain	Graafwater	Light grey quartzitic sandstone with thin siltstone, shale and polymictic conglomerate beds
		Piekenierskloof	Grey to reddish quartzitic sandstone with miner grit, conglomerate and reddish shale lenses
		Peninsula	Light grey quartzitic sandstone with thin siltstone, shale and polymictic conglomerate beds
Proterozoic	Malmesbury	Bridgetown	Greenstone with dolomite and chert lenses, graphitic schists, metavolcanic rocks with WPB-MORB affinities
		Moorreesburg	Greywacke and phyllite with beds and lenses of quartzite schist, limestone and grit, quartz-chlorite-muscovite-feldspar schists, graphitic schists and arenitic layers near the Klipplaat contact
		Klipplaat	Quartz schist with phyllite beds and minor limestone and chlorite schist lenses, sericite and limestone
		Berg River	Schist and fine-grained greywacke with beds and lenses of quartz schist and impure limestone lenses, graphitic schists quartz-chlorite-muscovite-feldspar schists toward the top of the formation
Pre- to Early Cambrian	Cape Granite suit	-	Hybrid granodiorite

2.3 Geomorphology

Surface drainage is largely dependent on the geomorphology or topographic gradient (see **Figure 4**) of the area with the groundwater flow largely also following this trend (Demlie *et al.* 2011). The DEM will later be used in conjunction with **Figure 14** to populate the Excel cascade model.

Up to 61% of the catchment area slopes at gradients between 0 to 4 degrees, with 27% sloping at 4 to 7 degrees (Demlie *et al.* 2011).

Land cover in the study area is divided into 90% grain and 4% grapes, with the remaining 6% of land use being allocated to reserves and mountain veld (Demlie *et al.* 2011). This also implies that the largest portion of this land is ploughed annually, which impacts on groundwater recharge.

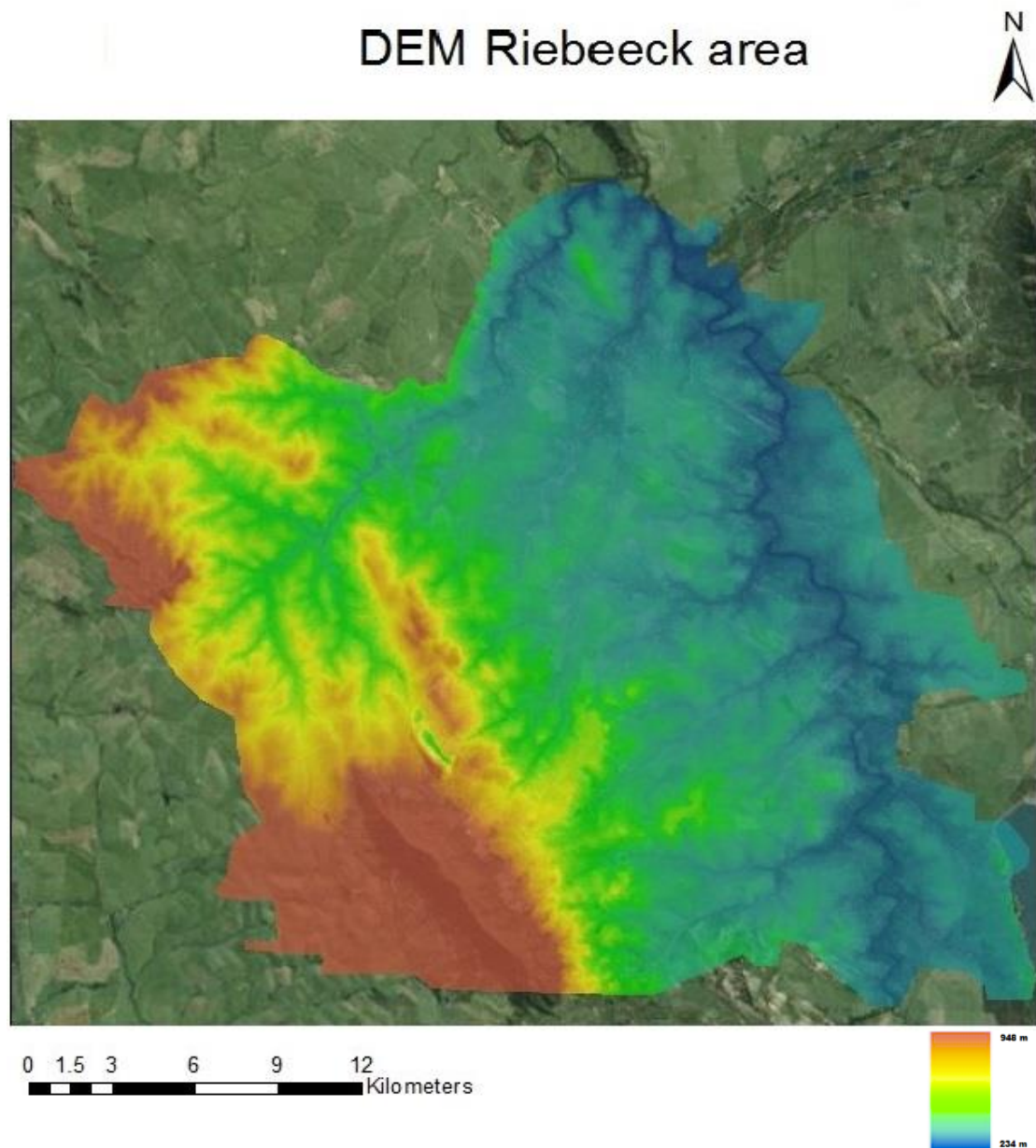


Figure 4 DEM of the study area

It is important to fully understand the geological setting of the Kasteelberg. In **Figure 10** one can see that the mountain has a major fault line along its southern side. In a NE to SW direction, there is a dip in the shale and sandstone. This means that water that penetrates the sandstone will be trapped at the base of the sandstone and on the less penetrable shale formation. This provides the opportunity for groundwater to accumulate in and below the mountain, except if

the fault system plays a role in decanting water to the shale layers below. It was therefore necessary to understand what the typical rates of water movement in the shales would be, as this defines the temporal storage effect in the system. This section therefore reflected on all the shale components of the Malmesbury formation and the reported physical character of these layers was used in the next section.

2.4 Study area

The research was conducted in a tributary or sub-catchment area that feeds into the Berg River. The Berg River currently supplies freshwater to the Greater Cape Town area and is a major freshwater source in the Western Cape. The Berg River combined with the Rivieronderend contributes 80% of the water needed by the Greater Cape Town and West Coast regions annually, contributing 450 million m³ of freshwater. In 2004, 12% of South Africa's Gross Domestic Product (GDP) was generated in this management area (De Clerq *et al.* 2013, WWF 2012).

An estimated 9% of the annual rainfall contributes to river flows, of which 4% recharges the local aquifers (De Clerq *et al.* 2013; WWF 2013). Studies focusing on groundwater recharge started in the mid-1980s, becoming more frequent and utilising modern technologies during the last couple of decades. It is thus important to reflect on the progress made and the current body of knowledge acquired in the field.

Groundwater recharge is subject to temporal and spatial variation of both the precipitation and geology. Groundwater recharge is a notorious component of the hydrological budget to accurately quantify (Stephens & Knowlton 1986; Jackson & Rushton 1987; Cook & Kilty 1992; Stone *et al.* 2001; Conrad *et al.* 2004). With the study area being in an area allocated to an arid zone, the task of establishing a water budget further increases the difficulty due to recharge factors such as time, space and geomorphology (Verma 1979; Yair & Lavee 1985; Simmers 1988; Conrad *et al.* 2004).

Inputs used in relation to water balance equations can be defined by direct or vertical recharge, rivers and lateral inflow mechanisms (Conrad *et al.* 2004). The study area (**Figure 5**) was selected because it receives seasonal rainfall and has an "isolated" mountain. This means that the mountain does not form part of a larger mountain chain, and limited geological variation is expected. Studies have also been conducted in this area to determine the possibility of commercialising the groundwater, but have yet not attempted to determine the water storage capacity of the aquifer.

The study area boundary was set to establish and ensure that the study area is not influenced by “outside” impacts (**Figure 16**). This means that the catchment area represented a closed system regarding water fluxes. These boundaries separated this catchment area from the adjacent catchment system, e.g. watersheds. This was essential in ensuring accurate assessments of geology, soil type and land cover (agriculture) that influence water movement. To achieve this, a watershed analysis was prepared in Map Window, based on a DEM from the USGS.

- Precipitation data was obtained by using data captured by local weather stations. The mountain (Kasteelberg) as focus had higher rainfall than the surrounding regime, with a reduction in rainfall relative to the distance from the mountain.
- Infiltration rates are important to the study as this will be the basis of the recharge potential calculations later in the study. This will be essential during the building of the cascade model. The influence of the geology, the soil type and agriculture will add to our understanding of the infiltration potential of the top soil (soil type and agriculture) and the permeability of deeper rock layers.

Table 3 illustrates the Water Source Areas (WSAs) of South Africa. The distribution is not equal and areas such as the study area need another water source for sustainable development. Due to the local economy being mostly based on agriculture, industries reliant on the agricultural sector are employing thousands of workers. The resulting need for sustainable growth is felt in the entire community.

Table 3 Water Source Areas (WSAs) are grouped into 21 areas in South Africa, water source areas in bold are classified as the country's strategic water source areas (WWF 2013)

Water Source Area	Main Rivers	Threats
Amatole	Great Kei; Keiskamma; Great Fish, Tyume; Amatele	Land degradation; fires; alien invasive vegetation
Boland Mountains	Berg; Breede; Riviersonderend	Large-scale plantations; land degradation; climate change; alien invasive vegetation; fires
Eastern Cape Drakensberg	Mzimvubu; Orange; Bokspruit; Thina; Klein Mooi; Mthatha	Land degradation; fires; climate change
Enkangala Drakensberg	Pongola; Bivane; Assegai; Vaal; Thukela; Wilge	Coal mining; large-scale plantations; land degradation
Grootwinterhoek	Olifants River; Klein Berg; Doring	Land degradation; climate change; alien invasive vegetation; fires
Kougaberg	Kouga; Baviaanskloof; Olifants; Gamtoos; Gouritz	Climate change; alien invasive vegetation; fires
Langeberg	Doring; Duiwenhoks; Naroo; Gouritz; Breede.	Climate change; alien invasive vegetation; fires
Maloti Drakensberg	Caledon; Orange; Senqu	Large-scale cultivation; land degradation
Mbabane Hills	Usutu; Lusushwana; Mpuluzi; Inkomati, Pongola	Large-scale plantations; land degradation
Mfolozi Headwaters	Lenjane, Black Mfolozi; Pongola	Large-scale plantations and cultivation; coal mining land degradation
Mpumalanga Drakensberg	Elands; Sabie; Crocodile; Olifants	Large-scale plantations; coal mining; land degradation
Northern Drakensberg	Senqu; Caledon; Thukela; Orange; Vaal	Coal mining; land degradation
Outeniqua	Groot Brak; Olifants	Large-scale plantations; alien invasive vegetation; fires
Pondoland Coast	Mzimvubu, Mngazi, Mntafufu; Msikaba	Large-scale cultivation and plantations; coal mining; land degradation
Southern Drakensberg	uMngeni; Mooi; Thugela; Mkomasi; uMzimkulu	Large-scale plantations; land degradation
Soutpansberg	Luvuvhu; Little Letaba; Mutale; Mutamba; Nzhelele	Large-scale plantations and cultivation; land degradation
Swartberg	Gamka; Sand; Dorps; Gouritz; Olifants	Climate change; alien invasive vegetation; fires
Table Mountain	Hout; Diep	Climate change; alien invasive vegetation; fires
Tsitsikamma	Groot Storms; Klip; Tsitsikamma	Large-scale plantations; land degradation; alien invasive vegetation
Wolkberg	Middle Letaba; Ngwabitsi; Oliphants	Large-scale plantations; land degradation; climate change
Zululand Coast	Mvoti; Thukela; Mhlatuze	Large-scale cultivation; coal mining; land degradation

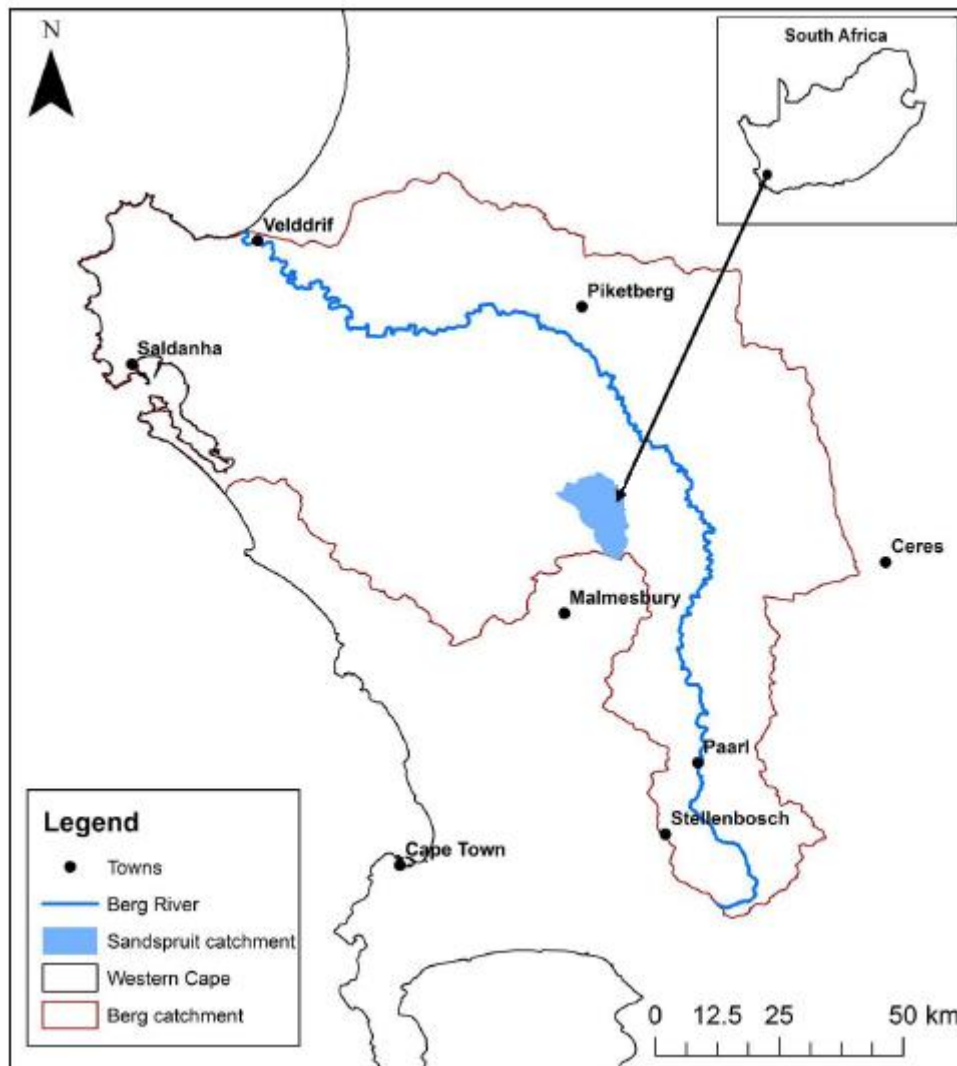


Figure 5 The location of the study area, which is part of the Sandspruit, Western Cape, South Africa

2.4.1 Local dam levels and water availability

Cape Town recently suffered from drought, and dam levels were extremely low. **Table 4** shows how water security was compromised. The dams were estimated to run dry early 2018 and this was referred to as Day Zero by local authorities. The crisis led to the Western Cape Province being proclaimed a disaster zone due to the widespread drought.

Table 4 Dam levels in the Western Cape, for the years 2016 and 2017 (Head 2017)

Dam	% 2016 (start of December)	% 2017 (start of December)	% difference
Cape Town System Dams (Combined)	52	34	-18
Theewaterskloof	45	21	-24
Voëlvlei Dam	61	26	-35
Clanwilliam Dam	82	30	-52
Brandvlei Dam	48	28	-20
Berg River Catchment	61	50	-11
Breede River Catchment	54	29	-25
Gouritz River Catchment	30	20	-10
Olifants River Catchment	81	30	-51
Western Cape state of dams	52	32	-20

Freshwater ecosystems in South Africa were mapped and classified into National Freshwater Ecosystem Priority Areas (NFEPSs). The NFEPS show that 60% of river ecosystems and 65% of wetlands are being threatened (WWF 2013), with 23% of river ecosystems and 48% of wetlands being at critical risk (WWF 2013). Only 12% of South Africa's land surface currently generates more than 50% of the country's surface water supply (WWF 2012). The WWF and Council for Scientific and Industrial Research (CSIR) have combined resources to conduct a water run-off study, which revealed that only 8% of South Africa's surface is responsible for 50% of the run-off (WWF 2013). Apart from this, 21% of South Africa receives less than 200 mm annual rainfall (WWF 2012). Two thirds of South Africa's water resources are also shared with South Africa's neighbouring countries (WWF 2013).

South Africa is divided into nine Water Resource Management (WRM) areas, which are each responsible for the management of water resources in their area. The division of these areas is based on geology (aquifer systems), geography (catchment area), financial viability, stakeholders and equity consideration. WRMs are in turn managed by Catchment Management Agencies (CMA) which monitor and control the integrated water resource management.

In 2012, the World Economic Forum (WEF) released a Global Risk Report (World Economic Forum 2012) which stated that the number one risk was a total financial collapse, followed by global freshwater supply (WWF 2012). It is noteworthy that the third greatest risk (global food shortage) and fourth (volatility in energy and agricultural prices) are both directly related to

water supply. In the 2015 *Global Risk Report*, the top risk in terms of impact is listed as a water crisis (World Economic Forum 2015).

The Western Cape encountered a further water-related challenge, which was eutrophication of water resources due to cyanobacteria blooms, causing the microcystin levels to rise in dams (Turton 2009). Turton (2009) also shows the correlation between climate change and these cyanobacteria blooms.

Water is also partially “lost” (non-revenue water) during agricultural practices, industry and mining. Industry makes use of inefficient water-reliant processes, not reusing water and limited reduction in water pollution. Mining companies also vary in their water usage due to fluctuations in mineral prices, but mostly fail to reuse water. The agricultural sector may be the largest challenge in reducing water loss, due to water lost in canal systems, irrigation systems and crop selection.

2.4.2 Water security

Which factors define water security? First, the physical (hydrological) environment must be considered. This will include the water availability, annual water budget and variables that influence water access. Other factors include the socio-economics of the area in question, type of industries (if present), agriculture and anthropogenic water management infrastructure. Last, future climate variation should be considered (Grey & Sandoff 2007).

2.5 Groundwater and hydrology

During a similar study by Haws *et al.* (2005) using HYDRUS-1D, it was found that the use of dual-porosity resulted in improved accuracy with regard to water flow modelling. It was also noted in the study that solute transport was not modelled with success. This study only focuses on water flow and thus chose to use this modelling method due to its limitations not influencing the current study in its current form.

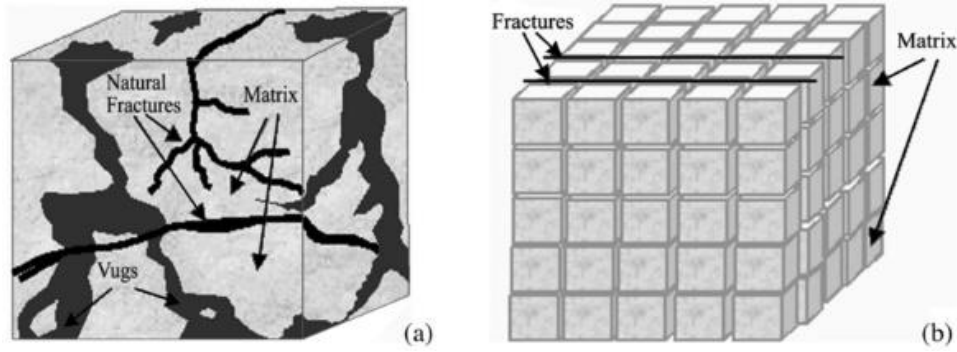


Figure 6 Actual (a) and idealised (b) dual-porosity reservoir model (Warren & Root 1963) used in the HYDRUS-1D model

Interporosity flow is the fluid exchange between two media, namely matrix and fractures, that constitute a dual-porosity system. Warren and Root (1963) defined the inter-porosity flow coefficient, λ , as

$$\lambda = \alpha r_w^2 \frac{k_m}{k_f},$$

Equation 1

where k_m is the permeability of the matrix, k_f is the permeability of the natural fractures, and α is the parameter characteristic of the system geometry (Gringaten 1984; Serra *et al.* 1983).

The interporosity flow coefficient is a measure of how easily fluid flows from the matrix to the fractures (Gringaten 1984). The parameter α is defined below by Equation 2.

$$\alpha = \frac{4j(j+2)}{L^2},$$

Equation 2

where L is a characteristic dimension of a matrix block and j is the number of normal sets of planes limiting the less-permeable medium ($j = 1, 2, 3$). On the other hand, for the multi-layered or "slab" model letting $L = k_m$, as the thickness of an individual matrix block (Serra *et al.* 1983), λ can then be described as in Equation 3.

$$\lambda = 12r_w^2 \frac{k_m}{k_f h_m^2}$$

Equation 3

The storativity ratio, ω , is defined by Gringaten (1984) as

$$\omega = \frac{(\phi V c_t)_f}{(\phi V c_t)_{f+m}} = \frac{(\phi V c_t)_f}{(\phi V c_t)_f + (\phi V c_t)_m},$$

Equation 4

where V is the ratio of the total volume of one medium and ϕ is the ratio of the pore volume of the medium to the total volume of that medium. Subscripts f and $f + m$ refer to the fracture and to the total system that constitutes fractures and the matrix. Consequently, the storativity ratio is a measure of the relative fracture storage capacity in the aquifer (Gringaten 1984).

De Clercq *et al.* (2010) monitored the climate of the Sandspruit since 2004. There are also other climate stations in the region, used in the studies of Wasserfall (2010) and Vermeulen (2013). Vermeulen (2010) studied the difference between two land uses: renosterveld and a wheat production system. See **Figure 8** and **9**, with their respective impacts on groundwater levels. This study along with the study conducted by De Clercq *et al.* (2009) in **Figure 9** illustrates past studies conducted in the area and the need to expand thereon.

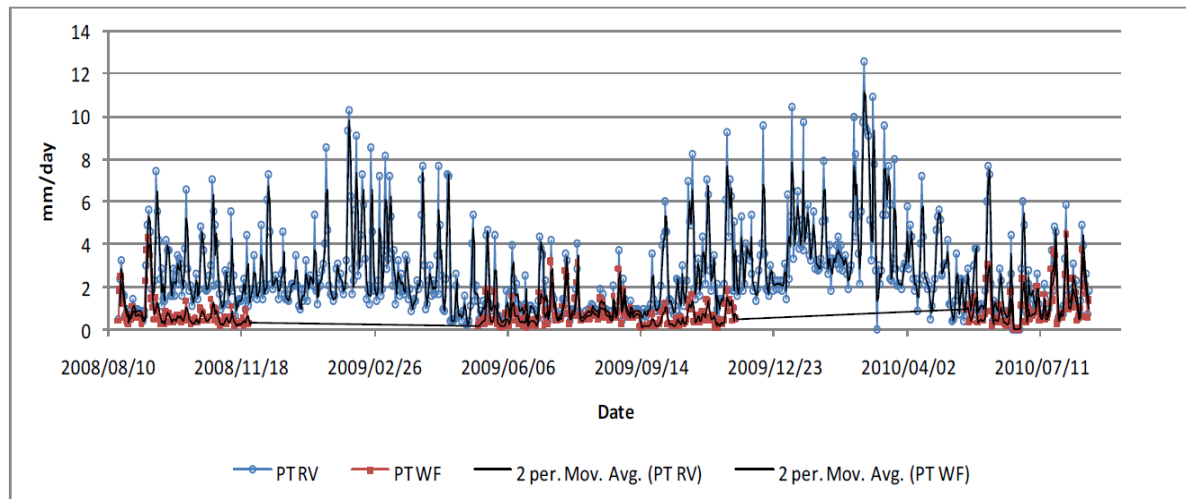


Figure 7 Estimated potential transpiration *PT* for renosterveld and wheat field with Hydrus (Vermeulen, 2010)

The use of weather station data and the monitoring of borehole formed the basis of this study. **Figure 8** shows the variation in precipitation and evapotranspiration in the area around the study area. **Figure 9** indicates the distribution of rainfall and evapotranspiration, indicating ET to be more dominant than rain.

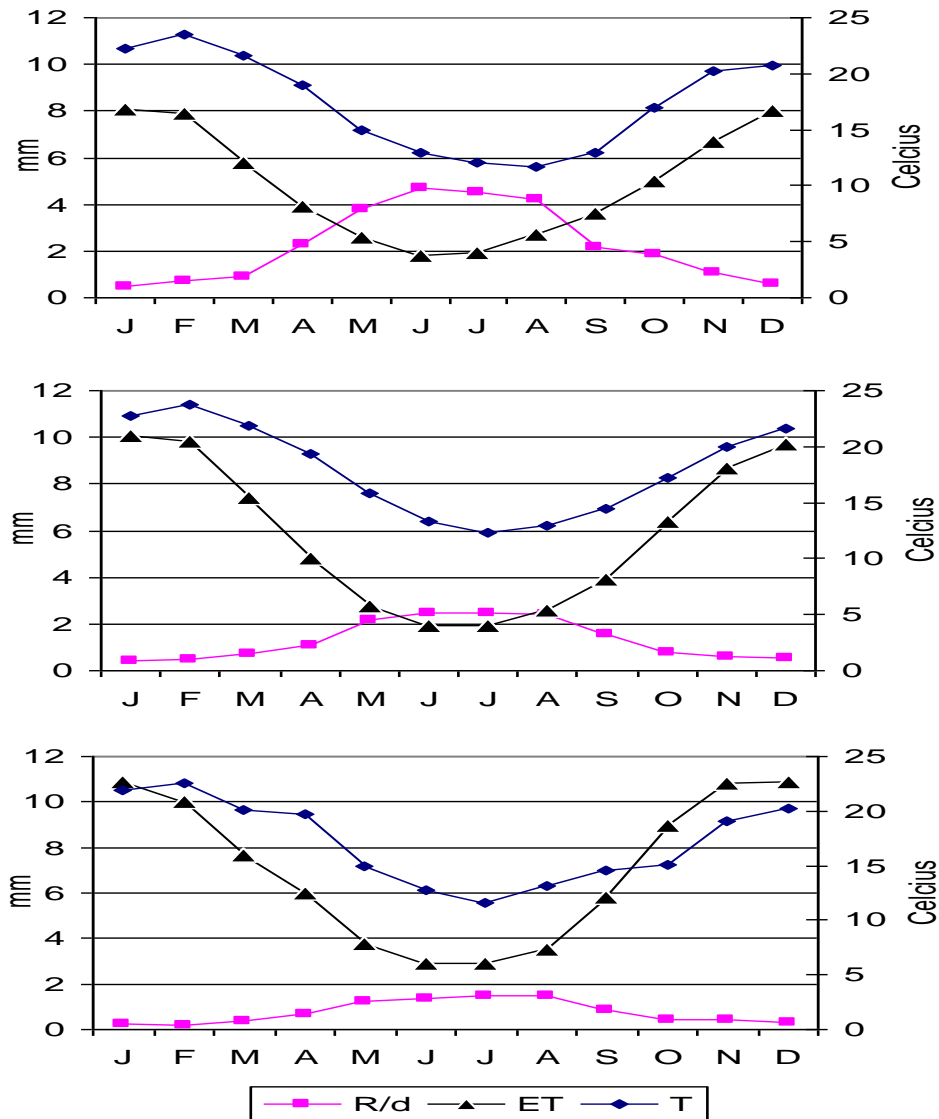


Figure 8 Characterisation of the climate variation through a comparison between (a) Franschhoek, (b) HLS Boland, and (c) Langebaanweg in terms of evapotranspiration (ET), average temperature (TM) and rainfall (R/d) (De Clercq et al. 2009)

2.5.1 Groundwater monitoring and modelling

Groundwater and HYDRUS-1D modelling were used by Bagan (2014) to investigate the hydrology of the Sandspruit. This study, on the edge of the Sandspruit, will use the same but more detailed information as the aims of this study are similar to Bagan’s (2014).

Table 5 Geological characteristics of the local lithology (Lin 2007)

Lithology	Density (g/m ³)	Porosity (%)
Clean sandstone	2.65	5.7
Fractured sandstone	2.3	16.4
Siltstone	2.45	17.1
Shale	2.35	14

When considering **Table 5**, the focus is rightly on the Kasteelberg Mountain and not the surrounding area due to the much larger yield in the fractured TMG. As shown in **Figure 9**, the mountain mostly comprises the Fractured TMG and the surrounding mainly the Malmesbury Group.

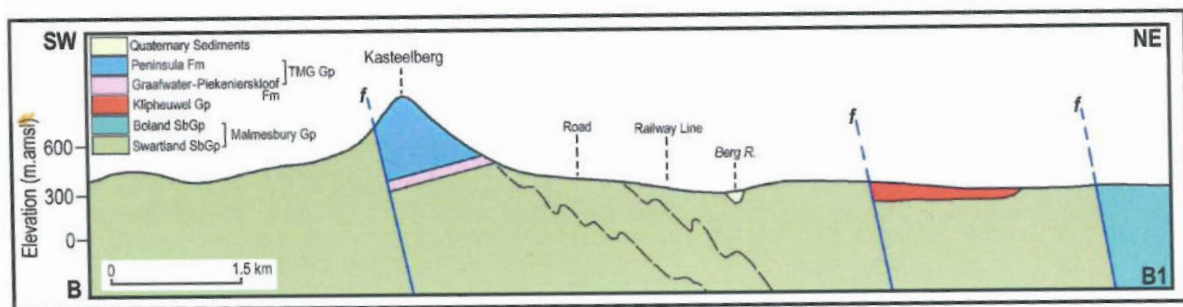


Figure 9 Geological cross section of the Kasteelberg region, with the SW fault possibly causing a permeable barrier to impede free flow of water (SRK, 2007)

2.5.2 Hydrological modelling

De Clercq *et al.* (2010) showed through hydrological modelling how the Sandspruit responded to flows from the Kasteelberg. This study by De Clercq *et al.* (2010), Bugan (2014), Wasserfall (2013), Vermeulen (2010) and Fey & De Clercq (2004b) focus on the area surrounding the study area. The studies by Bugan (2014) focused on the salinity in the Sandspruit, Wasserfall (2013) focused on hillslopes and Vermeulen (2010) on groundcover and evapotranspiration (Figure 8 and 9). These studies are important but lack the focus on the Mountain aquifer and the role it plays in the hydrological cycle of the Sandspruit. This study will follow a similar approach and methodology but will be adapted to indicate the role of the Kasteelberg Mountain Aquifer. Hydrological modelling will thus make use of multiple sources and various techniques

to increase accuracy of the results. HYDRUS-1D will be used to verify data collected and compare results from Excel, GIS, climate and borehole data.

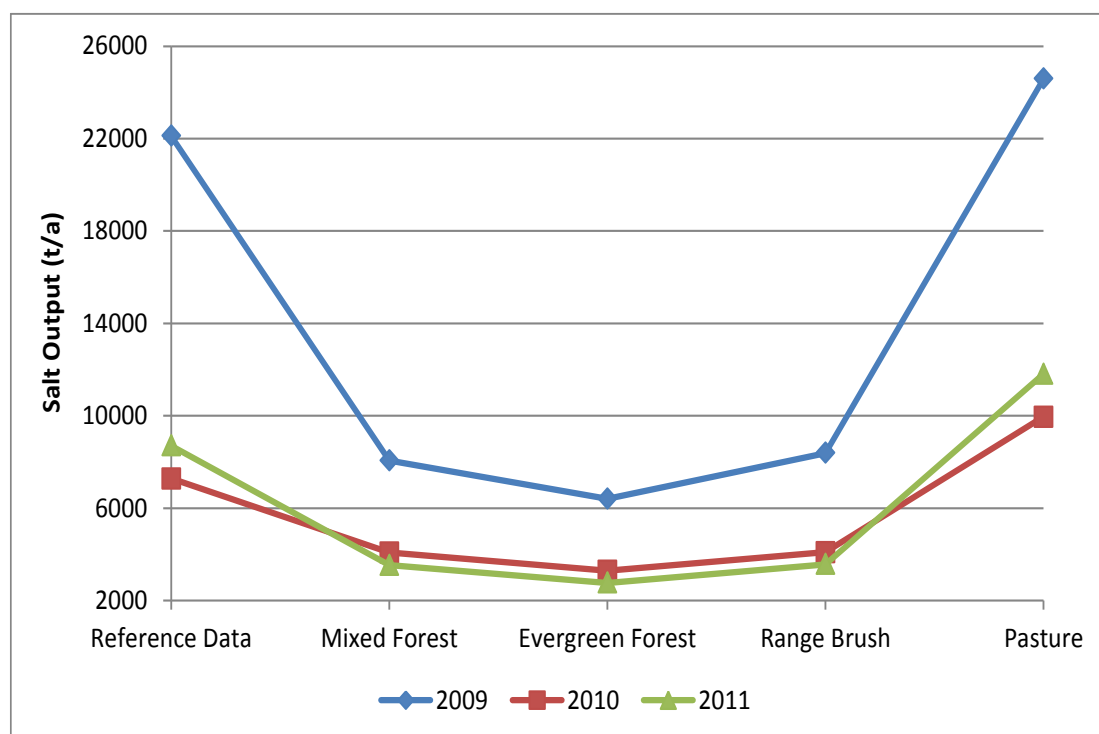


Figure 10 The modelled results in salt movement from the Sandspruit catchment linked to water movement, (De Clercq 2015).

Figure 13 summarises the current understanding of the hydrogeological setting of the Berg River catchment, indicating the seasonal responses of the perched water table in relation to the movements of salt. It is noteworthy that the salt output is minimal in relation to the other environments in **Figure 10**. This could be due to minimal agricultural-related chemicals or fertiliser being used in these areas, with constant recharge of the mountain aquifer from precipitation and the geological make-up of the aquifer not being high in salt. These facts from literature and field observations will later be used in determining parameters in the modelling of the aquifer in HYDRUS-1D. **Figure 12** is a graphic representation of the dynamic in groundwater occurrence in the Kasteelberg to the Berg River landscape by De Clercq (2015). The weathering zone, as indicated in **Figure 12**, shows the response of the perched water table to seasonal precipitation in the study area. This will be monitored over multiple seasons during this study. The results from monitoring the boreholes in the study area will later be used to correlate the results from the HYDRUS-1D model.

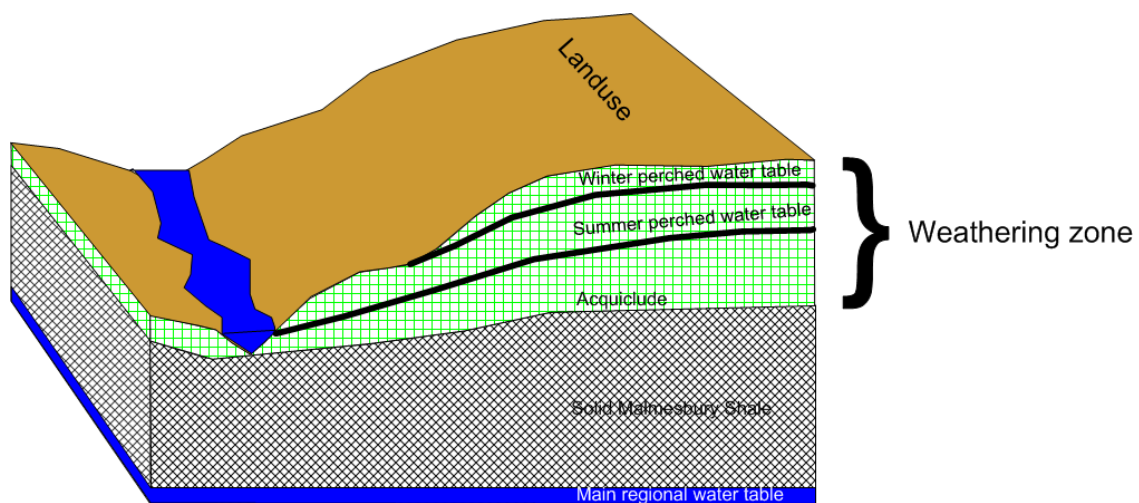


Figure 11 A graphic representation of the dynamic in groundwater occurrence in the Kasteelberg to Berg River landscape (De Clercq 2015)

2.6 Concluding remarks

Geology in the study area was extensively researched by Verwoerd *et al.* (1974) and the fault on the western side of the mountain makes the geological characteristics of the Kasteelberg Mountain unique and distinct from its surroundings, see **Figure 15**. With the geology being distinctly different from its surroundings, the establishment of boundaries was also that much easier. The geomorphology is also central to determining the boundary limits of the study area. This was due to the slope of the mountain, which made it distinct from its surroundings. This in turn resulted in very limited to no agricultural activity in the study area, which could augment the amount of water introduced into the system. This limitation to the local agricultural industry resulted in vegetation being natural and homogeneous, which will later reduce the number of unknown factors, with soil being limited on top of the mountain and the slopes. From literature and field observations the majority of water is sorted in joint and cracks rather than through soil infiltration. This also made the determining of the pressure head in modelling homogenous for this study.

Initially, the local mine was thought to be a challenge due to its manipulation of the water table so as to prevent flooding. This challenge was overcome due to using and observing boreholes between the mine and the mountain.

Expected challenges are that precipitation will be measured from a weather station next to the mountain. This is noteworthy in that it will undoubtedly influence the accuracy of the amount

of excess water in the system. With the focus of this study being the creation of a model and not the volume available for extraction, which is secondary, this was decided to be a sufficient source of precipitation data for the study.

Chapter 3 METHODOLOGY

3.1 Introduction

The reason for choosing the study area is due to the presence of an aquifer system that has been used for more than a century with multiple studies regarding geology, water use and local catchment management. This will make it possible to build a hydrological model from the abovementioned studies when combined with volume studies conducted during this study. The possible environmental impact that relate to improved water resource management at local level will be discussed. The aim should thus be to find a balance between a sustainable environment and sustainable land use. Aspects of the model population will also be discussed in this section.

Water accumulates in shallow fractures can differ in orientation, size and interconnectedness. This is important to consider, seeing that the major geology in the aquifer is fractured sandstones. The precipitation that percolates into these voids then migrate between each other or remain isolated above an aquitard. If the void is unable to distribute its excess water, it may become a perched spring or seep. Due to gravity, the groundwater in these systems might eventually migrate to deeper fractures that might lead to influencing the regional water table and the piezometric surface. One example of the piezometric surface in the Kasteelberg Mountain being reached, was during the month of August when streams started flowing from the mountain.

To achieve a balance between environment and sustainable land use, monitoring of the local boreholes was undertaken and it will be addressed in this chapter. Following this, GIS software is central to the understanding of hydrological systems and was utilised during this study. GIS software was first used to create a DEM map of the area; after this a watershed could be created with the help of SWAT software (Kiesel *et al.* 2013). Lithology is also important in understanding the workings of the aquifer and its interaction with a range of factors such as recharge and porosity. Precipitation and evapotranspiration data from year to year was used. QGIS was also used to calculate the surface area and volume of the Kasteelberg Mountain. With the surface calculated and the rough edges excluded to increase accuracy (see **Figure 15**), volume calculations were now possible. With the volume of the aquifer now known, the porosity of the strata was used to estimate the water storage potential of the aquifer. With the precipitation and evapotranspiration data sets, the water storage potential and the overflow

could now be calculated and modelled. Making use of the final calculations in Excel, the modelling was completed in Hydrus-1D.

The model concept in Excel was created to illustrate the response from the data gathered during the investigation of the Sandspruit catchment. From the conceptual model created by Bagan (2014) (see **Figure 12**), it is known that the Sandspruit catchment receives on average 473 mm/a precipitation (De Clercq *et al.* 2013). The model also shows the increased amount of precipitation as one moves closer to the mountain (494 mm/a) and the opposite is true when moving away from the mountain, with precipitation shown to be 321 mm/a. This also impacts the infiltration rates due to slope and varying precipitation. The vegetation also changes and this will affect the leaf area index in calculations in Hydrus. Due to that study area being limited to the mountain, this study will use a constant value when calculations require a leaf area index. Evapotranspiration was calculated at 443 mm/a from the Hortec datasets seen in the addendum. As expected, the precipitation is still indicated to recharge the water table. This change in precipitation decreasing from the mountain to the lowland have led this study to take note of the study conducted by Bagan (2014) and will thus only focus on the Kasteelberg Mountain. Groundwater in the study area is heavily relied upon by the local communities for various daily activities. Research in the area has thus far been restricted to field scale compared to the catchment studies, of which Bagan (2014) is a good example.

In this study, the catchment area will be spatially defined and mapped using QGIS and Swat software (Kiesel *et al.* 2013). Defining the catchment area will enable measuring of the annual precipitation and evapotranspiration. Measurements will be used to link rainfall, surface runoff and infiltration rate in the catchment area. Geology and subsequent geological processes will increase the understanding of the subsurface environment to better model the Kasteelberg Mountain Aquifer. Soil type data (topsoil) in the catchment area will be used to study the infiltration rates, impermeable layers and surface runoff of the aquifer. Infiltration reduction caused by agriculture may also be incorporated.

Findings include borehole readings that were monitored in the study area over multiple seasons. Precipitation from local weather stations was also used in this study. These data sets were also considered during GIS processes. Lithology and ground cover is also used in calculations that are later used to calculate the volume of the aquifer as well as the porosity thereof.

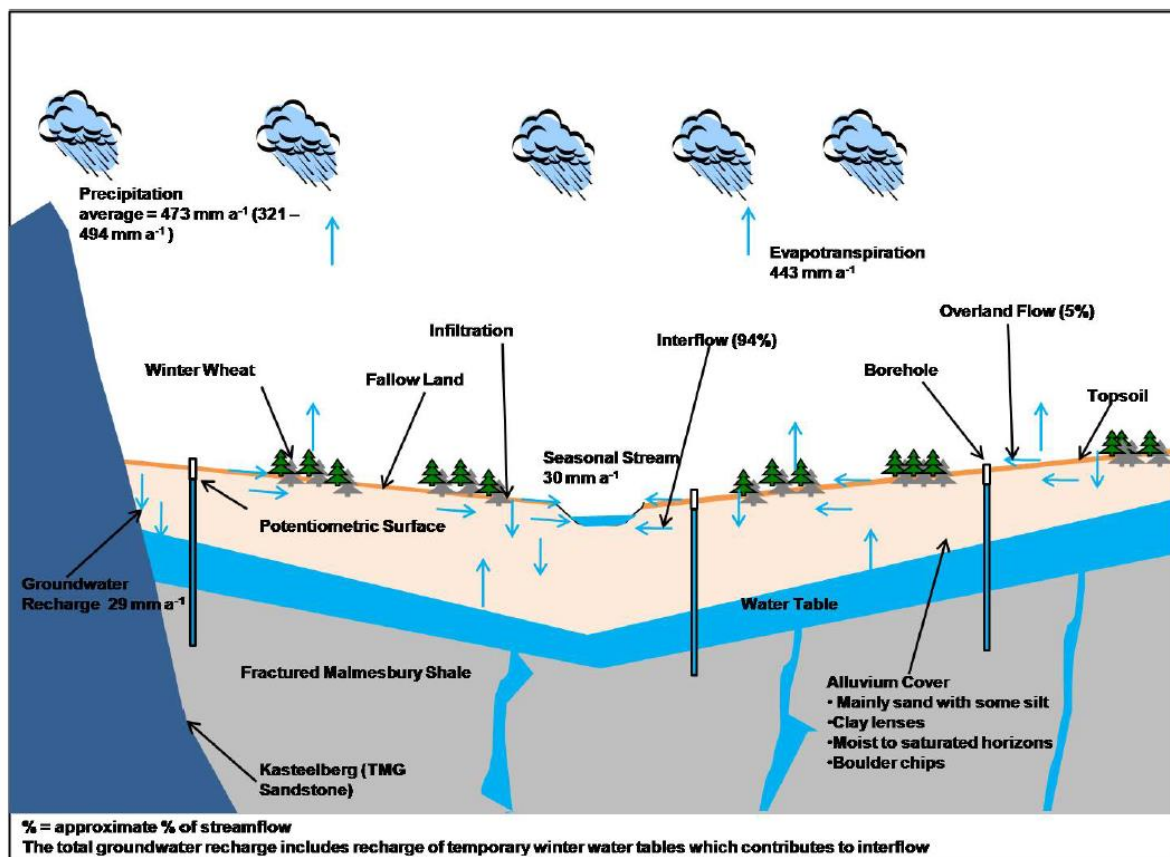


Figure 12 Conceptual flow model of the Sandspruit catchment area (Jovanovic et al. 2011a)

3.2 Lithology and hydrology

Groundwater quality in the lower reaches of the study area are predominantly saline, with EC ranging between 33 mS/m and 2 060 mS/m (Jovanovic *et al.* 2009). Past studies have shown groundwater yields of 0.9-2 l/s in the Malmesbury Group, 2.25 l/s in the TMG and 0.1-20 l/s in the Cape Granite Suite (Demlie *et al.* 2011). **Table 6** summarises the yield results documented by Demlie *et al.* (2001) which will be used to calculate the cascade model in Excel. The reported mean water yield in the two groups (in the study area) are 0.5 to 2.0 l/s, which is classified as medium to low yield (SRK, 2007).

Geology in the study area is dominated by the Malmesbury Group in the mid to lower reaches of the mountain. The upper reaches of the mountain (900 mamsl) are dominated by the Table Mountain Group (TMG) formations. Alluvial sediments also cover the foot slopes and increase in thickness towards the lower elevations. The bottom section of the mountain is classified as Graafwater – Piekenierskloof Formations. The remaining geology in the watershed area is grouped as the Malmesbury Group (**Table 6**), and this group is representative of low-grade metamorphic rocks such as phyllitic shale, quartz, sericrete shist, siltstone, sandstone and

greywacke. Field investigations have pointed out that some hills in the area are granite plutons protruding through the Malmesbury Formation. These granite hills are also characteristically distinct due to the hills being surrounded by clayey soil, which is derived from the weathered granite (Anchor Environmental and Freshwater Consulting Group 2007).

Table 6 Shows the minimum, maximum, mean and standard deviation with regard to borehole yields (l/s) linked to geological units, adapted from Demlie et al. 2011)

Geological association	Malmesbury	TMG	Cape Granite
Rock type	Shale	Sandstone	Granite
Number of test sites (boreholes)	12	12	11
Minimum	0.02	0.01	0.01
Maximum	3.38	17.07	1.60
Mean	0.83	2.28	0.38
Standard deviation	0.94	4.47	0.45

3.1 Monitoring of boreholes

The key data collected during this study consist of borehole water depth measurements and stream flow monitoring. This was done during the period of 4 June 2013 to 4 April 2016. These readings were acquired through direct measurement and using borehole level loggers (Solinst), logging change of the water levels and temperature of boreholes with Solinst loggers. Borehole level logging was used to indicate the water fluxes during the seasons, and to observe the responses of the water table with regard to precipitation.

The relative levels of the boreholes in the landscape and the relative depths of the water table at the different boreholes were studied, making use of the SRTM 30 m elevation data in QGIS, see **Figure 13**.

The spatial distribution of these monitored boreholes is also visually displayed in **Table 7** and **Figure 13**. Boreholes chosen for this study were distributed around the Kasteelberg Mountain and were only used for monitoring and not for other uses, such as abstraction. One of the boreholes was on the western slope of the mountain and was located near a streamflow monitor position (Hobo data logger used to monitor streamflow). The other boreholes were located mostly to the north-east and were existing boreholes used for scientific monitoring. Other boreholes were accessible, but were used by farmers, and therefore would not necessarily reflect the correct water table responses for that region due to periodic extraction.

Table 7 Locations of the boreholes monitored during the study

X-Longitude	Y-Latitude	Z (m)	Name of borehole location	Water table depth 2015 (m)					Water table depth 2016 (m)					Water table depth 2017 (m)				
				April	May	June	July	August	April	May	June	July	August	April	May	June	July	August
Farms																		
18°51.08 6.49"E	33°20 20.222"S	284.8	De Gift boerdery	8.84	0.7	0	0	0	7.62	0	0	0	0	8.1	0	0	0	0
18°51 46.505"E	33°20 46.222"S	268.5	Groenrivier function centre	3	3.5	3.2	3.2	3	2.6	2.9	3	3	3	3	3.2	3	2.9	2.9
18°49 40.672"E	33°19 24.214"S	245.9	Left side of the Klawervlei road	2.27	1.9	2	2.3	1.7	2	1.6	1.6	1.8	2.1	2.1	2	1.9	2.2	1.9
18°50 40.245"E	33°17 47.755"S	235.6	Vlakkerug	17.89	17.9	17	17	17.7	15.8	15.7	14.9	14.8	15.1	16.4	16.3	16.3	16.2	16.8
18°53 42.280"E	33°18 29.941"S	158.0	Goedertrou - among reeds	2.85	2.85	3	2.7	3	2.6	2.5	2.7	2.7	2.6	2.5	2.7	2.8	2.8	2.9
18°53 42.853"E	33°18 35.809"S	163.7	Goedertrou - in field	14.38	14.35	14.7	14.7	15	11	11.6	11.7	11.7	12	13.1	13.1	13.2	13.3	13.3
18°52 25.093"E	33°21 24.798"S	244.1	Allesverloren	1.32	2.3	1.7	1.7	1.1	.3	0.2	0.2	0	0	1	1.3	1.2	0.8	0.9
School																		
18°51'43.2"E	33°21'05.3"S	264.0	Bone-wood	13.33	16	16.5	16.5	16.6	Sealed									
18°51'55.8"E	33°21'09.7"S	256.3	School rugby field	13	dry	13	10	10.1	10.1	10.7	10.7	10	9.8	13	Used on day	dry	12.4	11
PPC mine																		
18°50 16.65"E	33°19 22.9"S	239.9	Site 1 (BH1)	23.5	25.1	25.5	25.6	26.3	See addendum									
18°51 24.35"E	33°19 8.48"S	209.9	Site 2 (BH2)	12	12	11.7	11.5	12.2										
18°51 20.61"E	33°18 28.4"S	204.7	Site 3 (BH3)	4.8	4.8	5	5.1	5.3										
18°50 7.85"E	33°18 1.26"S	216.5	Site 4 (BH4)	4.41	4.45	4.6	4.7	4.5										

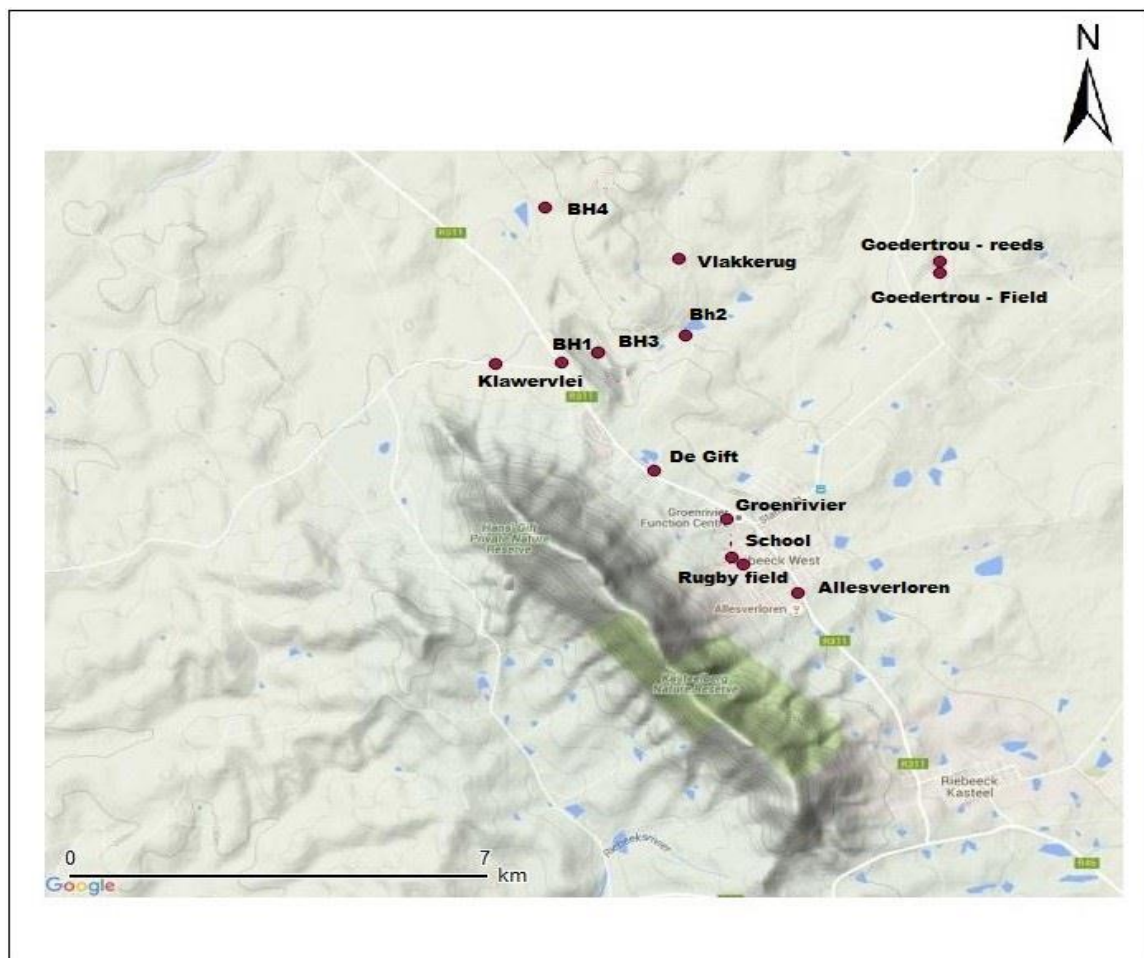


Figure 13 Locations of boreholes monitored during the study are indicated in purple. Those that are numbered are the property of PPC and have the longest continual datasets, 4 June 2013 to 4 April 2016.

3.2 Atmospheric data

Atmospheric variables that directly impact the hydrological processes are the amount of rainfall and its intensity over a period. Other hydrological processes also influenced by rainfall include infiltration rate, storage capacity and drainage. Atmospheric data also assists in estimating the evapotranspiration in the area, which in turn influences the recharge of the groundwater. Evapotranspiration is mainly controlled by air temperature, solar radiation, wind speed and relative humidity. Climate data was collected and used to apply in the temporal modelling of the aquifer.

3.3 GIS

In this section, the Soil and Water Assessment Tool (SWAT) was used along with Map Windows GIS software to determine the hydrological boundaries of the study area, seen in **Figure 15** (Kiesel *et al.* 2013). ArcMap was used to improve the display of the findings from Map Windows. This was done due to ArcMap consisting of more options when displaying the findings, legend, scale, values and a North arrow. QGIS was used, if not otherwise stated in

the study. QGIS was central in determining geological boundaries and the volumetric calculations of the Kasteelberg Mountain and its surroundings using the 30 m SRTM dataset.

Two Shuttle Radar Topographical Mission (SRTM) 30 m resolution data were used in this study (USGS 2015). These data sets are near-global Digital Elevation Models (DEMs), used to obtain elevation data for GIS software simulations. This data set was used in the flowing GIS section for volume calculations. The SRTM elevation data is based on radar information, meaning the true geological surface was used and not the canopy top or vegetation top surface.

SWAT was developed at the Blackland Research Centre in Texas. It was initially developed for the United States Department of Agriculture (USDA) Agricultural Research Service (SWAT 2017). This modelling method is based on a daily time step model, including amongst others the effects and changes in management practices. Further uses include the simulation of catchments in lumped or distributed mode (Kiesel *et al.* 2013), which is achieved by automatically delineating the catchment into either sub-catchments of numerous smaller grid cells, which in turn are based on a DEM. Following over 30 years of ongoing development by the USDA, the full background is explained in detail in both Arnold *et al.* (1999) and Neitsch *et al.* (2001). However, only the tools within SWAT, used to derive hydrological relevant information for this research from the elevation models, were used as SWAT is imbedded in ARCMAP, MapWindows and now also QGIS.

A preliminary graphical image of the study area was created in Map Window, using the SWAT hydrology extension, which is based on TauDEM. The input files are restricted to the SRTM's merged DEM and a projected geographical map. This image was further edited using the ArcMap software (Kiesel *et al.* 2013), where the smaller catchments were assigned different shades to better distinguish between these catchments, as shown in **Figure 15**. Last, QGIS was finally used in mapping the study area, determining geological boundaries and executing the volumetric calculations needed for the mass balance calculations.

Mapping of the geological boundaries, geological lithology and geological structures was achieved with the help of a study by Verwoerd *et al.* (1974). The presence of mostly sandstone in the Kasteelberg Mountain helped with the porosity calculations, due to the relative homogenous nature of the lithology. It also helped with the watershed delineation used in identifying the study area. The watershed or basin was then used in conjunction with a DEM for later volumetric calculations.

The DEM (30 m SRTM as seen in **Figure 14**) was obtained from USGS Earth Explorer (<https://earthexplorer.usgs.gov/>). A 30 m resolution did result in adequate volumetric calculations of the Kasteelberg Mountain Aquifer for this study.

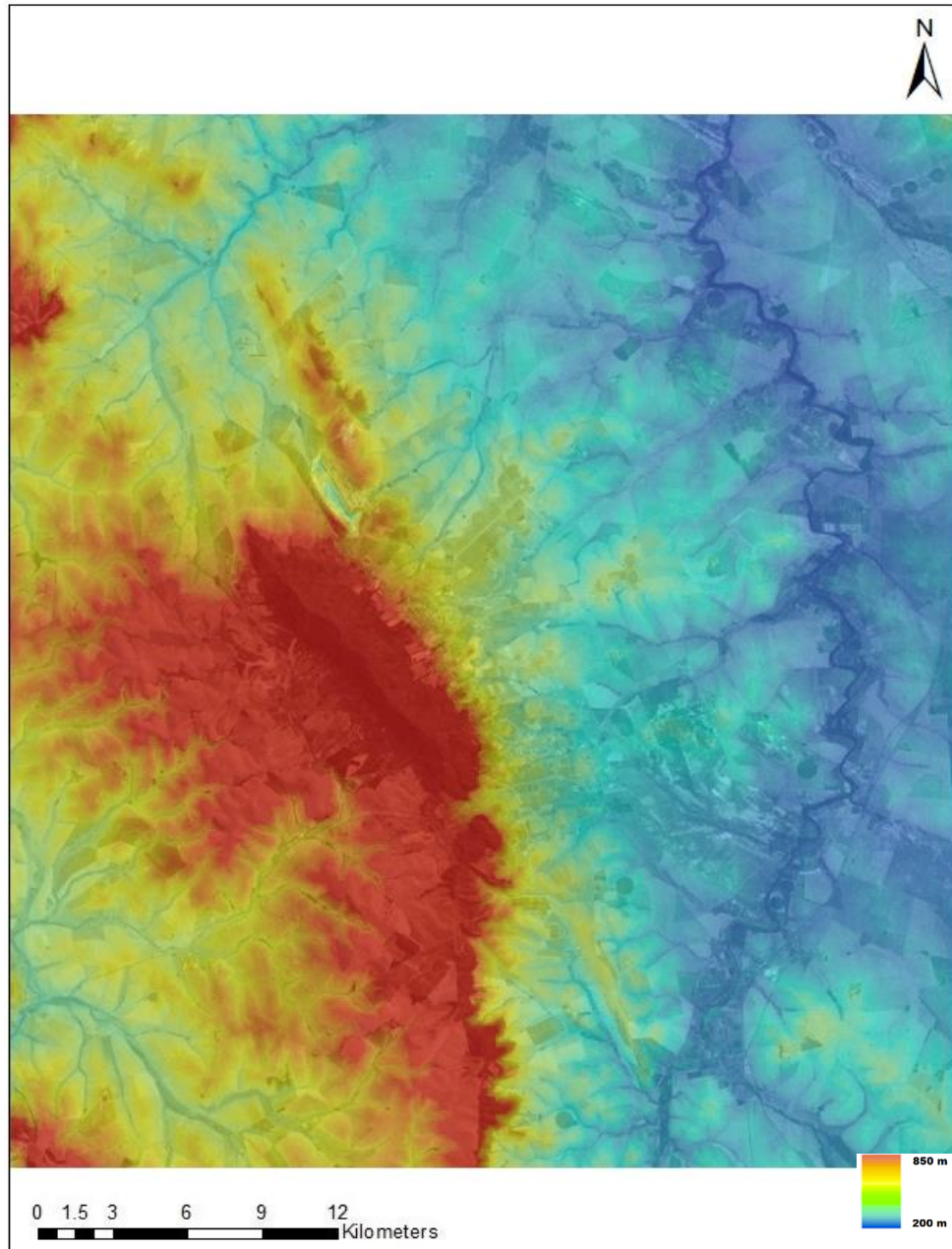


Figure 14 DEM of the study area and surrounding area

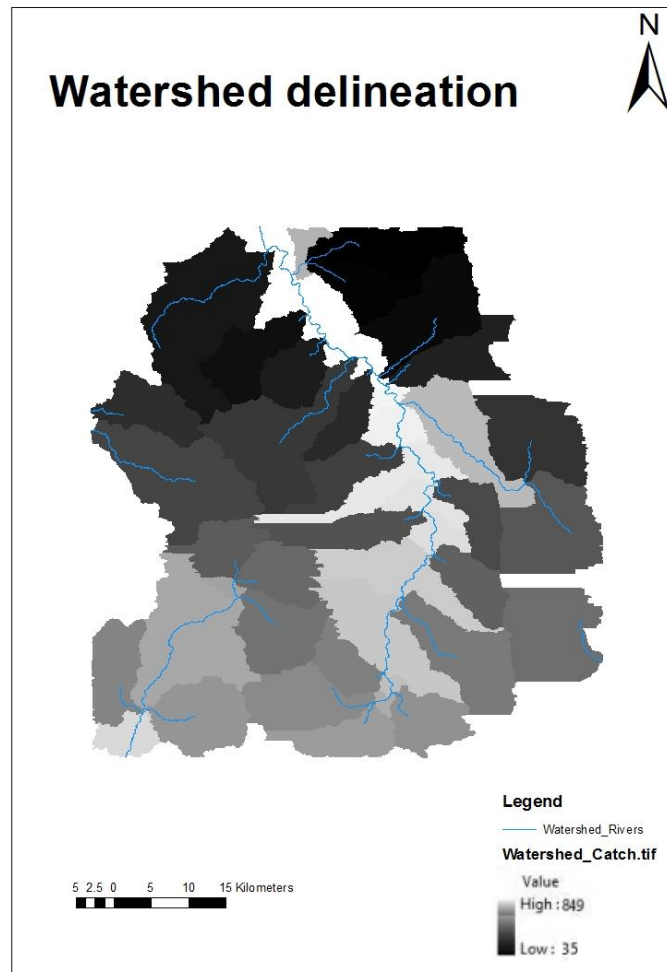


Figure 15 Watershed model created with GIS software

3.4 Spatial and temporal rainfall variability and associated trends in the Kasteelberg area – precipitation and evapotranspiration

As indicated by De Clercq *et al.* (2012), the distribution of rainfall in the catchment is primarily influenced by elevation and especially the high mountains of the region. There is a general precipitation trend where 1 000 mm/a is indicated on top of the mountain, 600 mm/a at the foot of the mountain and 400 mm/a close to the Berg River itself. In an arid environment, such as the study area, the effect of evapotranspiration is one of the main, if not the dominant, water loss process in this area, after local abstraction for crops and vineyards. The focus of the project was however not to provide a regional temporal groundwater response, but to estimate the temporal storage volume of the mountain aquifer. The primary reason for modelling the precipitation gradient for the mountain was to provide differential input to a regional model.

The focus of this study was however to estimate the aquifer response in a one-dimensional system. Therefore, the temporal climate response of a single point was more important than regional distributed estimates.

3.5 Land cover

Water source areas (WSAs) are grouped in 21 districts and spatially reserved for uses as natural vegetation, cultivation, plantations, degraded land and mining. Natural vegetation is restricted to 63% at the land surface due partly to altitude and sloped areas having been limited by development (WWF 2013).

Indigenous vegetation includes the Swartland renosterveld and Hawekwas, which form part of the fynbos biome. In the catchment area the natural vegetation, fynbos, has mostly been replaced with cultivated lands and pastures intended for agricultural use. Wheat is the main cultivated crop of the study area. Other crops include grapes, lupins and canola is present on a smaller scale. Farmers mostly follow a three-year planting rotation, i.e. cultivation only occurs every third year (Jovanovic *et al.* 2011b), which is why a stable and sustainable water supply is central to planning. During the fallow years, the land is used for grazing, during which groundwater extraction will be limited resulting in unhindered groundwater recharge and affecting evapotranspiration and infiltration rates due to change in vegetation. Construction of man-made erosion contours, erosion in the study area are thus considered to be minimal (Jovanovic *et al.* 2011b).

3.6 Aquifer volume calculations

Figure 16A shows the estimated water table in the Kasteelberg Mountain during the summer. This also shows the reason why the DEM was created (see **Figure 15**). From the created DEM the volume could be calculated using **Figure 15** as an overlay boundary, which resulted in the aquifer being divided into layers for an Excel cascade model. **Figure 16B** shows the surface receiving rain and exposed to the effects of evapotranspiration. **Figure 16C** illustrates the reasons why the volume of the aquifer was calculated using blocks and not the entire surface area. By excluding the edges, the accuracy of the calculations is thus higher. Note that the limited surface area influenced by vegetation cover is severely limited, thus the decision was made to use a default value of 1 for leaf index during HYDRUS-1D modelling.

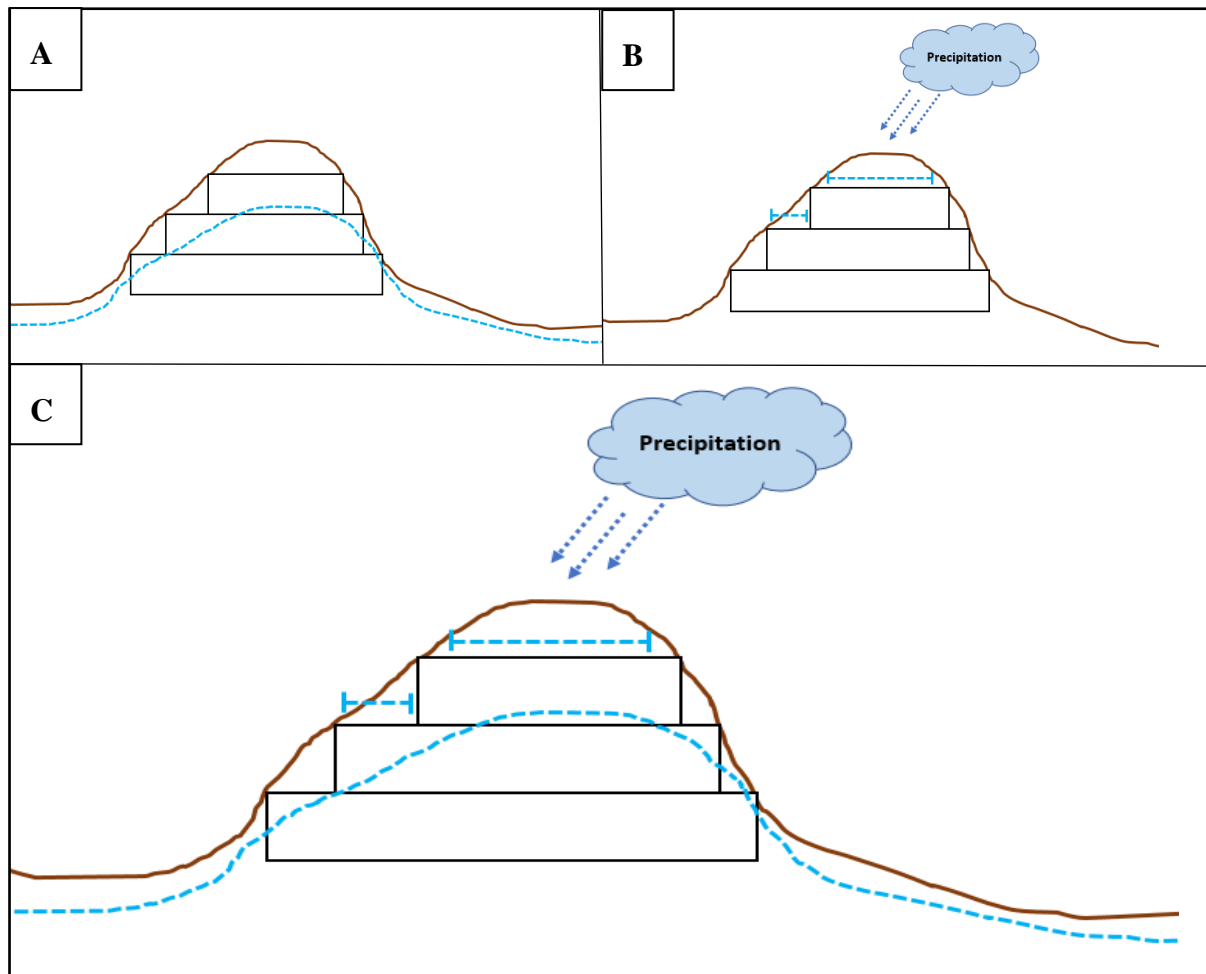


Figure 16 Illustrates the change in the water table before and after recharge for the Kasteelberg Mountain. A) shows the rough estimated water table in the Kasteelberg Mountain during the summer when recharge is at its lowest due to limiter precipitation during the summer months. It can thus be regarded as the minimum level of the water table. The three rectangles represent the blocks into which the mountain was divided for modelling purposes. B) shows the surface area receiving precipitation with the rectangles illustrating how the surface recharge was calculated. C) This figure should also be viewed along with the cascade model calculations in Excel. It also illustrates the reason why the volume of the aquifer was first calculated to later be used in the cascade system.

3.7 Porosity calculations

3.7.1 Porosity

Porosity (Φ) is the ratio of the void space divided by the bulk volume of the material being measured, see **Equation 5**. Porosity can be measured in both a fraction and a percentage. The equation for calculating the porosity is given by **Equation 1**.

$$\text{Porosity } (\phi) = \frac{\text{Volume of Pores}}{\text{Total Volume of Rock}} \quad \text{Equation 5}$$

The importance of the porosity or total “free” space in a rock relates to the storage capacity of the material (aquifer in this study). The porosity value on its own is not representative of the true holding capacity. This is due to a generalised porosity for the aquifer. This sampling assumes homogeneous composition. Effective porosity refers to the interconnectedness of voids.

Below in **Table 8**, the pore space is shown along with the aquifer being divided into eight layers. The layers represent horizontal section of 100 m each, based on the DEM that was overlain with a 2D contour map in **Figure 17**. This is due to the surface of each 100 m section being both exposed to precipitation and overlain by a top layer, which results in the cascade effect (Kiesel *et al.* 2013). The top layer is thus the only layer where the surface and rain surface are equal, due to no overlaying layer. **Table 8**. shows the formulas used in these volumetric calculations.

Table 8 Screenshot from Excel, showing the division of the aquifer into eight layers, as well as density and porosity values that are used during modelling

			Layer 1	Layer 2	Layer 3	Layer 4	Layer 5	Layer 6	Layer 7	Layer 8
Vol total poros			16	16	16	16	16	16	16	16
Surface (m2)			314045	1305586.007	1927384.993	2860636	3175836	5935174	12014298	37638682
Rain surface (m2)			314045	991541	935844	1924792	1251044	4684130	7330168	30308514
Volume (m3)			31404500	130558600.7	192738499.3	286063600	317583600	593517400	1201429800	3763868200
Contour (m)			900	800	700	600	500	400	300	200
Total pore volume	Rain mm	ETo mm	5,150,338	21,411,611	31,609,114	46,914,430	52,083,710	97,336,854	197,034,487	617,274,385
			Density (g/m3)	Porosity (%)						
Clean Sandstone			2.65	5.7						
Fractured Sandstone			2.3	16.4						
Siltstone			2.45	17.1						
Shale			2.35	14						

Effective porosity thus excludes isolated voids/pores and volumes occupied by air (Schalkwyk, 2005). Total porosity refers to the total void space which includes the effective, non-effective, and isolated and the volume taken up by absorbed air and water on grain surfaces (Levorsen 1967).

Porosity can originate from both primary and secondary processes. Primary porosity is the space/void that remains after deposition. While secondary porosity is attributed to: vugs (a small to medium-sized cavity inside rock), solution channels, diagenesis and in some cases

dolomitisation (Schalkwyk 2005). Fractures, shrinkage and dissolution are the most common. (Schalkwyk, 2005)

3.7.2 Permeability

Permeability is a physical property of any material, such as reservoir rock or porous medium, which allows the migration of fluid. It is related to effective porosity, yet not entirely dependent on it. Fluid flow is influenced by the size of the connection between voids and is measured in milidarcies (md). Permeability is measured in darcies where the SI unit of 1 darcy is equal to 10^{-12} m^2 .

A viable reservoir rock should display between 5 to 500 md size connections between pores.

Darcy's law $Q = -KIA$ Equation 6

Darcy's law ($Q=KIA$) is commonly used in the hydro industry to measure fluid flow, where Q is the flow discharge, K represents the specific permeability, with I being the hydraulic gradient, and A the area.

Fluid saturation is expressed as a fraction or percentage that represents the pore volume occupied by fluid, mostly water or hydrocarbons (Schalkwyk, 2005).

Fluid saturation (Sf) = $\frac{\text{Fluid occupying pores}}{\text{Total pore space in rock}}$ Equation 7

This saturation concept is important for the calculation of total water volume available, and is done by subtracting water saturation from the bulk volume. Water saturation (Sw) is normally indicated as a percentage of the total volume.

3.8 Water table and factors that influence recharge

Each respective layer has different water retention attributes, influencing the volume of water passed to the layer beneath it and the rate of flow thereof. This is central to understanding the recharge process in the Kasteelberg Mountain Aquifer as it shows that the rate is determined by soil type, vegetation and lithology, with slow initial water absorption in the top layers, contributing to the high evapotranspiration rates observed by Bagan (2014) in the study area. Bagan (2014) reported that evapotranspiration constitutes 94% of the water balance in the Sandspruit catchment, resulting in it being one of the most important factors to consider when

calculating recharge. Therefore, the layers were divided into thinner layers (horizontally) in **Table 8**, to improve the accuracy of the surface area affected by evapotranspiration.

3.9 Cascade model

Excel was used to convert the surface data obtained from QGIS. Multiple calculations could be done where layer responses were linked and dependant on one another. This provided the ability to easily generate graphs from both the non-refined and the refined data sets. That was essential to the modelling process and the first estimates of the water volumes in question and the type of responses to expect (Kruijne *et al.* 2008).

The cascade model was calibrated using field data collected over a period of 30 months (25 June 2015 to 22 December 2017), which represents different agrometeorological conditions in both the wet and dry periods. The cascade model used in this project was applied to the Kasteelberg Mountain Aquifer to apprise its storage capacity and runoff potential, as was also shown in studies such as those of Singh and Buapeng (1981), Kiesel *et al.* (2013) and Kruijne *et al.* (2008).

By using this simple cascade water balance modelling approach, the total water storage of the study area's aquifer was estimated. This was done by using the porosity of the aquifer, which is based on the lithology and meteorological data. The meteorological data as driver for the model included the field data collected over a 30-month period, which include borehole level readings, temperature, precipitation and evapotranspiration. The cascade model uses these data sets to determine the rate at which the top layer will reach its saturation point, which will then cascade to the following, underlying layer. The rate at which, if at all, the aquifer will fill (till it reaches the saturation point) will differ from year to year due to different precipitation and evapotranspiration parameters. Yet the potential volume of groundwater the aquifer is capable of retaining will remain relatively constant and was the focus of this study. From this, the sustainable use of the aquifer was also incorporated into the calculations and the average excess water. After the saturation point was reached, it was calculated based on the 30-month average.

The eight layers chosen in this study were based on 100 m thick sections of the mountain to break up the cross-section of the mountain to improve accuracy due to rough surfaces and a 30 m DEM. This could be refined for a more accurate estimation of the water-carrying potential, yet for the purposes of this study these parameters will suffice.

Below is a screenshot from the Excel spreadsheet used for the main calculations (**Table 9**). The Kasteelberg Mountain was divided into eight layers, each being 100 m thick. The contour

values refer to the elevation above sea level. Data used include fractured sandstone density and porosity. The surface area (row 3) is the values obtained from QGIS. Rain surface was calculated by subtracting the bottom layer from the top layer due to the bottom layer only being exposed to rainfall where the top layer does not overlay the bottom layer, (see **Figure 16** where the blue lines illustrate this point).

Table 9 Screenshot from Excel, showing the division of the aquifer into eight layers, illustrating the values used in modelling, fractured sandstone, density and porosity and percentage infiltration rate

	A	B	C	D	E	F	G	H	I
1		Layer 1	Layer 2	Layer 3	Layer 4	Layer 5	Layer 6	Layer 7	Layer 8
2	Vol total poros	16	16	16	16	16	16	16	16
3	Surface (m ²)	314045	1305586	1927385	2860636	3175836	5935174	12014298	37638682
4	Rain surface (m ²)	314045	991541	935844	1924792	1251044	4684130	7330168	30308514
5	Volume (m ³)	31404500	130558600,7	192738499,3	286063600	317583600	593517400	1201429800	3763868200
6	Contour (m)	900	800	700	600	500	400	300	200
7	Total pore volume	5 150 338	21 411 611	31 609 114	46 914 430	52 083 710	97 336 854	197 034 487	617 274 385
8	Percent infil	10	10	10	10	10	10	10	10
9		Density (g/m ³)	Porosity (%)						
10	Fractured Sandstone	2,3	16						

Table 9 was constructed along with values obtained from the GIS model with the mountain being divided (based on **Figure 17**) by elevation. In **Table 9** row 3, the value obtained from the metadata in the GIS model shows the surface area of layer one, which acted as the top of the mountain, at 900 m. The area that is referred to in layer two is calculated by dividing the previous (top) layer so as to not overestimate the exposed area.

Table 9 features the calculations executed in Excel to determine the excess groundwater potential of the Kasteelberg Mountain Aquifer. In this figure, evapotranspiration (ET_0) was divided from the rain data. Results in column F show the net effect of the two factors: a positive value will result in water added to the aquifer system and a negative value in the loss thereof. The first row (highlighted in green G, 10) is the total pore potential in the fractured sandstone. The second column, F, is the amount of rain/ ET_0 per rain surface area. An “IF” function was used in column G. Here the cascade effect applies, if the amount of groundwater entering the layer is more than the maximum water potential and the excess is transferred to the adjacent column. Column H is also used as a check, where negative values are normalised to 0. If the values are positive, it shows the net excess water that has accumulated through the system thus

far. This value (if positive) from column H is then transferred to column I, where the value recorded represents the amount of water transferred to the directly underlying layer.

The approach followed in Excel was based on a typical cascade modelling approach. The measured precipitation and the calculated ET_0 was used as the drivers for the approach. The following steps indicate the basis of the calculations and the approach followed.

1. The mountain was divided into 8 x 100 m thick layers
2. The total porosity of the fractured sandstone was calculated for each layer.
3. The rainfall and evapotranspiration were factored in; in turn the response could now be calculated using these two values.
4. As soon as a layer was saturated – not filled due to gravity making it unlikely to occur – the excess water was transferred to the deeper layer.
5. The water-carrying capacity was then calculated resulting in the excess recharge to account for the surface runoff. This is where the HYDRUS-1D model was used to correlate the results of this model and the HYDRUS model.

To summarise, the cascade model was started with the following data set known: the surface of each layer, the surface area of each layer exposed to precipitation and evapotranspiration, and the volume. Previously mentioned data was generated in QGIS from the 30 m SRTM DEM and superimposed 2D contour map, **Figure 17**.

The percentage infiltration rate was chosen to be “10” and the thickness of each layer was chosen to be 100 m respectively.

The first calculation done in Excel was to subtract the Et_0 from the precipitation. On days where precipitation was nil or less than the Et_0 it would result in a negative value. This negative value would then be used as a starting value for the next day. This is done to “make up” for the water loss the previous day/period. This value response is then multiplied by the surface area that is exposed to precipitation, giving the recharge value. The porosity is then calculated by multiplying the porosity and dividing it by 100 to give the porosity percentage.

$$\text{Rain} - Et_0 = \text{Response} \quad \text{Equation 8}$$

$$\text{Response} * \text{surface exposed to precipitation} = \text{Recharge}$$

$$\text{Recharge} + \text{pore space} = \text{Runoff}$$

Recharge was calculated as:

$$R_c = R - Et_0 \quad \text{Equation 9}$$

where, R_c is the recharge (mm/day), R is the rainfall (mm/day) and ET_0 is the evapotranspiration (mm/day).

Porosity percentage was calculated as:

$$P = TP V \quad \text{Equation 10}$$

where, P is the porosity percentage (%), TP is the total pore volume (%), V is the volume (m^3).

Recharge per exposed surface area is calculated as:

$$R_{cs} = R_s R_c \quad \text{Equation 11}$$

where, R_{cs} is the recharge per surface area (mm^3/m^2), R_s is the surface area exposed to precipitation/recharge (m^2), R_c is the recharge per day (mm/day).

$$R_{pcs} = \text{If } ((P + R_{cs}) > P, (P + R_{cs}) - P, P) \quad \text{Equation 12}$$

Where, R_{pcs} is the recharge that occur after factoring in the ET_0 and the available pore volume, P is the porosity percentage, R_{cs} is the recharge per surface area.

Following this step, it is calculated if there is excess water to what the layer can accommodate; this will result in a positive number or a nil.

$$\text{If } (R_{pcs} > 0, R_{pcs}, 0) \quad \text{Equation 13}$$

Over flow was calculated as:

$$\text{Overflow} = \text{If } (R_{cs} - R_{pcs} > 0, R_{cs} - R_{pcs}, 0) \quad \text{Equation 14}$$

where the values were given in m^3 .

Table 10 Screenshot from Excel, showing the division of the aquifer into eight layers, and the input data to the left, rain and evapotranspiration

	A	B	C	D	E	F	G	H	I	J
1							Layer 1			
2							Density (g/m ³)			
3	Fractured Sandstone						2,3			
4	percent infil						10			
5	Vol total poros						16			
6	Surface (m ²)						314045			
7	Rain surface (m ²)						314045			
8	Volume (m ³)						31404500			
9	Contour (m)						900			
10	Total pore volume		Rain mm		ETo mm		5 150 338	5 150 338		Runoff
11		1	3,2		1,23	1,97	618 669	618 669	618 669	
12		2	0		1,89	-1,89	-593 545	25 124	25 124	0
13		3	0		1,67	-1,67	-524 455	0	0	0
14		4	0,2		1,26	-1,06	-332 888	0	0	0
15		5	0		1,04	-1,04	-326 607	0	0	0

Table 11 Screenshot from Excel, showing the division of the aquifer into eight layers, and the input data in the left, rain and evapotranspiration and the calculations used to calculate the excess water in the system

	A	B	C	D	E	F	G	H	I
1						Layer 1			
2						Density (g/m ³)			
3	Fractured Sandstone					2,3			
4	percent infil					10			
5	Vol total poros					16,4			
6	Surface (m ²)					314045			
7	Rain surface (m ²)					=F6			
8	Volume (m ³)					31404500			
9	Contour (m)					900			
10	Total pore volume		Rain mm	ETo mm		=F8*F5/100	5150338		Runoff
11		1	3,2	1,23	=C11-D11	=F6*E11	=IF((G10+F11)>F\$10;(G10+F11)-F\$10;G10+F11)	=IF(G11>0;G11;0)	
12		2	0	1,89	=C12-D12	=F6*E12	=IF((G11+F12)>F\$10;MOD((G11+F12);F\$10);IF((G11+F12)<0;0;G11+F12))	=IF(G12>0;G12;0)	=IF((F12-G12)>0;F12-G12;0)
13		3	0	1,67	=C13-D13	=F6*E13	=IF((G12+F13)>F\$10;MOD((G12+F13);F\$10);IF((G12+F13)<0;0;G12+F13))	=IF(G13>0;G13;0)	=IF((F13-G13)>0;F13-G13;0)
14		4	0,2	1,26	=C14-D14	=F6*E14	=IF((G13+F14)>F\$10;MOD((G13+F14);F\$10);IF((G13+F14)<0;0;G13+F14))	=IF(G14>0;G14;0)	=IF((F14-G14)>0;F14-G14;0)
15		5	0	1,04	=C15-D15	=F6*E15	=IF((G14+F15)>F\$10;MOD((G14+F15);F\$10);IF((G14+F15)<0;0;G14+F15))	=IF(G15>0;G15;0)	=IF((F15-G15)>0;F15-G15;0)
16		6	0	1,73	=C16-D16	=F6*E16	=IF((G15+F16)>F\$10;MOD((G15+F16);F\$10);IF((G15+F16)<0;0;G15+F16))	=IF(G16>0;G16;0)	=IF((F16-G16)>0;F16-G16;0)
17		7	0	1,97	=C17-D17	=F6*E17	=IF((G16+F17)>F\$10;MOD((G16+F17);F\$10);IF((G16+F17)<0;0;G16+F17))	=IF(G17>0;G17;0)	=IF((F17-G17)>0;F17-G17;0)
18		8	0	2,32	=C18-D18	=F6*E18	=IF((G17+F18)>F\$10;MOD((G17+F18);F\$10);IF((G17+F18)<0;0;G17+F18))	=IF(G18>0;G18;0)	=IF((F18-G18)>0;F18-G18;0)
19		9	0	1,93	=C19-D19	=F6*E19	=IF((G18+F19)>F\$10;MOD((G18+F19);F\$10);IF((G18+F19)<0;0;G18+F19))	=IF(G19>0;G19;0)	=IF((F19-G19)>0;F19-G19;0)
20		10	0	2,13	=C20-D20	=F6*E20	=IF((G19+F20)>F\$10;MOD((G19+F20);F\$10);IF((G19+F20)<0;0;G19+F20))	=IF(G20>0;G20;0)	=IF((F20-G20)>0;F20-G20;0)
21		11	0	1,78	=C21-D21	=F6*E21	=IF((G20+F21)>F\$10;MOD((G20+F21);F\$10);IF((G20+F21)<0;0;G20+F21))	=IF(G21>0;G21;0)	=IF((F21-G21)>0;F21-G21;0)

3.10 Water storage

Bugan (2008) logged soil samples from both outside and inside the Sandspruit area, and part of the current study area, and found that the surrounding area has similar soils, climate and geology, justifying sampling outside that study boundaries.

3.10.1 Local studies in the past

Past studies have attempted to quantify the specific yield of the aquifers in the greater Berg River basin, with the Sandspruit catchment being divided into two sections. The fractured sections are (see **Table 6**) divided based on their yield potential, respectively 0.1 - 0.5 L/s and 0.5 – 2 L/s (Jovanovic *et al.* 2011b). The study by Jovanovic *et al.* (2011b) also noted the relationship between faulting and high yield and linking the groundwater recharge rate to the topographic elevation. Recharge is a combination of episodic and prolonged rainfall, generally in the winter months, from May to October. Groundwater in the study area were found both confined and unconfined (Demlie *et al.* 2011).

Table 6 shows the groundwater yield of the Sandspruit area, indicating the two observable aquifer yield possibilities. The question remains whether the areas with similar yield are part of a larger system. An alternative could be that the independent isolated fractured systems behave similarly due to similar geology. This study treated the areas with similar yield as a single interconnected system.

The Malmesbury Group hosts, spatially, most of the aquifers (Parsons 1995). With the rocks having an argillaceous nature along with poor groundwater quality, the economic potential is limited (Jovanovic *et al.* 2011b). With these limitations, their role in the environment cannot be understated as they are essential in the local community and maintain local smaller river flows in the area.

The Sandspruit catchment is made up of a fractured aquifer system, found in the TMG, Malmesbury and Cape Granite suites, with the aquifers being defined as low to moderately productive (Jovanovic *et al.* 2011b). Aquifer characteristics are generally uniform in the TMG (Demlie *et al.* 2011). This is due to the isotropic nature of the lithological units found in this group (Demlie *et al.* 2011).

3.10.2 Groundwater

Groundwater can be visualised as a liquid phase that fills the pores and fractures of the regolith. The top of this water body is referred to as the water table. The area between the water table layer and the surface is referred to as the unsaturated or vadose zone. In this unsaturated zone, groundwater moves downward toward the water table, recharging the layer, assuming normal pressure gradients (Bugan R. D., 2014).

Groundwater flow is generally slow – approximately a few centimetres to a couple of meters per day. The water pressure surface and water table depth are known as the hydraulic head. The hydraulic head is the main driving force in groundwater flow. Thus, with a hydraulic head present, the flow will be downward, away from high pressure towards lower pressure; no hydraulic head, no groundwater flow.

3.10.3 Soil

Generally, the soil present in the catchment area exhibits poor development, shallow and hard or weathering rock and brownish sandy loams (Jovanovic *et al.* 2011b). Also present is an abundance of lime, found naturally in the ground; hence the presence of local lime mining operations. Other soils found in the region are red and yellow with low- to medium-base status (Jovanovic *et al.* 2011b). The alluvial cover in the area is characterised as loam and sandy loam soils (Jovanovic *et al.* 2011b).

Drainage in the catchment is greatly hindered by the Malmesbury shales due to its low conductivity along with low to medium swelling clays found in the area (Jovanovic *et al.* 2011b).

3.11 Hydrus model

During the HYDRUS modelling, dual porosity was used to model this hydrological system. The naturally fractured sandstone in the aquifer along with the matrix of the surrounding rock were factored into the model. This dual-porosity approach is expected to result in more accurate results than only factoring in one of these parameters. The choice for this decision is based on the work of Haws *et al.* (2005). During the literature review, it is noted that this approach resulted in improved accuracy during a similar study.

The one-dimensional Hydrus model, version 4.0 was parameterised for the study site and used to predict daily aquifer water content and daily evapotranspiration. Field data were compared to HYDRUS-1D predicted data (a one-dimensional water flux model).

For this study, the Hydrus-1D model was preferred due to the functionality that was required for this study, the availability of the model and the parameterisation that can be done at this scale. The Richardson equation is used to simulate soil water content in the model and an imbedded model by Feddes (1987) to simulate the uptake of water by roots (Šimunek *et al.* 2005). Hydrus-1D expresses water content as water per volume, thus water content is expressed in volumetric units.

HYDRUS-1D is a program designed to simulate one-dimensional movement of water in various porous media. To improve our understanding of the changes brought about by land use changes and their effect on the movement of water, both above and below surface, water simulation models like Hydrus become valuable tools.

Hydrus was parameterised for this project, implementing the same criteria and data used in the Excel model explained above.

3.11.1 Model setup

Richards's equation:

$$\frac{\partial \theta}{\partial t} = \frac{\partial}{\partial x} \left[K \left(\frac{\partial h}{\partial x} + \cos \alpha \right) \right] - s$$

Equation 15

is used for simulating water movement in a partially saturated porous medium, where h is the water pressure head, θ the volumetric water content, t the time, x the spatial coordinate (positive upward), S is the sink term, α is the angle between the flow direction and the vertical axis and K is unsaturated hydraulic conductivity (Šimunek *et al.* 2005).

The water flow equation incorporates a sink term (S) to account for root water uptake. S is defined as the volume of water removed from a unit volume of rock (Šimunek *et al.* 2005).

Allen *et al.* (1998) define ET_0 as the evaporation from a reference surface, not short of water. The only factors affecting ET_0 are climatic conditions and these parameters were captured by local weather stations; therefore, ET_0 can be calculated from meteorological data.

The FAO Penman-Monteith (FAO-PM) method (FAO-ET₀ calculator) was used to calculate the daily ET₀ values by using the long-term meteorological data collected from the Swartberg weather station. The FAO-PM equation (6) was used for daily ET₀ estimation.

$$ET_0 = \frac{\Delta(R_n - G) + \rho_a c_p \frac{(e_s - e_a)}{r_a}}{\Delta + \gamma \left(1 + \frac{r_s}{r_a}\right)}$$

Equation 16

Where R_n is the net radiation, G soil heat flux, (e_s - e_a) represent the vapour pressure deficit of the air, ρ_a is the mean air density at constant pressure, c_p specific heat of the air, Δ the slope of the saturation vapour pressure temperature relationship, γ psychrometric constant, and r_s and r_a are the (bulk) surface and aerodynamic resistances (Allen *et al.* 1998).

To calculate PET from ET₀ the following equation was used:

$$PET = ET_0$$

Equation 17

Where K_{cmax} is a function of weather data and vegetation height (Allen *et al.* 1998). Crop coefficient data was kept at a default value of one.

Hydraulic parameters from soil data (aquifer parameters in this study) collected throughout the study were also imported into the model to predict water flow and root water uptake.

3.12 Specifics of the model setup in HYDRUS-1D

Within the HYDRUS model setup, specific routines were selected for this research. This is indicated as follows:

1. Main processes:
 - a. Water flow
 - b. Root water uptake
2. Geometry information
 - a. Number of materials = 3
 - b. Number of layers for mass balance = 4
 - c. Depth of profile = 800 m (200 m per layer)
3. Time information
 - a. Delay time steps
 - b. Final day = 902
4. Output or print information
 - a. Every 30.5 days
5. Iteration criteria
 - a. Max = 11

- b. Water content tolerance 0.001
- c. Pressure head = 1 m
- 6. Soil hydraulic model
 - a. Dual porosity (Durner, Van Genuchten – Mualem)
 - b. Hysteresis = no
 - c. Water flow parameters (see **Table 12**)
- 7. Water flow boundary conditions
 - a. Upper: Atmospheric BC with Surface layer
 - b. Lower: Constant pressure head
- 8. Root water uptake
 - a. Reduction model: Feddes
 - b. Solute stress model: No Solute stress
- 9. Root water uptake
 - a. Pasture (Weeseling, 1991) (See **Table 13**)
- 10. Time variable boundary conditions:
 - a. Precipitation
 - b. Potential ET
 - c. Minimum allowed pressure head = 0.1 m
 - d. LAI = 1
- 11. Profile summary = 4 times 200m layers

Within the HYDRUS model, specific water flow and rock hydraulic parameters were used and are provided in **Table 12**. These values were used based on the standardised values within the software, where the degrees of freedom are quite limited. **Table 13** provides the values used related to root water uptake. Different from normal soil water modelling, in this research all layers in the model had a surface area, where exposed to the atmosphere, but only the top layer had full exposure to the atmosphere (see **Figure 17**).

*Table 12 Water Flow and rock hydraulic parameters where Θ_r is the residual soil water content, Θ_s the saturated soil water content, **Alfa** the parameter α in the soil water retention function [L⁻¹], **n** the parameter n in the soil water retention function, **Ks** the saturated hydraulic conductivity, K, [LT⁻²], **1** tortuosity parameter in the conductivity function [-], **w2** the parameter w for material M [-]. Relative weighting factor for the sub curve of the second overlapping sub-region, **Alfa2** the parameter a for material M [L⁻¹], for the second overlapping sub-region and **n2** the parameter n for material M [-], for the second overlapping sub-region.*

Θ_r	Θ_s	Alfa	N	Ks	1	W2	Alfa2	N2
0.07	0.45	0.014	1.56	6	0.5	0.5	3	1.5
0.08	0.5	0.014	1.37	3	0.5	0.5	3	1.5
0.09	0.4	0.014	1.3	1	0.5	0.5	3	1.5

*Table 13 Root water uptake where **P0** is the value of the pressure head below which roots start to extract water from the soil, **POpt** the value of the pressure head below which roots extract water at the maximum possible rate, **P2H** the value of the limiting pressure head, below which roots cannot longer extract water at the maximum rate (assuming a potential transpiration rate of **r2H**), **P2L** as above, but for a potential transpiration rate of **r2L**, **P3** the value of the pressure head, below which root water uptake ceases (usually taken at the wilting point), **r2H** the potential transpiration rate [LT^{-1}] (currently set at 0.5 cm/day) and **r2L** the potential transpiration rate [LT^{-1}] (currently set at 0.1 cm/day).*

P0	P2H	P2L	P3	r2H	r2L
-0.1	-2	-8	-80	0.005	0.001

3.1 Conclusion

Field observations made during the study assisted in choosing the correct parameters during modelling. From interviews with multiple farmers it became apparent that the water extracted was used for human consumption, while moving closer to the river, groundwater salinity increased. The local geology also showed that the rocks contain little salts and that regular water recharge due to precipitation washed away many of the salts. This observation, along with the previous statement regarding the water quality, according to the locals, influenced the parameters used in the HYDRUS-1D model.

The question remains whether accurate data could be found in literature. Due to this study's focus on the calculation of the water-carrying capacity of the Kasteelberg Mountain Aquifer. Data such as density and porosity of the local geology were used from literature. Weather data was also collected from a nearby station and not on the mountain itself. This influenced the recharge data to an unknown degree. With the study's focus on modelling the aquifer system and not the accuracy of groundwater available for extraction, this was acceptable for the purpose of this study.

The process followed during this study was that of field data collection, interpretation of that data and supplementing it with data from literature and acquired weather data. GIS was used to determine volume by creating a DEM. The DEM was used as necessary in creating a 3D model of the study area, which resulted in the dimensions of this model being used to determine the volume of the aquifer. GIS was also used for defining boundary limits in **Figure 4** and **15** so as to determine the extent of the study area, creating a watershed model. Boundary conditions included soil, rocks, and vegetation. **Figure 17** shows the extent of the aquifer, and

these limits were used due to known geology, vegetation and no additional water being introduced into the system by means of agriculture. These factors limited the unknowns during modelling, which will be expanded on in the next chapter.

An understanding of porosity in the aquifer was important in determining the parameters necessary to set up the model. These values were obtained from the local mine (SRK, 2007). True water table reactions in the region were measured for correlating the correctness of modelling. The field observations were thus necessary to confirm the accuracy of the model in the following section, which will also be discussed in the conclusion of the study. Modelling parameters were determined in this section to set up the model used in GIS, Hydrus and Excel. These results obtained from these models are discussed in the following section.

Hydrus was selected as the modelling program of choice for this study. The reasons for this decision are that it is Windows-based, free to use and has free tutorials to help to use the program. It has also been used for over two decades and has a focus on water movement, which made it perfect for this study.

Chapter 4 RESULTS AND DISCUSSION

4.1 Introduction

The results pertain to the information generated in QGIS as derivatives from the SRTM elevation data. It also relates to the information gathered from boreholes and borehole loggers. The information was used in Excel modelling of the aquifer responses and lastly used in Hydrus modelling of the aquifer, specific data about the water-holding capacity of the different geological members were provided in the methods and literature section.

4.2 The role of DEM's in the study

QGIS was used to generate a surface map for the study area. After this, a watershed map was created using the DEM. **Figure 17** is the final product where the previous maps were combined to create a map where the surface area of the mountain could be calculated. HYDRUS-1D was used and discussed at the end of this chapter. The aquifer was modelled using only three layers in HYDRUS-1D and eight layers in Excel. This was done due to a modelling error in HYDRUS-1D when using eight layers (see **Table 8**). The map (**Figure 17**) shows that to increase accuracy in Excel, the mountain was divided into 100 m segments – eight in total. For this study, 100 m was chosen due to the steep slope of the mountain and because land cover would be negligible, as shown in **Figure 17**.

The use of borehole data was paramount in observing the water table changes in the catchment area as it was expected to flux during the seasons. As was indicated in the literature study, the mountain aquifer and the adjacent groundwater aquifer are linked and therefore should be sensitive to changes in the mountain aquifer. The elevation of the boreholes with the occurrence of water depth is indicated in **Table 14**.

Borehole data was collected using level loggers and can be found in the addendum of this study. Some of the boreholes monitored during this study can be seen in **Figure 18** and **19**. Data from the Water Council and the PPC cement mine were also used in this study.

Table 14 The regional water table is shown with measurements at the start of the rainy season and at the end of the rainy season. The last two columns are calculated by subtracting the measured water level in the borehole from the Z value, height of the borehole, as indicated on the DEM, shown in **Figure 15**. **Table 14** shows the results of the regional water table before and after the main rainfall period for 2015.

Z (m) hasl	Water table depth 2015 (m)		
	Name of borehole location	April	September
268.5	Groenrivier	3.0	3.0
245.9	Klawervlei	2.3	1.7
235.6	Vlakkerug	17.9	17.7
158.0	Goedertrou - reeds	2.9	3.0
163.7	Goedertrou - field	14.4	15.0
244.1	Allesverloren	1.3	1.1
264.0	Wood	13.3	16.6
256.3	School	13.0	10.1
239.9	Site 1	23.5	26.3
209.9	Site 2	12.0	12.2
204.7	Site 3	4.8	5.3
216.5	Site 4	4.41	4.5

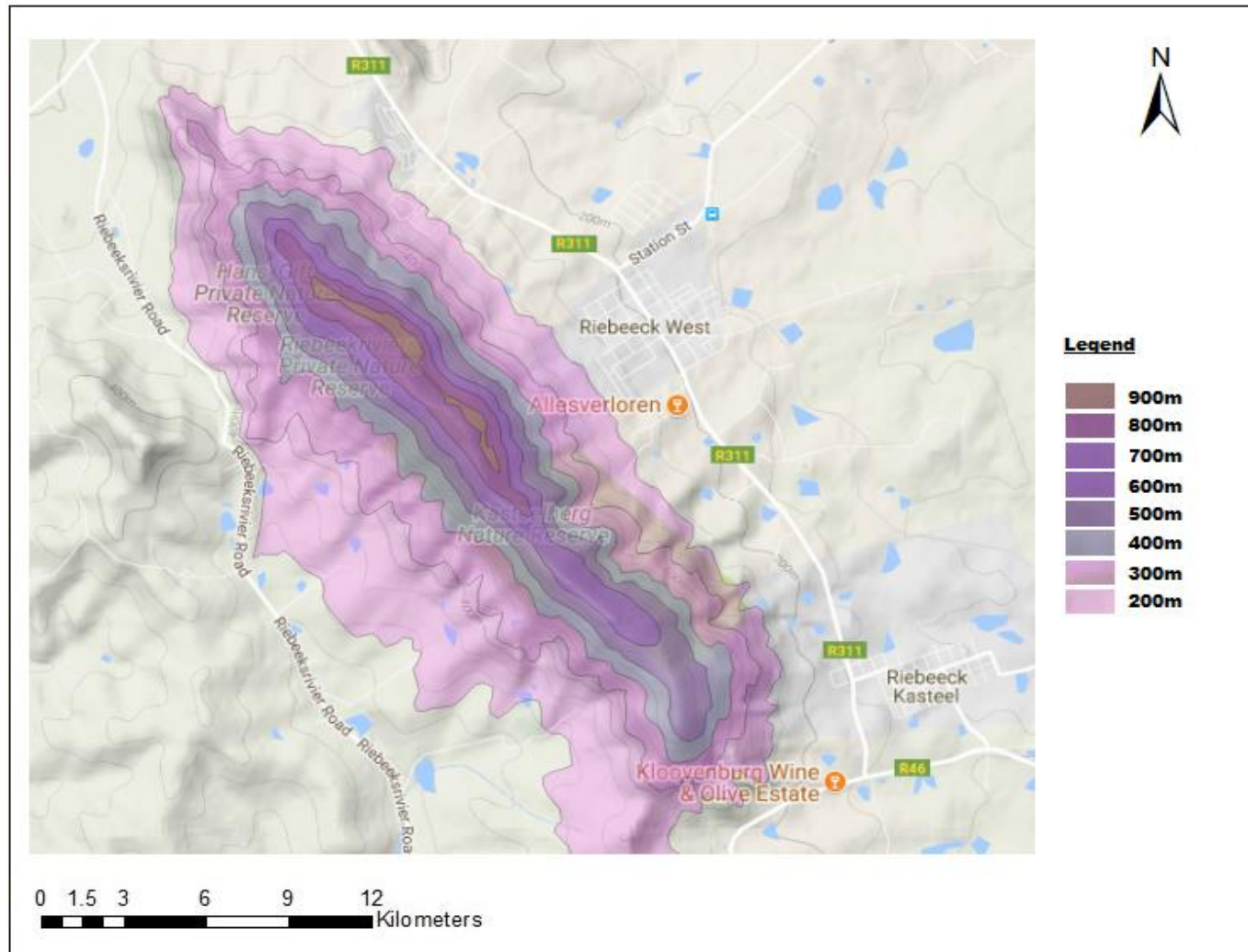


Figure 17 Surface of the Kasteelberg Mountain Aquifer, showing elevation starting at 200 m with 100 m increments

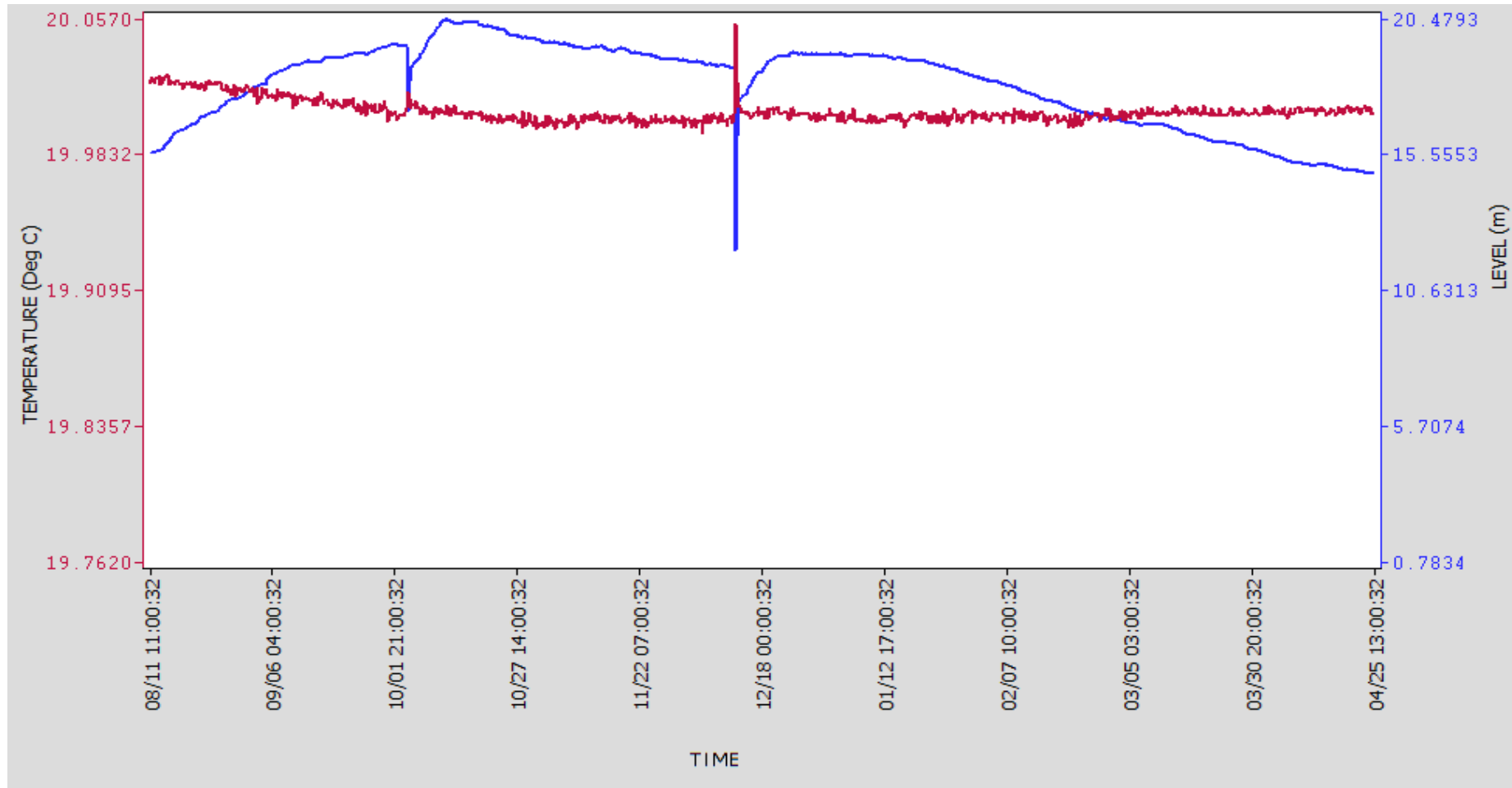


Figure 18 BH1 (Foot slope) – Water level from 11 August 2015 to 25 April 2016, this is indicated by the red line. The blue line indicates temperature during this time (generated by Solinst software).

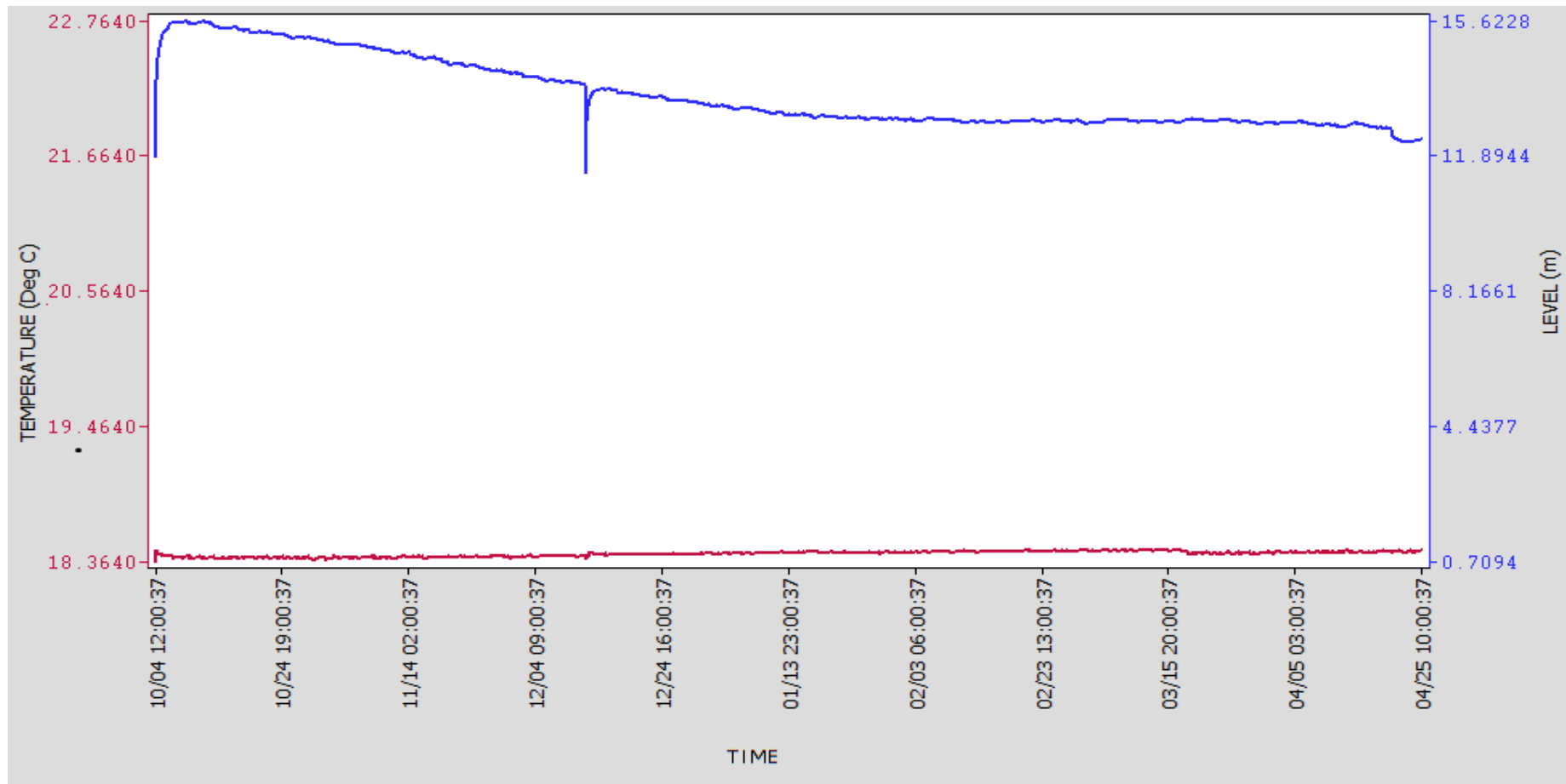


Figure 19 BH2 (Mid slope) – Water level from 4 October to 25 April 2017, left to right, this is indicated by the red line. The blue line indicates temperature during this time.

4.3 Climate and borehole response data

The use of weather stations in the near vicinity to study the meteorological conditions prevalent in the study area was also a priority.

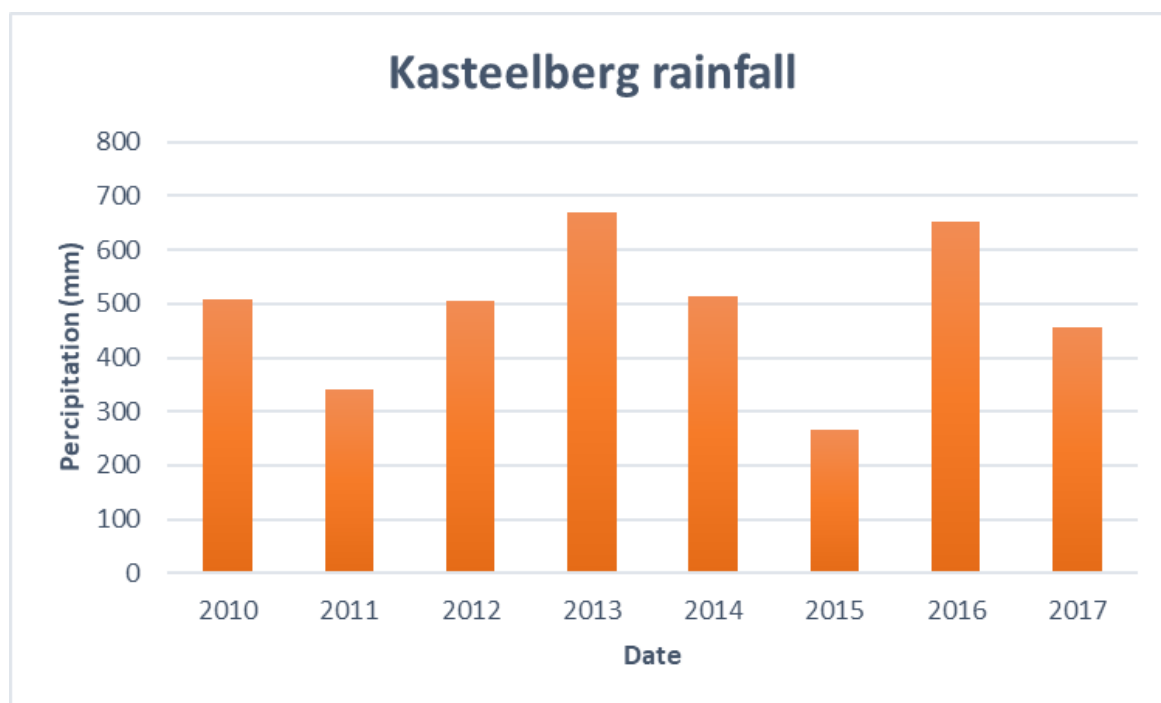


Figure 20 Rainfall in the study area, 2010 to 2017 (Hortec, 2018)

Figure 20 shows the precipitation data acquired from Hortec for the years 2010 to 2017. The years 2011 and 2015 experienced less precipitation than the years 2010 and 2014. This may be due to the El-Niño effect. Data used to populate **Figure 25** and **26** can be viewed in the addendum.

The result in **Figure 21** shows the groundwater response during the seasons when compared with rainfall in **Figure 23**. Borehole 1 (BH1) is situated closest to the Kasteelberg Mountain. Borehole 3 (BH3) is located further away from the mountain. Borehole 2 (BH2) was also located further away from the mountain, but is also nearest to the local open-pit mine. **Figure 24** also shows five noticeable response events. Three “high” points where the water level was relatively high can be observed on the far left, middle and far right of the figure. Two points where the water level decreased can be observed at 11th of the month in 2013 and 12th of the month in 2014.

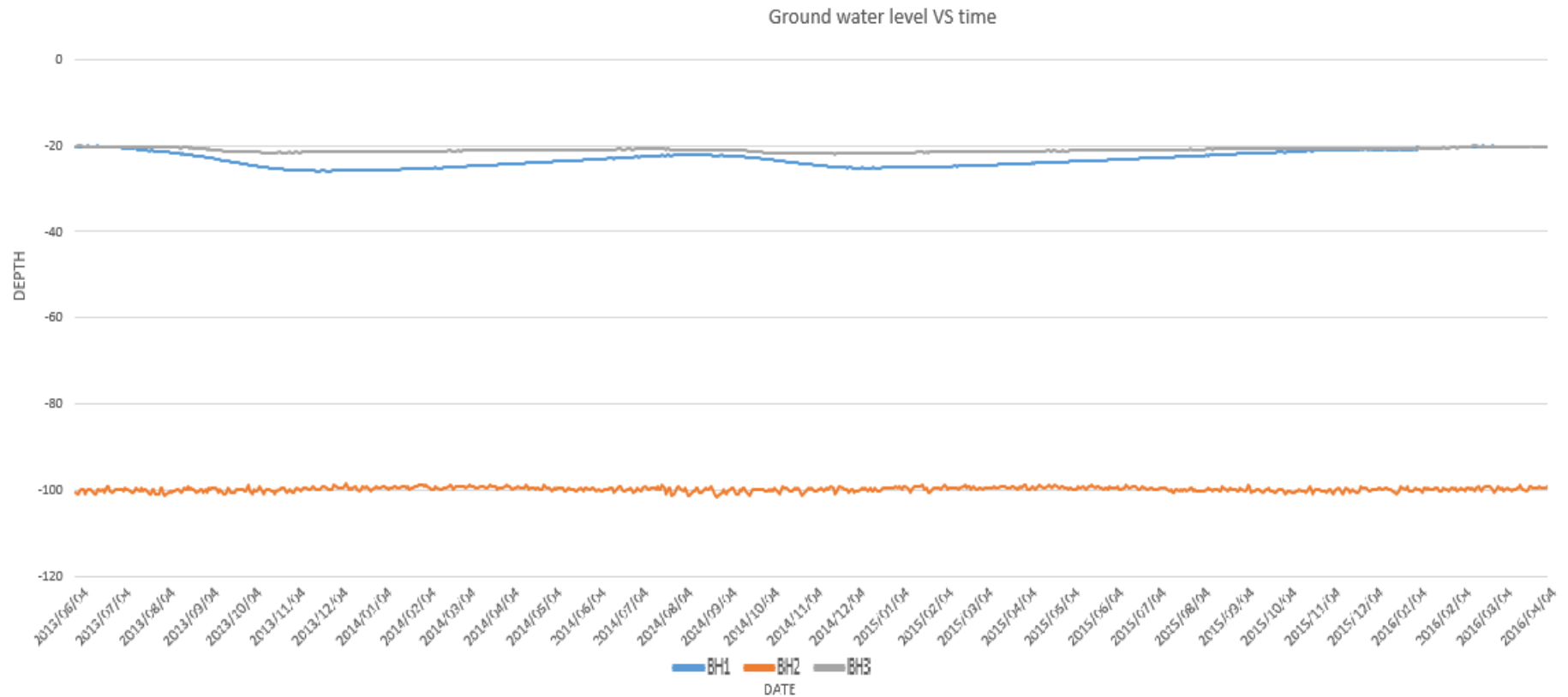


Figure 21 Ground water levels in the boreholes, BH1 is located closest to the Kasteelberg Mountain, with BH2 and BH3 both located further east, but BH2 being near a local open mine (data from 4 June 2013 to 4 April 2016)

The rainfall data used in **Figure 21** are used in calculations with the results shown in **Figure 23** and **24**. In **Figure 22** the periods from day 100 to 281 and days 491 to 701 represent the summer months, and the three spikes during day 1 to 100, 281 to 491 and 701 to 876 represent the winter months or winter rain season. This is linked to the HYDRUS-1D modelling results seen in **Figure 25** and **26**. The results show correlation between precipitation and surface runoff. It is interesting to note that the precipitation between day 701 and 876 is not significant enough to show a response in the HYDRUS-1D model. Arrows are also used in **Figure 23** to indicate the periods with no to limited precipitation. This data set will later be used to assess the accuracy of the HYDRUS-1D model, in **Figure 25** and **26**.

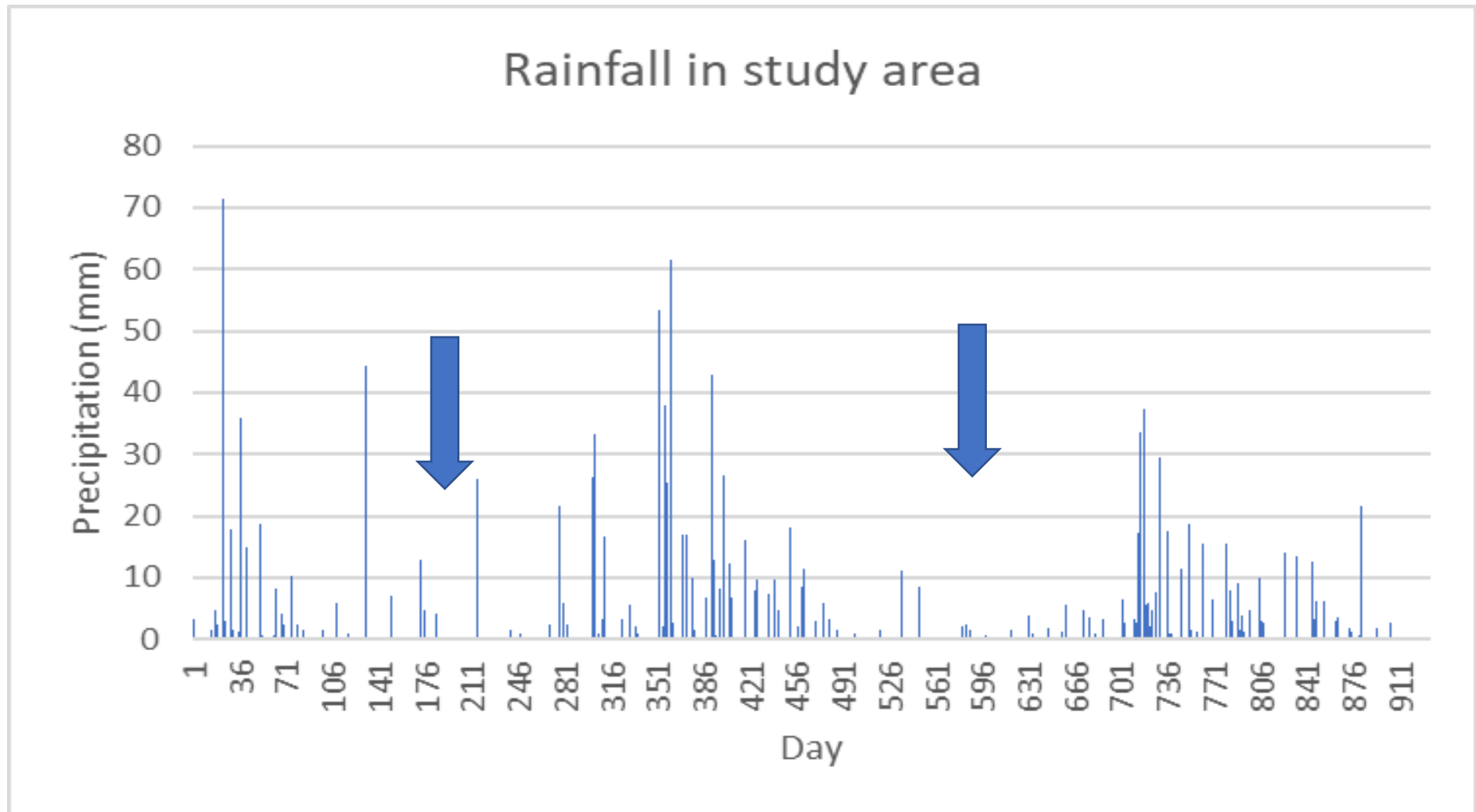


Figure 22 Weekly rainfall in the study area, used in HYDRUS-1D modelling. Day 1 is 25 June 2015 to 22 December 2017; high precipitation is indicative of winter due to predominant winter rainfall in the study are (Hortec, 2018).

In **Figure 24**, the available weather and borehole data that overlap are combined to illustrate the borehole response. From the figure it can be derived that the groundwater level “rises” during months with high precipitation. This is however not the case at the end of the rainy season in the year of 2014. It is unclear why this occurred. A possible explanation could be that the weather station was adjacent to the mountain and not on top of the Kasteelberg Mountain. As the mountain received higher rainfall than the surrounding, it could be postulated that this might have contributed to the observed discrepancy.

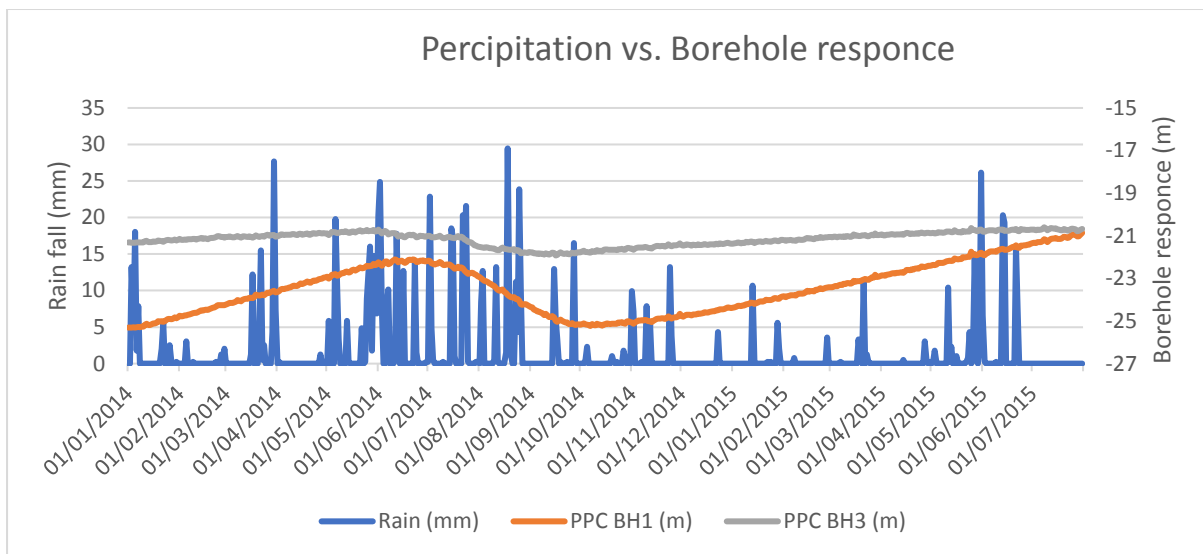


Figure 23 Daily precipitation and borehole water level

In an attempt to better understand the correlation and abovementioned discrepancy, both the precipitation and water level fluxes were averaged in **Table 15**. As observed, the mentioned discrepancy occurred during the end of the eighth month of 2014. From **Table 15**, the total precipitation for a month can be observed along the averaged borehole response. From this perspective, the total precipitation is seen to correlate with the borehole responses, with a clear drop after the eighth month. This indicates a near instantaneous response to precipitation in the Kasteelberg Mountain Aquifer.

Table 15 Total monthly precipitation and average water level responses

Year	Rain (mm)	BH1 (m)	BH3 (m)
01/01/2014	57.14	-25.32	-21.32
01/02/2014	6.85	-24.5357	-21.1294
01/03/2014	76.21	-23.9223	-21.032
01/04/2014	1.52	-23.2951	-20.9307
01/05/2014	127.24	-22.6597	-20.8175
01/06/2014	126.24	-22.2132	-20.9397
01/07/2014	123.94	-22.4647	-21.1293
01/08/2014	125.73	-23.607	-21.6407
01/09/2014	39.61	-24.8231	-21.8295
01/10/2014	6.86	-25.137	-21.6898
01/11/2014	47.49	-24.9384	-21.5197
01/12/2014	4.57	-24.5936	-21.4034
01/01/2015	18.79	-24.1378	-21.2902
01/02/2015	4.32	-23.6617	-21.1544
01/03/2015	16.76	-23.1711	-21.0109
01/04/2015	4.06	-22.6612	-20.9146
01/05/2015	66.29	-22.1191	-20.8087
01/06/2015	70.34	-21.6818	-20.746

4.4 Implications of the Excel model

During the modelling process in HYDRUS-1D, the program experienced problems with the huge database partly due to separating the Kasteelberg Mountain into eight segments of 100 m each, as shown in **Table 16**. This was solved by using the values calculated by the three layers, as indicated in **Table 9**.

Table 17 mention surface area and effective surface area. The volume was calculated using **Figure 27**. By using **Figure 12**, a DEM of the study area and **Figure 27**, the aquifer was divided into eight layers. The surface area refers to the total area of the layers. This surface area was only used for the first layer that had no overlaying layers and thus impacting direct recharge by precipitation. Effective precipitation refers to the area with “direct” access to recharge, independent of overlaying layers. **Figure 17** illustrates this surface area using a blue line.

With the aquifer being split into three layers instead of eight (see full description in methodology), the straight blue lines show the surface area that was used (**Figure 17b** and **17c**) to calculate the effective surface. The amount of excess water in the aquifer system available for extraction, averaging as $2,8 \times 10^9 \text{ m}^3$ per year was calculated in Excel, adding up the overflow for a full year.

Table 16 Summary of the eight layers used in the Excel calculations, Table 11

Layer	Volume m³	Total Porosity m³	Surface Area m²	Effective Surface Area m²
1	31404500	5,150,338	314045	314045
2	161963101	26,561,949	1619631	1305586
3	354701600	58,171,062	3547016	2241430
4	640765200	105,085,493	6407652	4166222
5	958348800	157,169,203	9583488	5417266
6	1551866200	254,506,057	15518662	10101396
7	2753296000	451,540,544	27532960	17431564
8	6517164200	1,068,814,929	65171642	47740078

Table 16 was constructed along with values obtained from the GIS model, with the mountain being divided into eight layers (based on **Figure 18**) by elevation. The GIS model gave the total volume of the mountain and with the contour map (see **Figure 18**) overlain on the DEM (see **Figure 15**) it was possible to horizontally divide the mountain into these 100 m layers and use these parameters when constructing the cascade model in Excel.

Table 17 Altered division of the Excel summary used in HYDRUS-1D modelling

Layer	Volume m ³	Total Porosity m ³	Surface Area m ²	Effective Surface Area m ²
1	354701600	89883349	5480692	3547016
2	1197164600	516760753	31509802	11971646
3	4965298000	1520355473	65171642	49652980

4.5 The Hydrus model and the Excel model in comparison

With HYDRUS, it was important to use the correct hydrogeological parameters and understand the factors that impact on these parameters. This is often an arduous task to achieve due to the sheer number of options in the model.

The modelling strategy rested on porosity and preferential flows through fractures, where preference was also provided for the simulation of water in the aquifer through preferential flows. The results generated in HUDRUS-1D are presented in **Figure 24** and **25**. The potential surface flux shows multiple negative peaks pointing to the driest periods in the data, with the potential surface flux being stable during the rainy season. Actual surface flux shows the fluxes more accurately than the potential flux. If viewed along with **Figure 24** and **Figure 25**, the smaller-scale dry and wet increments are also depicted; thus the multiple smaller peaks. Between days 650 and 700, the peak perfectly corresponds to the measured rainfall. Surface run-off, if viewed alongside **Figure 25**, shows that the slow pace of recharge and the saturation point held over time also perfectly corresponds with this prediction. The peaks in **Figure 24** correspond with the point after the rain season when the maximum water table was not yet reached, due to relatively slow recharge. After this point, the water table is maintained for roughly 90 days before the groundwater starts to subside.

The HYDRUS-1D model and its results are thus an accurate representation of the true events, as compared to real-world data. It is noteworthy that the peaks in HYDRUS-1D are not as accurate when it came to illustrating the steep slope in **Figure 24**. The HYDRYS-1D model shows peaks to be mostly symmetrical, yet the data show a steep slope during the dry seasons (see **Figure 24**). Field data also show a slow recharge rate, not depicted in the HYDRUS-1D model.

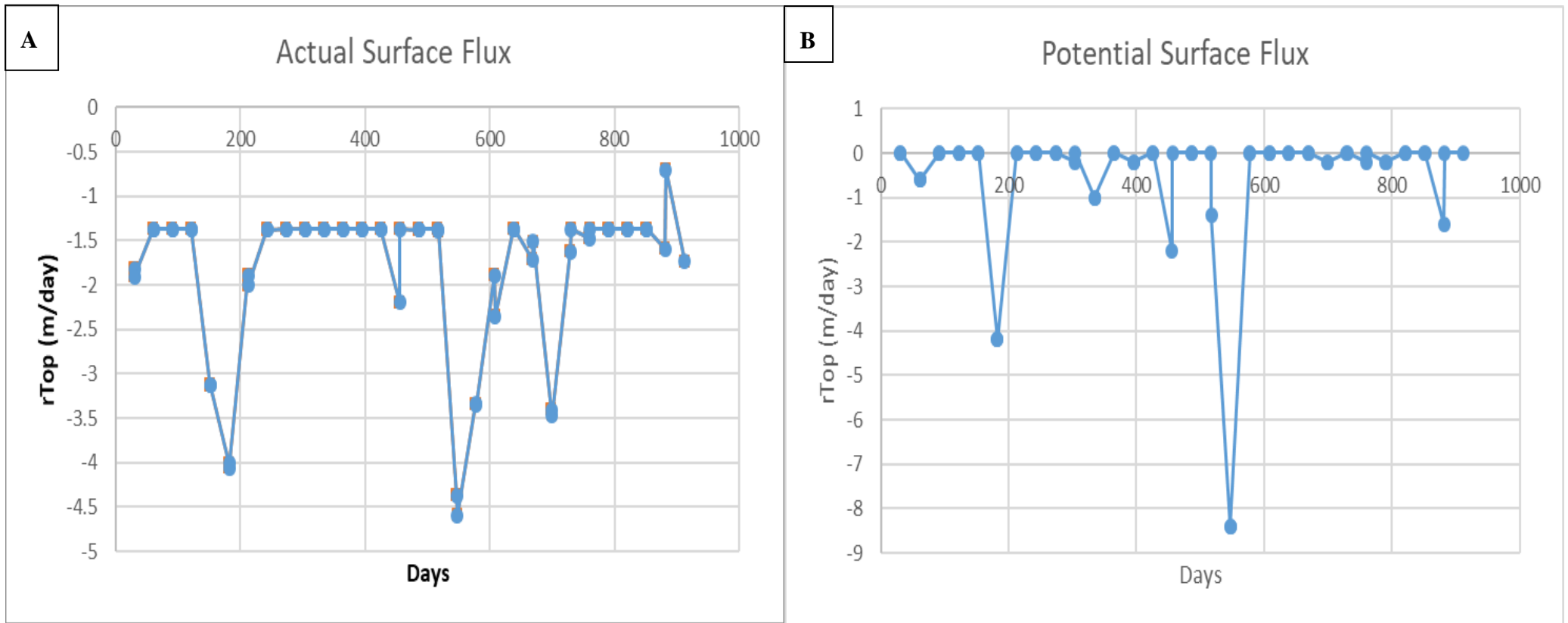


Figure 24 HYDRUS-1D results, A) Actual Surface Flux, B) Potential Surface Flux

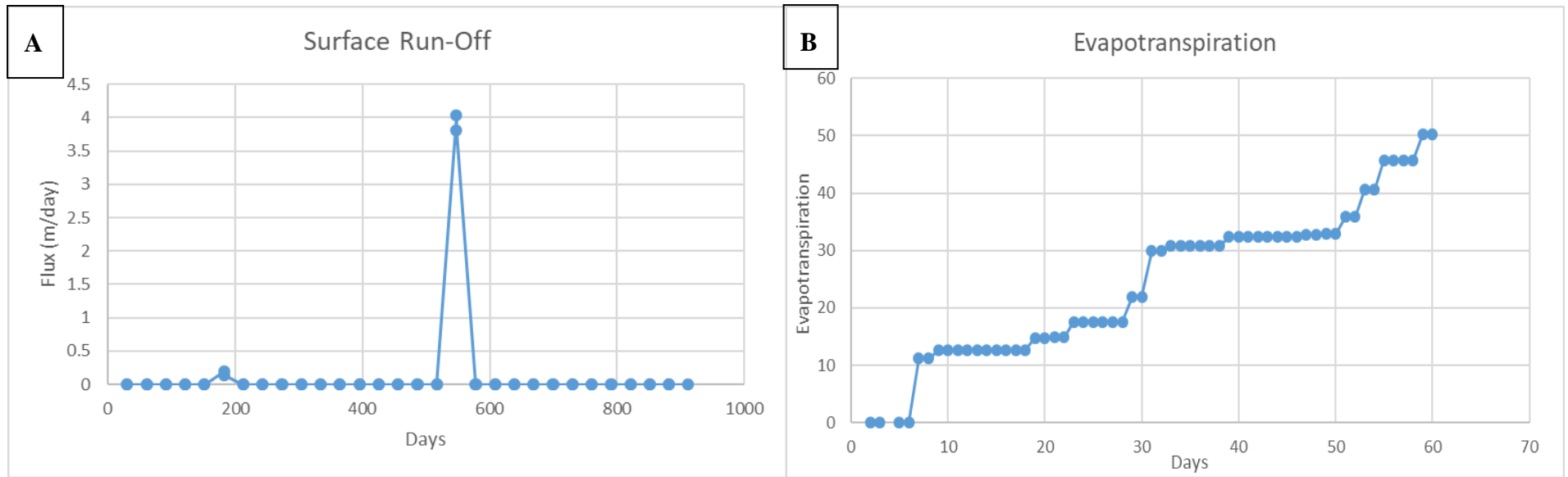


Figure 25 HYDRUS-1D model results, A) Surface Run-Off, B) Cumulative Evaporation graph

4.6 Conclusion

From the result section the indication is clear that the boreholes do respond to precipitation as hypothesised. It should be noted that conflicting to this are the boreholes between the local mine and the Kasteelberg Mountain. BH2 shows a very high frequency with regard to flux, with BH1 showing the strongest response to the precipitation during the winter months and BH3 mirroring BH1, but with lower flux, adding to the argument of the Kasteelberg Mountain Aquifer being a major source of groundwater in the area. It is also interesting to note the sudden “dip” in groundwater before the rainy seasons. This is due to the recharge occurring at a significantly slower rate.

Figure 19 & 20 showed how the BH1 and BH2 responded to precipitation. BH1 and BH2 in **Figure 19 & 20** are explained in **Table 15**. It is shown for the period 11 August 2015 to 25 April 2016 and 4 October 2016 to 25 April 2017, how BH2 at the foot slope responded to rain and BH1 for the same period did not.

Figure 22 can also be viewed with the HYDRUS-1D result in that dual porosity was used in the modelling to imitate the true environment of the aquifer. It is reasonable to believe that the mountain would consist of numerous fractures and cracks along its extremities, but that weathering had not penetrated the core of the mountain. The core being less porous would fill slower and possibly from the bottom up, where the fractures and cracks would fill at a much higher rate. This was one of the observations made, but no core sample was available to verify this idea.

Figure 22 indicates that during the rainy season, the BH2 borehole in this part of the study area was not visibly recharged. This may, however, not be a realistic reflection of the truth. The local mine pumps water from its pit to not have the open-cast pit flooded. This may keep the water table relatively stable and not reflect the true effect of the recharge.

It may also be attributed to the geology into which the boreholes are drilled, with the boreholes being drilled into non-porous material thus not reflecting recharge. This may be investigated in future studies where chemical analysis is done to determine the age and possible origin of the groundwater.

Chapter 5 CONCLUSION

Prospects for new dams and redesigning the current dams are approaching practical limitations and is placing South Africa in a position where storage capacity is diminishing and does not adequately guarantee sustainable reserves, which subsequently compromises national water supply security. With this said, the need for this research was conceptualised to supplement similar studies being conducted with similar outcomes.

The Kasteelberg Mountain, part of the Table Mountain Group (TMG), is a regionally fractured and predominantly sandstone aquifer. This study showed the potential of utilizing it as a source for bulk water supply in the local municipality to augment local demands in both the agricultural and residential sectors by use of the cascade model and the HYDRUS-1D model. From this perspective, the total precipitation is seen to correlate with the borehole responses, with a clear drop after the eighth month. This indicates a near instantaneous response to precipitation in the Kasteelberg Mountain Aquifer.

The first studies relating to water systems in the Sandspruit were undertaken by Vermeulen (2010) and Bugar (2014). The first study by Vermeulen (2010) in part studied the water loss due to changes in vegetation. Another study by Bugar (2014) saw the assessment of dryland salinity in the Sandspruit and methods to combat salinity. With these studies completed and Wasserfall (2013) and Vermeulen (2010) investigating the surrounding area, the first investigation of Kasteelberg Mountain as a water source could begin. This study now contributes to the greater study to ultimately determine the viability of mountain aquifers being used by the City of Cape Town.

The perched water table was directly monitored during this study. Field data collected over a period of 30 months (25 June 2015 to 22 December 2017), which represents different agrometeorological conditions in both the wet and dry periods, were also collated to supplement water levels in the observed boreholes. The water table showed a response to the precipitation and those mostly stable during both the dry and wet seasons were close to mining operations. This may however not be a realistic or natural reflection. The local mine extracts water from its pit to not have its open-cast pit flooded. The mine pumps the excess water to holding dams between itself and the Kasteelberg Mountain. Local farmers use it for irrigation. Thus, seepage from the holding dams and the seepage from the irrigation see the reintroduction

of the water and might be the reason boreholes in this area show minimum response. This may keep the perched water table relatively stable and not reflect the true effect of the recharge.

The De Gift borehole showed the highest rate of response and recharge. This might be since this borehole is the closest to the mountain, or other geological factors might be responsible. Interaction between the aquifer and the surrounding study area could not definitively be proven. This was due to limited geological data available for the study area. A more detailed geological study will be needed to clearly identify boundaries between the different aquifer systems. This will also be advantageous in characterising the properties of the respective aquifer systems.

The study was also conducted during some of the driest seasons in a century: 2011 and 2015. Measuring boreholes during this time, did not always produce a clear link between climate data and observation in the boreholes. However, with the major rain events that occurred, a correlation could be made between rain and borehole responses.

The rainfall data used in these calculations show that during the periods from days 100 to 281 and days 491 to 701 represent the summer months, and the three spikes during days 1 to 100, 281 to 491 and 701 to 876 represent the winter months or winter rain season. This is linked to the HYDRUS-1D modelling results. The results show correlation between precipitation and surface run-off. It is interesting to note that the precipitation between day 701 and 876 is not significant enough to show a response in the HYDRUS-1D model. This might be due to parameters that are not sensitive enough to pick up this less significant spike in the data. It should be noted that if this study should be used to include the study of salinity, such as was done by Bugan (2014), the HYDRUS-1D dual-porosity methods should be replaced with a model capable of simulating solute transport. It was not under investigation in this study, but the limitation of this method should be noted as observed in Haws *et al.* (2005).

The interconnectedness of fractured aquifer systems requires extensive knowledge about their ability to “communicate”. The interconnectedness is thus hard to prove and results in isolated aquifer systems or isolated fractures. The study focused on the theoretical capacity of the Kasteelberg Mountain Aquifer, regional recharge potential and changes in groundwater. The most significant changes observed in the water level occurred in boreholes with the closest proximity to the Kasteelberg Mountain. Bugan (2008) logged soil samples outside the Sandspruit area and on part of the current study area of this study and found that the surrounding area has similar soils, climate and geology, justifying sampling outside those study

boundaries. Results from his study showed variations (on annual scale) to be negligible regarding soil characteristics with regard to water storage. The responses from the two sporadic springs monitored, proved fruitful in understanding the fracture system and the calibration of the models.

The 30 m SRTM DEM was obtained from NASA Earth Explorer. A resolution of 30 m may result in biased volume calculations for the Kasteelberg Mountain Aquifer, which may cause an overestimation or underestimation during volume calculations. This will be an important consideration if the aquifer is to be utilised in the future. Due to this study exploring the methods for calculating the water potential for the aquifer, the 30 m SRTM was sufficient for a rough estimate. The rough estimate of $2,8 \times 10^9 \text{ m}^3$ per year is both dependent on the precipitation and the parameters that were used in the modelling process.

The cascade model executed in Excel was central in calculating the estimated $2,8 \times 10^9 \text{ m}^3$ extractable water per year from the aquifer. From the GIS data, both obtained and created in this study, a clear understanding of the water-carrying capacity could be postulated. From this model the study was able to establish the surface area exposed to recharge and accordingly the recharge after factoring in the evapotranspiration. The subdivision of the aquifer into eight equal (only equal in thickness) units resulted in more accurate results than using only three layers in the HYDRUS-1D model, but lacked the response sensitivity needed in a dual-porosity system. To improve the results, the eight “layers” could be increased to accommodate even finer discrepancies in the surface of the mountain, such as valleys and crests. From the cascade model, the eight units were also modelled as lithologically homogeneous. From the geological maps of Verwoerd *et al.* (1974) and SRK (2007), this was a reasonable assumption to make during the testing of this model.

The HYDRUS 1D results, however brief, shows two peaks on the surface runoff that coincide with observed sporadic stream flow events (days 184 and 587) from the south-western slope of the mountain – a good indication of the accuracy of the HYDRUS-1D model when correctly parameterised by accurate data.

Borehole responses may also be attributed to the specific geology in the region of the boreholes, with the boreholes being drilled into non-porous material, thus not reflecting recharge adequately. This may be investigated in future studies where chemical analysis is done to determine the age and possible origin of the groundwater in the observed boreholes.

Reviewing the hypothesis, aim and objective, the following was achieved in this study:

- A rough estimation was obtained with regard to the Kasteelberg Mountain's volume and lithology.
- Water storage potential was calculated.
- The next step was monitoring the water responses across multiple years, to measure the water table responses to natural and anthropogenic events, with the possible stabilising effect of the mine.
- Field data confirmed the hypothesis with regard to the water table being influenced by the seasons.
- The study roughly measured the volume of water flow in the aquifer based on recharge, evapotranspiration and porosity.
- The study measured the amount of excess water in the aquifer system available for extraction, averaging $2,8 \times 10^9 \text{ m}^3$ per year.
- Additionally, a HYDRUS-1D model was also created to present the knowledge gained and calculate additional data with regard to groundwater flow and at what point rivers would respond, by starting to flow that would mark the saturation of the aquifer.

South Africa is facing a slow-onset disaster with regard to pollution of the environment and natural resources (Barnes 2015), as seen in the past three years in the Western Cape.

With the completion of this research project it is the hope of the author that the study will be used by local government to assist in water management planning in the area, with local municipalities and academics furthering the study to assist in managing an ecologically responsible and sustainable water resource in the municipality. The usage of this aquifer for local agriculture and households, will greatly assist in relieving strain on the larger Cape Town Metropole.

5.1.1 Recommendations for future research

Due to limited hydrogeological data regarding the core of the mountain, values from studies in the vicinity were used in calculations. In the future, test samples should be collected to verify the density and porosity of the sandstone through the entire mountain. It may justify this study for treating the mountain as a homogeneous sandstone aquifer or result in additional information generated to put these results in perspective.

The study treats the system as a closed system. To a degree this holds true, but the study assumed that the aquifer consisted at zero stored water during the calculations. If the permanent water table values can be obtained, the results of this study will also improve.

The speed (precipitation and evapotranspiration were averaged) at which the aquifer filled was unexpected. Yet future studies now have a starting point from a known water storage point to

increase the accuracy of future studies. Dual porosity that was used during modelling (the HYDRUS-1D model used dual porosity) to treat the mountain with a fractured “crust” and solid centre, resulted in two recharge paths and two different rates of recharge. This theory was discussed in Chapter 4, but requires more investigation to be proved or refuted.

To further increase accuracy, the water from local dams (on farms) could also be factored in when calculating the available water in the aquifer. Some of the water used also returns to the system during agricultural practices, leaking pipes and leaking dams.

In a follow-up study, the modelling should be done with a regionalised hydrological model, using the true rainfall distribution over the mountain. This will require rainfall distribution modelling to be done first.

The local mine also pumps water from its pit into dams used by local farmers. This practice should also be studied due to the artificial recharge and recycling of the water in the system.

An interesting part of the geology was that the results showed that the mountain aquifer and the lower slopes could possibly be disconnected hydrologically. This is due to the differences in response to precipitation and evapotranspiration. A chemical analysis and structural investigation may explain these discrepancies. It is also mentioned in Chapter 2 that the mine pumps water from their excavated area to prevent flooding, thus keeping the water table relatively stable. It was also discussed in Chapter 4 that the groundwater chemistry changes as one moves further away from the mountain. It may also be attributed to the geology into which the boreholes were sunk. However, De Clercq *et al.* (2010) indicated the relationship between rainfall distribution and the electrical conductivity of groundwater. There is still a need to investigate in future studies the age and possible origin of the groundwater.

Calculating the water requirement of the local ecosystems would be beneficial for future ecological diversity studies; in other words, determining the minimum amount of water needed to sustain the local ecosystems. This will enable responsible water extraction by the local community and other possible interested parties.

SRTM 30 m resolution images were used in the DEM and volume calculations. In future studies, 5 m resolution images would be advised to improve volume calculations. This will increase the DEM resolution and subsequently the area calculations used to derive the volume during Excel calculations.

Invasive plant species also reduce the water budget and need to be cleared from the ecosystem. This has been shown to release water back into the water cycle. Current initiatives by the WFWP (Working for Water Programme) and mostly farmers include an alien-clearing effort.

References

- Allen, R., Pereira, L., Raes, D., & Smith, M. (1998). *Crop evapotranspiration: guidelines for computing crop requirements*. Rome, Italy: FAO Irrigation and Drainage Paper No. 56.
- Anchor Environmental, & Freshwater Consulting Group. (2007). *Berg River baseline monitoring programme. Final report*. DWA Report. Pretoris: Department of Water Affairs and Forestry. doi:P WMA 19/G10/00/2107
- Arnold, J. G., Williams, J. R., Srinivasen, R., & King, K. W. (1999). *SWAT: Soil and Water Assessment Tool, Model Documentation*. USDA, Texas.
- Barnes, J. M. (2015). Marine Outfall Sewers Discharging into Table Bay. *Camps Bay Ratepayers & Residents Association*. Cape Town. Retrieved 8 7, 2015
- Belcher, R. W. (2003). *Tectonostratigraphic Evolution of the Swartland Region and Aspects of Orogenic Lode-Gold Mineralisation in the Pan-African Saldania Belt, Western Cape, South Africa*. PhD: Stellenbosch .
- Boston University. (2015). *Terrestrial Lidar Scanning Research*. Retrieved 04 10, 2015, from <http://sites.bu.edu/lidar/>
- Broquet, C. A. (1992). The sedimentary record of the Cape Super group: A review. In M. De Wit, & I. Ransome (Eds.), *Inversion Tectonics of the Cape Fold Belt Karoo and Cretaceous Basins of Southern Africa*. (pp. 159-183). Rotterdam: Balkena.
- Bugan, R. D. (2014). Modeling and regulating Hydrosalinity dynamics in the Sandspruit River catchment, Western Cape. Stellenbosch: University of Stellenbosch.
- Bugan, R. D. (2014). *Modeling and regulating hydrosalinity dynamics in the Sandspruit river cathment (Westen Cape)*. Stellenbosch: Stellenbosch University.
- Bugan, R. D., Jovanovic, N. Z., & De Clercq, W. P. (2012). The water balance of a seasonal stream in the semi-arid Western Cape (South Africa). *Water SA*, 38(ISSN 1816-7950).
- Cleaver, G., Brown, L. R., Brendenkamp, G. J., Smart, M. C., & Rauternbach, C. J. (2003). *Assessment of environmental impacts of groundwater abstraction from Table Mountain Group (TMG) aquifers on ecosystems in the Kammanassie nature reserve and environs*. WRC. Pretoria: Water Research Commission. doi:ISBN: 1 77005 034 5
- Coetzee, H. (1995). Radioactivity and the Leakage of Radioactive Waste Associated with Witwatersrand Gold and Uranium Mining. In B. J. Merkel, S. Hurst, E. P. Lohnert, & W. Struckmeier (Eds.), *Proceedings Uranium Mining and Hydrogeology*. Freiberg, Germany. doi:ISBN 3-87361-256-9
- Coetzee, H., Venter, J., & Ntsume, G. (2005). *Contamination of Wetlands by Witwatersrand Gold Mines – Processes and the Economic Potential of Gold in Wetlands*. Pretoria: Council for Geosciences. doi:Report No 5005-0106
- Coetzee, H., Wade, P., & Winde, F. (2002b). Reliance on Existing Wetlands for Pollution Control Around the Witwatersrand Gold Uranium Mines in South Africa - Are They Sufficient? In B. J. Merkel, B. Planer-Friederich, & C. Wolkersdorfer (Eds.), *Uranium in the Aquatic Environment* (pp. 59-65). Berlin: Springer.

- Coetzee, H., Wade, P., Ntsume, G., & Jordaan, W. (2002a). *Radioactivity Study on Sediments in a Dam in the Wonderfonteinsspruit Catchment*. Department of Water Affairs and Forestry. DWAF Report.
- Coetzee, H., Winde, F., & Wade, P. W. (2006). *An Assessment of Sources, Pathways, Mechanisms and Risks of Current and Potential Future Pollution of Water and Sediments in Gold-Mining Areas of the Wonderfonteinsspruit Catchment*. Water Research Commission, WRC. doi:Report No 1214/1/06
- Conrad, J., Nel, J., & Wentzel, J. (2004). The challenges and implications of assessing groundwater recharge: A case study – northern Sandveld, Western Cape, South Africa. *Water SA*, 30(5 Special edition, ISSN 0378-4738), 75-81.
- Cook, P. G., & Kilty, S. (1992). A helicopter borne electromagnetic survey to delineate groundwater recharge rates. *Water Resources Research*.
- Cowan, K. (2017). *Timeslive, The great thirst: water crisis paralyzes rural towns*. Retrieved from <https://www.timeslive.co.za/news/south-africa/2017-11-13-the-great-thirst-water-crisis-paralyses-rural-towns/>
- Dalvie, M. A., Cairncross, E., Solomon, A., & London, L. (2003). *Contamination of rural surface and ground water by endosulfan in farming areas of the Western Cape, South Africa*. Environmental Health.
- De Clercq, W. (2015). Land use impacts vs sustainability: Are we the first to apply minimum tillage. George, South Africa: SSSSA conference.
- De Clercq, W. P., Jovanovic, N. Z., & Fey, M. V. (2010). *Land use impacts on salinity in Berg River water*. Water Research Commission, Pretoria. doi:Report No K5/1503
- De Clercq, W. P., Jovanovic, N., Bugar, R., Mashimbye, E., De Toit, T., Van Niekerk, A., . . . Flugel, W. A. (2013). *Management of human-induced salinisation in the Berg River catchment and development of criteria for regulating agricultural land use in terms of salt generating capacity*. Water Research Commission. WRC Report No. 1849/1/13. doi:ISBN 978-1-4312-0402-1
- De Villiers, S. (2007). The deteriorating nutrient status of the Berg River. *Water SA*, 33, 659-664.
- de Vries, J. J., & Simmers, I. (2002). Groundwater recharge: an overview of processes and challenges. *Hydrogeology Journal*, 10(DOI 10.1007/s10040-001-0171-7), 5-17.
- Dean, L. (2007). Reservoir engineering for geologists - Part 3 - Volumetric estimation. *Fekete Associates Inc*.
- Demlie, M., Jovanovic, N., & Naicker, S. (2011). *The origin of the groundwater salinity in the Sandspruit catchment, Berg river basin (South Africa)*.
- du Plessis, J., & Schloms, B. (2017). An investigation into. *Journal of the South African Institution of Civil Engineering*, 59(ISSN 1021-2019), 47-55. Retrieved from <http://www.scielo.org.za/pdf/jsaice/v59n4/05.pdf>
- Du Toit, A. (1954). *The Geology of South Africa*. Edinburgh: Oliver and Boyd.

- DWS. (2019). *Department: Water and Sanitation*. Retrieved 03 10, 2019, from <http://www.dwa.gov.za/drought/>
- Ferreira, E. (2017). *WaterCrisis: France offers Western Cape help with*. Cape Town: IOL .
- Fey, M. V., & De Clercq, W. P. (2004a). *Dryland salinity impacts on Western Cape rivers*. Pretoria: Water Research Commission. doi:Report No 1342/1/04
- Fey, M. V., & De Clercq, W. P. (2004b). *A Pilot Study Investigating the Role of Dryland Salinity in the Quality of the Water of the Berg River*. Pretoria: Water Research Commission Report No. 1342/1/04.
- Flugel, W. (1995). River salination due to Dryland agriculture in the Western Cape Province, Republic of South Africa. *Environment International*, 21, 679-686.
- Fourie, J. M. (1976). *Mineralization of Western Cape Rivers: An Investigation into the Deteriorating Water Quality Related to Drainage from Cultivated Lands along Selected Catchments, with Special Reference to the Great Berg River*. 146. Stellenbosch: University of Stellenbosch.
- Gorgens, A., & De Clercq, W. P. (2006). *Water Quality Information Systems for Integrated Water Resource Management: The Riviersonderend-Berg River System*. Pretoria: Water Research Commission Report No. TT 262/06.
- Greef, G. J. (1990). *Detailed Geohydrological Investigations in the Poesjesnel River Catchment in the Breede River Valley with Special Reference to Mineralization*. Pretoria: Water Research Commission Report No. 120/1/90.
- GreenCape. (2017). *GreenCape, 2017 Market Intelligence Report*. Retrieved from <https://www.greencape.co.za/assets/Uploads/GreenCape-Water-MIR-2017-electronic-FINAL-v1.pdf>
- Gresse, P. G., von Veh, M. W., & Frimmel, H. E. (2006). Namibian (Neoproterozoic) to early Cambrian successions. In M. R. Johnson, C. R. Anhaeusser, & R. J. Thomas (Eds.), *The Geology of South Africa* (pp. 405-409). Cape Town: CTP Printers.
- Grey, D., & Sandoff, C. W. (2007). Sink or Swim? Water security for growth and development. *Water Policy*, 9(doi: 10.2166/wp.2007.021), 545-571.
- Gringaten, A. C. (1984). Interpretation of Tests in Fissured and Multilayered Reservoirs With Double-Porosity Behavior: Theory and Practice. *Journal of Petroleum Technology*, 36(4), 549-564. doi:<https://doi.org/10.2118/10044-PA>
- Hälbich, I. W., de Villiers, J., Hartnady, C. J., Hugo, P. J., Joubert, P., Kröner, A., . . . Kent, L. E. (1980). Malmesbury Group (6.3). In A. De Grys, & S. Troskie (Eds.), *Stratigraphy of South Africa, Handbook 8* (pp. 455-465). Pretoria: Department of Minerals and Energy Affairs.
- Haws, N. W., Rao, S. C., Simunek, J., & Poyer, I. C. (2005). Single-porosity and dual-porosity modeling of water flow and solute transport in subsurface-drained fields using effective field-scale parameters. *Journal of Hydrology*, 313, 257-273.
- Head, T. (2017). *Western Cape latest dam levels: Water capacity drops again*. Retrieved from <https://www.thesouthafrican.com/western-cape-latest-dam-levels-water-11-december-2017/>

- Hortec. (2018). Swartdam & Riebeeksrivier weather data. Cape Town: Hortec.
- IOL. (2014). *Cape Town is SA's fastest growing city*. Retrieved from <https://www.iol.co.za/business-report/economy/cape-town-is-sas-fastest-growing-city-1767603>
- IWQS. (1999). *Report on the Radioactivity Monitoring Programme in the Mooi River (Wonderfonteinspruit) Catchment*. Institute for Water Quality, Pretoria. doi:Report No. N/C22/00/RPQ/2399
- Jackson, D., & Rushton, K. R. (1987). Assessment of recharge components for a chalk aquifer unit. *Journal of Hydrology*, 92, 1-15.
- Jovanovic, N. Z., Bugan, R. D., & Soltau, L. S. (2009). *Report detailing boreholes in the Sandspruit Catchment*. Natural Resources and the Environment. Stellenbosch: CSIR. doi:WRC Project K5/1849
- Jovanovic, N., Israel, S., Petersen, C., Bugan, R. D., Tredoux, G., de Clercq, W. P., . . . Demlie, M. (2011a). Guidelines for the integrated catchment monitoring: ICM mind map development and demonstration.
- Jovanovic, N., Israel, S., Petersen, C., Bugan, R., Tredoux, G., de Clercq, W. P., . . . Demlie, M. (2011b). *Optimized monitoring of the groundwater - Surface water - Atmospheric parameters for enhanced decision-making at a local scale*. Water research commission. doi:WRC Report No. 1846/1/11 ISBN No 978-1-4312-0125-9
- Kempster, P. L., Van Vliet, H. R., Looser, U., Parker, I., Silberbauer, M. J., & Du Toit, P. (1996). *Overview of Radioactivity in Water Sources: Uranium, Radium and Thorium*. Pretoria: Institute for Water Quality Studies. doi:Report, IWQS-No. N/0000/00/RPQ/0196
- Kiesel, J., Schmalz, B., Brown, G. L., & Fohrer, N. (2013). Application of a hydrological-hydraulic modelling cascade in lowlands for investigating water and sediment fluxes in catchment, channel and reach. *Journal*, 61(4), 334-346. doi:10.2478/johh-2013-0042
- Kruijne, R., van Bakel, P., Adriaanse, P., & Boesten, J. (2008). *Surface water hydrology for the Cascade model - Study area "Drentsch Veenkoloniën"*. ISSN - 1566-7197. Wageningen: Alterra Wageningen. Retrieved from www.alterra.wur.nl
- Levorsen, A. (1967). *Geology of Petroleum* (2nd Edition ed.). New York: W. H. Freeman and Company.
- Lin, L. (2007). *Hydrolic properties of the Table Mountain Group (TMG), aquifers*. Cape Town, PhD: University of the Western Cape.
- Middelton, B. J., & Bailey, A. K. (2009). Water resources of South Africa (WR2005). South Africa: Water Research Commission Report No. TT 382/08. doi:ISBN 978-1-77005-815-6
- Midgley, D. C. (1952). Preliminary Survey of the Surface Water Resources of the Union of South Africa. *Unpublished Ph. D. Thesis*. Pietermaritzburg, South Africa: University of Natal.
- Münch, Z. (2004). *Assessment of GIS-interpolation techniques for groundwater evaluation: A case study of the Sandveld, Western Cape, South Africa*. Stellenbosch: MSc .
- Neitsch, S. L., Arnold, J. G., Kiniry, J. R., & Williams, J. R. (2001). *Soil and Water Assessment Tool: Version 2001, Theoretical Documentation*. Agricultural Research Service, Texas.

- NWRS 2. (2013b). 4th Municipal Water Quality Conference. Sun City: National Water Resource Strategy 2.
- NWRS2. (2013a, June). Water for an Equitable and Sustainable Future. *Department Water Affairs, Second edition*. South Africa: National Water Resource Strategy.
- Oberholster, P. J., & Ashton, P. (2008). *State of the Nation Report: An Overview of the Current Status of Water Quality and Eutrophication in South African Rivers and Reservoirs*. Pretoria: Council for Scientific and Industrial Research (CSIR).
- Oberholster, P. J., Botha, A. M., & Cloete, T. E. (2005). An overview of toxic freshwater cyanobacteria in South Africa with special reference to risk, impact and detection by molecular marker tools. *Biokem*, 17, 57-71.
- Oberholster, P. J., Botha, A. M., & Grobbelaar, J. U. (2004). Microcystis aeruginosa: Source of toxic microcystins in drinking water. *Africa Journal of Biotechnology*, 3, 159-168.
- Oberholster, P. J., Cloete, T. E., Van Ginkel, C., Botha, A. M., & Ashton, P. J. (2008). *The use of remote sensing and molecular markers as early warning indicators of the development of cyanobacterial hyperscum crust and microcystin-producing genotypes in the hypertrophic Lake Hartebeespoort, South Africa*. Council for Scientific and Industrial Research (CSIR), Pretoria.
- Parsons, R. P. (1995). *A South African aquifer system management classification*. Pretoria: Water Research Commission. doi:Report No. 77/95
- Peyper, L. (2016). *Fin24*. Retrieved from <https://www.fin24.com/Economy/ct-city-population-up-almost-tenfold-in-10-years-20160413>
- Pitman, W. V. (2011). Overview of water resource assessment in South Africa: Current state and future challenges. *Water SA*, 37(ISSN 1816-7950), 659-664.
- Poncea, V. M., & Shetty, A. V. (1995). A conceptual model of catchment water balance: Formulation and calibration. *Journal of Hydrology*, 173(1), 27-40.
- Rabie, L. P., Smuts, H., & Verwoerd, W. J. (1974). *Geological map of the Mooriesburg-Wellington area*. Geology. Stellenbosch: Stellenbosch Universiteit.
- Rozendaal, A., & Scheepers, R. (1995). Magmatic and related mineral deposits of the Pan_african Saldania belt in the Estern Cape Province, South Africa. *Journal of African Earth Sciences*, 21(1), 107-126.
- RSA. (1998, August 20). *Department of Water Affairs*. Retrieved 05 31, 2015, from https://www.dwa.gov.za/Documents/Legislature/nw_act/NWA.pdf
- Rust, I. (1967). On the Sedimentation of the Table Mountain Group in the Western Cape Province. Unpubl. D.Sc. Thesis, Univ, Stellenbosch. 110pp.
- Rust, I. (1973). The evolution of the Paleozoic Cape Basin, southern margin of Africa. In A. Nairn, & F. Stehli (Eds.), *The Ocean Basins and Margins* (Vol. 1, pp. 247-276). New York: Plenum Publishing Corporation.

- Samuels, D. (2007). Hydraulic properties of the vadose zone at two typical sites in the Western Cape for the assessment of groundwater vulnerability to pollution. Bellville: University of the Western Cape.
- SAWS. (2015). *South African Weather Service*. Retrieved 09 13, 2015, from <http://www.kzndae.gov.za/Portals/0/weather%20report/2015/SCOLF201507.pdf>
- Schalkwyk, H. J.-M. (2005). *Assessment controls on reservoir performance and the affects of granulation seam mechanics in the Bredasdorp Basin, South Africa*, MSc. Cape Town: University of the Western Cape.
- Serra, K., Reynolds, A. C., & Raghavan, R. (1983). New Pressure Transient Analysis Methods for Naturally Fractured Reservoirs(includes associated papers 12940 and 13014. *Journal of Petroleum Technology*, 35(12), 2271-2283.
- Simmers, I. (1988). Estimation of natural groundwater recharge. 222. NATO ASI Series C.
- Šimunek, J., Sejna, M., & Van Genuchten, M. (2005). *The Hydrus 1D software package for simulating two-dimensional movement of water, heat and multiple solutes in variably saturated media*, Department of Environmental Sciences. Riverside, California: University of California.
- Singh, V. P., & Buapeng, S. (1981). A nonlinear hydrologic cascade. *Journal of Hydrology*, 51(1-4), 283-293. doi:10.1016/0022-1694(81)90136-0
- Slabbert, J. L., Venter, E. A., Moletsane, M., van Wyk, J. H., Blaise, C., & Aneck-Hahn, N. H. (2007b). *An investigation of the estrogenic activity in water from selected drinking water treatment processes*. Water Research Commission by CSIR Natural Resources and the Environment. CSIR. doi:Report No 1532/1/07
- Slabbert, J. L., Venter, E. A., Moletsane, M., van Wyk, J. H., Schillack, V., Aneck-Hahn, N. H., & Marais, P. (2007a). An investigation into the occurrence of steroidal hormones (estrogens) in sewage effluent using biological/biochemical and chemical techniques. In A. E. Burger (Ed.), *Implementation of a Research Programme for Investigating Endocrine Disrupting Contaminants in South African Water Systems* (Vol. 2, pp. 2003-2005). Pretoria. doi:WRC Report No 1402/1/07
- Spaull, N. (2012). *Politicsweb*. Retrieved 11 15, 2017, from <http://www.politicsweb.co.za/news-and-analysis/education-in-sa-a-tale-of-two-systems>
- SRK, C. (2007). *PPC Riebeek Wes Expansion Project: Specialist Hydrogeological Study*. Cape Town.
- SSWM. (2015). *Sustainable sanitation and water managemant (SSWM)*. Retrieved 5 26, 2015, from <http://www.sswm.info/content/waterbalanceestimation>
- Stephens, D. B., & Knowlton, R. (1986). Soil water movement and recharge through and at a semi arid site in New Mexico. *Water Resources Research*, 22(6), 81-889.
- Stone, D. B., Moomaw, C. L., & Davis, C. L. (2001). Estimating recharge distribution by incorporating runoff from mountainous area in an alluvium basin in Great Basin Region of the Southwestern United States. *Groundwater*, 39(6), 807-818.
- SWAT. (2017). *Soil & Water Assessment Tool (SWAT)*. Retrieved 02 24, 2017, from <https://swat.tamu.edu/>

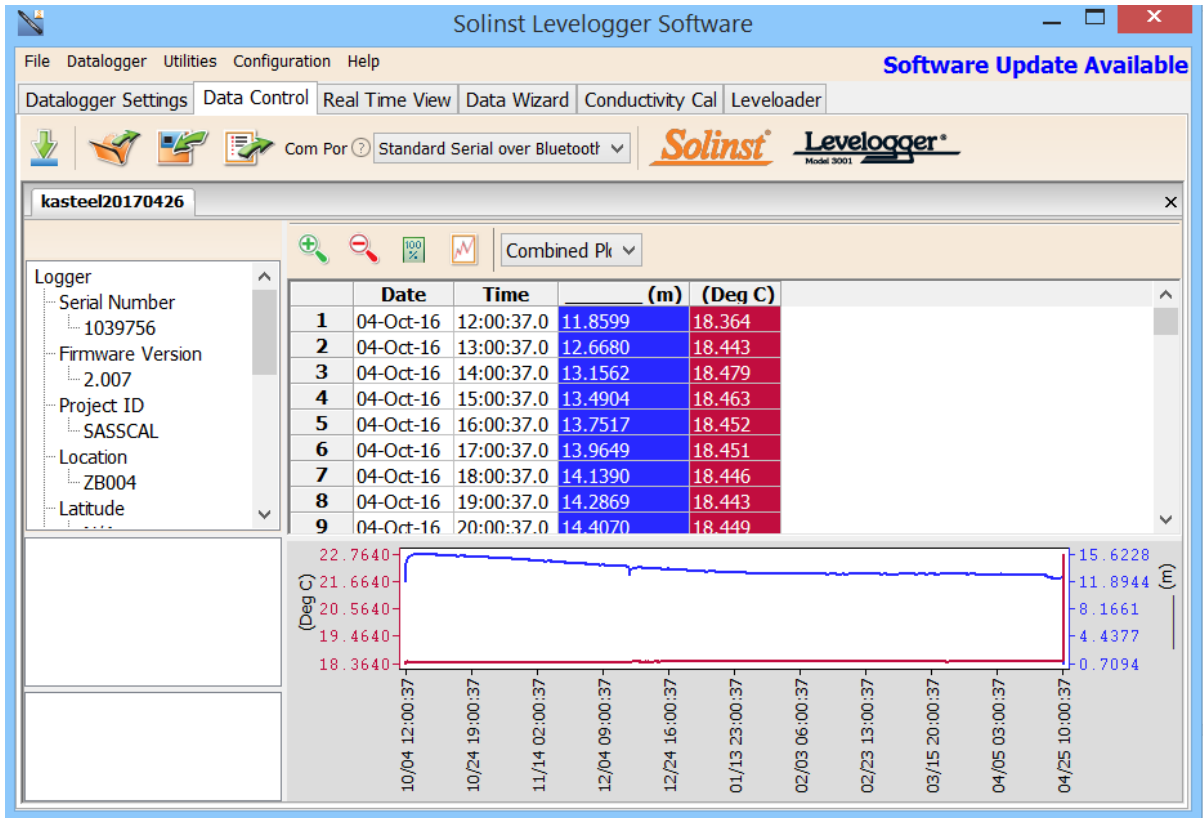
- Theron, J. (1962). An analysis of the Cape Folding in the District of willowmore. Unpubl. D. Sc. Thesis, Univ. Stellenbosch.
- Theron, J., & Loock, J. (1988). Devonian deltas of the Cape Supergroup, South Africa. In N. McMillan, A. Embry, & D. Glass (Eds.), *Devonian of the World* (Vol. 1, pp. 729-740).
- Toens, P. D., Stadler, W., & Wullschleger, N. J. (1999). *The Association of Groundwater Chemistry and Geology with Atypical Lymphocytes (as a Biological Indicator) in the Pofadder Area, North Western Cape, South Africa*. Pretoria: Water Research Commission. doi:Report No 839/1/98
- Turton, A. (2009). *South Africa's Own Inconvenient Truth(s)*. Retrieved from [http://www.anthonyturton.com/assets/my_documents/my_files/Turton_Inconvenient_Truth_2009_\[Compatibility_Mode\].pdf](http://www.anthonyturton.com/assets/my_documents/my_files/Turton_Inconvenient_Truth_2009_[Compatibility_Mode].pdf)
- USGS. (2015). *USGS - Earth Explorer*. Retrieved 04 15, 2015, from <http://earthexplorer.usgs.gov/>
- Van der Merwe, M. (2017). *Daily Maverick, Water, water nowhere: Update on the Western Cape's drought*. Retrieved from <https://www.dailymaverick.co.za/article/2017-10-25-water-water-nowhere-update-on-the-western-cape-drought-interventions/#.WjO6rd-WbIU>
- Van Rensburg, L. D., De Clercq, W. P., Barnard, J. H., & Du Preez, C. C. (2011). Salinity guidelines for irrigation: Case studies from Water Research Commission projects along the Lower Vaal, Riet, Berg and Breede Rivers. *Water Research Commission Report No. 5, 37*(ISSN 1816-7950).
- Verma, R. D. (1979). A physical model of the rainfall-runoff relationship for semiarid lands. The hydrology of areas of low precipitation. *128*, pp. 215-217. Canberra Symposium: International Association of Hydrological Sciences (IAHS) .
- Vermeulen, T. (2010). *Plant water relations of Elytropappus Rhinocerotis with specific reference to soil restrictions on growth*. Stellenbosch: Stellenbosch University, MSc .
- Verwoerd , W. J., Rabie, L. P., & Smuts, H. (1974). Geological Map of the Moorreesburg-Wellington Area. University of Stellenbosch.
- Von Veh, M. W. (1983). Aspects of sedimentation, structure and tectonic evolution in the Tygerberg Terrane, South-western Cape Province. *Bull. Precamb. Res. Unit, University of Cape Town*, *32*, 88pp.
- Wade, P. W., Woodbourne, S., Morris, W. M., Vos, P., & Jarvis, N. W. (2002). *Tier 1 Risk Assessment of Selected Radionuclides in Sediments of the Mooi River Catchment*. Water Research Commission. Pretoria: WRC. doi:Project No K5/1095
- Warren, J. E., & Root, P. J. (1963). The Behavior of Naturally Fractured Reservoirs. *Society of Petroleum Engineers Journal*, *3*(3), 245–255. doi:<https://doi.org/10.2118/426-PA>
- Wasserfall, N. M. (2013). *Rain events based hillslope hydrological processes at the Langgewens experimental farm, Western Cape, South Africa*. Stellenbosch, MSc: University of Stellenbosch.
- Wickens, H. (2012). *Welcome to the southwestern Karoo Basin Deep-water Field Experience*. Stellenbosch.
- World Economic Forum. (2012). *Global Risk Report*. Retrieved 07 27, 2015, from <http://www.weforum.org/reports/global-risks-2012-seventh-edition>

- World Economic Forum. (2015). *Global Risk Report*. Retrieved 07 27, 2015, from http://www3.weforum.org/docs/WEF_Global_Risks_2015_Report15.pdf
- WWF. (2012). WWF - South Africa : Water Balance Programme. 1-7. WWF Booklet. Retrieved 5 26, 2015, from www.wwf.org.za/waterbalance
- WWF. (2013). *An introduction to South Africa's Water Source Areas*. Retrieved 5 27, 2015, from http://awsassets.wwf.org.za/downloads/wwf_sa_watersource_area10_lo.pdf
- WWF. (2015). *WWF South Africa*. Retrieved 5 26, 2015, from http://www.wwf.org.za/what_we_do/freshwater/water_balance/
- Yair, A., & Lavee, H. (1985). Runoff generation in arid and semiarid zones. In M. G. Anderson, & T. P. Burt (Eds.), *Hydrological Forecasting* (pp. 183-220). New York: Wiley.
- Zille, H. (2017). *The Cape Water Crisis – FAQs and honest answers, Daily Maverick*. Retrieved from <https://www.dailymaverick.co.za/opinionista/2017-10-30-the-cape-water-crisis-faqs-and-honest-answers/#.WjO6s9-WbIU>

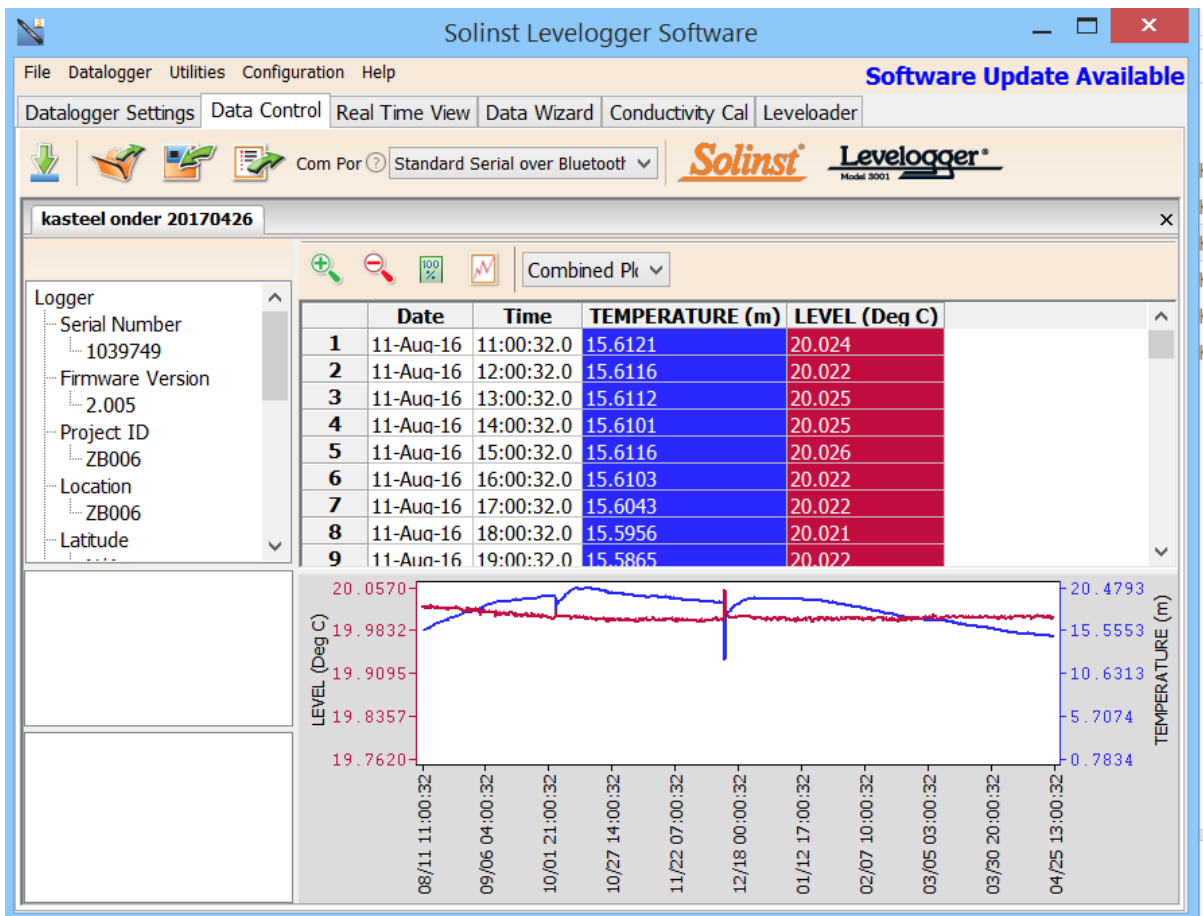
Addendum

Borehole information and software used.

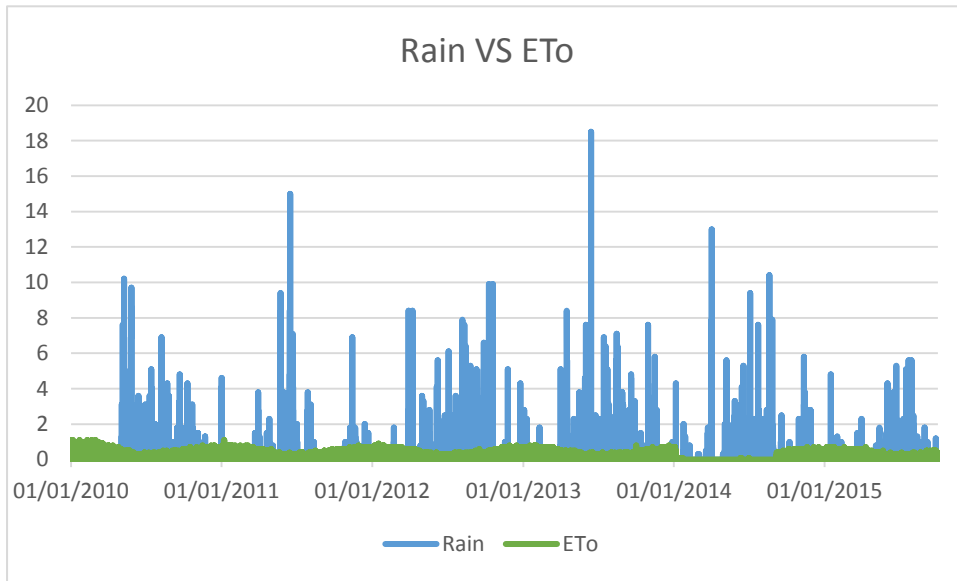
BH1 Kasteelberg midslope.



BH2 Kasteelberg footslope



Precipitation vs Evapotranspiration (2010-2015)



HYDRUS-1D Mass Balance Information generated during the modelling process.

***** Program HYDRUS

Welcome to HYDRUS-1D

Date: 3. 1. Time: 21:45:59

Units: L = m , T = days , M = mmol

 Time [T] 0.0000

Sub-region num. 1 2 3 4

Length [L] 0.80000E+03 0.13667E+03 0.20167E+03 0.19667E+03 0.26500E+03
 W-volume [L] 0.18205E+03 0.29283E+02 0.49981E+02 0.45060E+02 0.57728E+02
 In-flow [L/T] 0.00000E+00 0.00000E+00 0.00000E+00 0.00000E+00 0.00000E+00
 h Mean [L] -0.10000E+03 -0.10000E+03 -0.10000E+03 -0.10000E+03 -0.10000E+03
 Top Flux [L/T] -0.22785E-05
 Bot Flux [L/T] -0.22785E-05

Time [T] 30.4000

Sub-region num. 1 2 3 4

Length [L] 0.80000E+03 0.13667E+03 0.20167E+03 0.19667E+03 0.26500E+03
 W-volume [L] 0.29247E+03 0.61179E+02 0.99125E+02 0.74412E+02 0.57750E+02
 In-flow [L/T] 0.18202E+01 -0.85254E-01 0.00000E+00 0.18746E+01 0.30825E-01

h Mean [L] 0.22585E+02 0.36324E+02 0.12836E+03 0.69346E+02 -0.99698E+02

Top Flux [L/T] -0.19055E+01

Bot Flux [L/T] -0.22785E-05

WatBalT [L] 0.30534E+02

WatBalR [%] 27.654

Time [T] 60.8000

Sub-region num. 1 2 3 4

Length [L] 0.80000E+03 0.13667E+03 0.20167E+03 0.19667E+03 0.26500E+03

W-volume [L] 0.11844E+03 0.53114E+02 0.21799E+02 0.17817E+02 0.25709E+02

In-flow [L/T] 0.13916E+01 0.64549E+00 0.73598E+00 0.00000E+00 0.10146E-01

h Mean [L] -0.32745E+08 -0.17352E+02 -0.31341E+08 -0.69315E+08 -0.23562E+08

Top Flux [L/T] -0.13747E+01

Bot Flux [L/T] 0.10144E-01

WatBalT [L] -0.19306E+03

WatBalR [%] 139.976

Time [T] 91.2000

Sub-region num. 1 2 3 4

Length [L] 0.80000E+03 0.13667E+03 0.20167E+03 0.19667E+03 0.26500E+03

W-volume [L] 0.11663E+03 0.52165E+02 0.20774E+02 0.17861E+02 0.25828E+02

In-flow [L/T] 0.18890E+01 0.90619E+00 0.98059E+00 0.00000E+00 0.22340E-02

h Mean [L] -0.25774E+08 -0.29914E+02 -0.19883E+08 -0.52865E+08 -0.23445E+08

Top Flux [L/T] -0.13747E+01

Bot Flux [L/T] 0.22295E-02

WatBalT [L] -0.25922E+03

WatBalR [%] 128.062

Time [T] 121.6000

Sub-region num. 1 2 3 4

Length [L] 0.80000E+03 0.13667E+03 0.20167E+03 0.19667E+03 0.26500E+03

W-volume [L] 0.19740E+03 0.60537E+02 0.88865E+02 0.22111E+02 0.25882E+02

In-flow [L/T] 0.29522E+01 0.00000E+00 0.19043E+01 0.10464E+01 0.14687E-02

h Mean [L] -0.18676E+08 0.32993E+01 -0.32238E+02 -0.44394E+08 -0.23434E+08

Top Flux [L/T] -0.13747E+01

Bot Flux [L/T] 0.14706E-02

WatBalT [L] -0.23959E+03

WatBalR [%] 90.908

Time [T] 152.0000

Sub-region num. 1 2 3 4

Length [L] 0.80000E+03 0.13667E+03 0.20167E+03 0.19667E+03 0.26500E+03

W-volume [L] 0.19249E+03 0.61179E+02 0.85087E+02 0.20306E+02 0.25921E+02

In-flow [L/T] 0.31109E+01 0.00000E+00 0.23146E+01 0.79512E+00 0.11444E-02

h Mean [L] -0.20342E+08 0.15889E+02 -0.18006E+03 -0.51176E+08 -0.23429E+08

Top Flux [L/T] -0.31290E+01

Bot Flux [L/T] 0.11443E-02

WatBalT [L] -0.30978E+03

WatBalR [%] 94.203

Time [T] 182.4000

Sub-region num. 1 2 3 4

Length [L] 0.80000E+03 0.13667E+03 0.20167E+03 0.19667E+03 0.26500E+03

W-volume [L] 0.18522E+03 0.61171E+02 0.79303E+02 0.18790E+02 0.25953E+02

In-flow [L/T] 0.40084E+01 0.13387E+01 0.22542E+01 0.41464E+00 0.95113E-03

h Mean [L] -0.18812E+08 0.56500E+01 -0.25984E+04 -0.44953E+08 -0.23427E+08

Top Flux [L/T] -0.40075E+01

Bot Flux [L/T] 0.95556E-03

WatBalT [L] -0.38533E+03

WatBalR [%] 97.032

Time [T] 212.8000

Sub-region num. 1 2 3 4

Length [L] 0.80000E+03 0.13667E+03 0.20167E+03 0.19667E+03 0.26500E+03

W-volume [L] 0.17825E+03 0.60250E+02 0.73962E+02 0.18062E+02 0.25980E+02

In-flow [L/T] 0.18876E+01 0.25156E+00 0.14993E+01 0.13587E+00 0.82970E-03

h Mean [L] -0.29147E+08 -0.94771E-01 -0.47894E+05 -0.86952E+08 -0.23425E+08

Top Flux [L/T] -0.18916E+01

Bot Flux [L/T] 0.83012E-03

WatBalT [L] -0.45691E+03

WatBalR [%] 98.955

Time [T] 243.2000

Sub-region num. 1 2 3 4

Length [L] 0.80000E+03 0.13667E+03 0.20167E+03 0.19667E+03 0.26500E+03

W-volume [L] 0.17511E+03 0.60242E+02 0.70914E+02 0.17953E+02 0.26003E+02

In-flow [L/T] 0.14301E+01 -0.25526E+00 0.16314E+01 0.53177E-01 0.74625E-03

h Mean [L] -0.22119E+08 -0.98454E-01 -0.48561E+06 -0.57916E+08 -0.23423E+08

Top Flux [L/T] -0.13747E+01

Bot Flux [L/T] 0.73960E-03

WatBalT [L] -0.52837E+03

WatBalR [%] 99.203

Time [T] 273.6000

Sub-region num. 1 2 3 4

Length [L] 0.80000E+03 0.13667E+03 0.20167E+03 0.19667E+03 0.26500E+03

W-volume [L] 0.16705E+03 0.60537E+02 0.62606E+02 0.17887E+02 0.26025E+02

In-flow [L/T] 0.34323E+01 0.00000E+00 0.34311E+01 0.59605E-03 0.66916E-03

h Mean [L] -0.23427E+08 0.10668E+01 -0.34293E+07 -0.60220E+08 -0.23422E+08

Top Flux [L/T] -0.13747E+01

Bot Flux [L/T] 0.67061E-03

WatBalT [L] -0.59550E+03

WatBalR [%] 100.617

Time [T] 304.0000

Sub-region num. 1 2 3 4

Length [L] 0.80000E+03 0.13667E+03 0.20167E+03 0.19667E+03 0.26500E+03

W-volume [L] 0.16949E+03 0.60537E+02 0.65079E+02 0.17834E+02 0.26044E+02

In-flow [L/T] 0.35719E+01 0.00000E+00 0.35639E+01 0.74177E-02 0.61798E-03

h Mean [L] -0.24531E+08 0.42193E+00 -0.71770E+07 -0.60868E+08 -0.23421E+08

Top Flux [L/T] -0.13747E+01

Bot Flux [L/T] 0.61594E-03

WatBalT [L] -0.67428E+03

WatBalR [%] 99.975

Time [T] 334.4000

Sub-region num. 1 2 3 4

Length [L] 0.80000E+03 0.13667E+03 0.20167E+03 0.19667E+03 0.26500E+03

W-volume [L] 0.16750E+03 0.60537E+02 0.63040E+02 0.17859E+02 0.26062E+02

In-flow [L/T] 0.34520E+01 0.00000E+00 0.34499E+01 0.15227E-02 0.56903E-03

h Mean [L] -0.22424E+08 0.98398E+00 -0.61895E+07 -0.53309E+08 -0.23421E+08
 Top Flux [L/T] -0.13747E+01
 Bot Flux [L/T] 0.57134E-03
 WatBalT [L] -0.74873E+03
 WatBalR [%] 100.244

 Time [T] 364.8000

Sub-region num. 1 2 3 4

Length [L] 0.80000E+03 0.13667E+03 0.20167E+03 0.19667E+03 0.26500E+03
 W-volume [L] 0.16503E+03 0.60537E+02 0.60557E+02 0.17859E+02 0.26079E+02
 In-flow [L/T] 0.33761E+01 0.00000E+00 0.33754E+01 0.22769E-03 0.53406E-03
 h Mean [L] -0.22483E+08 0.13213E+01 -0.63859E+07 -0.53352E+08 -0.23420E+08
 Top Flux [L/T] -0.13747E+01
 Bot Flux [L/T] 0.53415E-03
 WatBalT [L] -0.81701E+03
 WatBalR [%] 100.528

 Time [T] 395.2000

Sub-region num. 1 2 3 4

Length [L] 0.80000E+03 0.13667E+03 0.20167E+03 0.19667E+03 0.26500E+03
 W-volume [L] 0.16504E+03 0.60537E+02 0.60638E+02 0.17768E+02 0.26095E+02
 In-flow [L/T] 0.33812E+01 0.00000E+00 0.33800E+01 0.66757E-03 0.50545E-03

h Mean [L] -0.37502E+08 0.13150E+01 -0.16970E+08 -0.10359E+09 -0.23420E+08

Top Flux [L/T] -0.13747E+01

Bot Flux [L/T] 0.50257E-03

WatBalT [L] -0.89662E+03

WatBalR [%] 100.134

Time [T] 425.6000

Sub-region num. 1 2 3 4

Length [L] 0.80000E+03 0.13667E+03 0.20167E+03 0.19667E+03 0.26500E+03

W-volume [L] 0.16903E+03 0.60537E+02 0.64554E+02 0.17833E+02 0.26110E+02

In-flow [L/T] 0.35089E+01 -0.29513E-01 0.35339E+01 0.40356E-02 0.47684E-03

h Mean [L] -0.26377E+08 0.57363E+00 -0.59463E+07 -0.69642E+08 -0.23419E+08

Top Flux [L/T] -0.13747E+01

Bot Flux [L/T] 0.47534E-03

WatBalT [L] -0.97331E+03

WatBalR [%] 99.216

Time [T] 456.0000

Sub-region num. 1 2 3 4

Length [L] 0.80000E+03 0.13667E+03 0.20167E+03 0.19667E+03 0.26500E+03

W-volume [L] 0.17065E+03 0.60799E+02 0.65881E+02 0.17842E+02 0.26124E+02

In-flow [L/T] 0.37075E+01 0.74907E-01 0.36227E+01 0.94364E-02 0.45432E-03

h Mean [L] -0.25543E+08 0.16430E+00 -0.49807E+07 -0.67242E+08 -0.23419E+08
 Top Flux [L/T] -0.21223E+01
 Bot Flux [L/T] 0.45158E-03
 WatBalT [L] -0.10463E+04
 WatBalR [%] 99.027

 Time [T] 486.4000

Sub-region num. 1 2 3 4

Length [L] 0.80000E+03 0.13667E+03 0.20167E+03 0.19667E+03 0.26500E+03
 W-volume [L] 0.17152E+03 0.60536E+02 0.67016E+02 0.17834E+02 0.26137E+02
 In-flow [L/T] 0.13798E+01 0.76469E-01 0.12804E+01 0.22440E-01 0.48154E-03
 h Mean [L] -0.24314E+08 0.17550E+00 -0.47458E+07 -0.62482E+08 -0.23419E+08
 Top Flux [L/T] -0.13791E+01
 Bot Flux [L/T] 0.43062E-03
 WatBalT [L] -0.11186E+04
 WatBalR [%] 99.012

 Time [T] 516.8000

Sub-region num. 1 2 3 4

Length [L] 0.80000E+03 0.13667E+03 0.20167E+03 0.19667E+03 0.26500E+03
 W-volume [L] 0.14784E+03 0.60409E+02 0.43411E+02 0.17874E+02 0.26150E+02
 In-flow [L/T] 0.13929E+01 -0.37584E+00 0.17684E+01 0.00000E+00 0.41127E-03

h Mean [L] -0.21017E+08 -0.88013E-01 -0.67934E+07 -0.46971E+08 -0.23419E+08

Top Flux [L/T] -0.13751E+01

Bot Flux [L/T] 0.41198E-03

WatBalT [L] -0.12059E+04

WatBalR [%] 101.049

Time [T] 547.2000

Sub-region num. 1 2 3 4

Length [L] 0.80000E+03 0.13667E+03 0.20167E+03 0.19667E+03 0.26500E+03

W-volume [L] 0.14138E+03 0.60934E+02 0.36445E+02 0.17838E+02 0.26162E+02

In-flow [L/T] 0.43684E+01 0.86939E+00 0.34986E+01 0.00000E+00 0.39101E-03

h Mean [L] -0.27750E+08 0.92546E+01 -0.21588E+08 -0.59191E+08 -0.23418E+08

Top Flux [L/T] -0.43680E+01

Bot Flux [L/T] 0.39526E-03

WatBalT [L] -0.12739E+04

WatBalR [%] 101.487

Time [T] 577.6000

Sub-region num. 1 2 3 4

Length [L] 0.80000E+03 0.13667E+03 0.20167E+03 0.19667E+03 0.26500E+03

W-volume [L] 0.13206E+03 0.58611E+02 0.29412E+02 0.17864E+02 0.26174E+02

In-flow [L/T] 0.33367E+01 0.94969E+00 0.23866E+01 0.00000E+00 0.38147E-03

h Mean [L] -0.24832E+08 0.29847E+01 -0.18167E+08 -0.50828E+08 -0.23418E+08

Top Flux [L/T] -0.33363E+01

Bot Flux [L/T] 0.38016E-03

WatBalT [L] -0.13364E+04

WatBalR [%] 102.138

Time [T] 608.0000

Sub-region num. 1 2 3 4

Length [L] 0.80000E+03 0.13667E+03 0.20167E+03 0.19667E+03 0.26500E+03

W-volume [L] 0.12248E+03 0.54950E+02 0.23485E+02 0.17865E+02 0.26185E+02

In-flow [L/T] 0.18936E+01 0.10292E+01 0.86403E+00 0.00000E+00 0.36526E-03

h Mean [L] -0.24833E+08 -0.54360E+01 -0.18289E+08 -0.50707E+08 -0.23418E+08

Top Flux [L/T] -0.18933E+01

Bot Flux [L/T] 0.36645E-03

WatBalT [L] -0.13995E+04

WatBalR [%] 102.757

Time [T] 638.4000

Sub-region num. 1 2 3 4

Length [L] 0.80000E+03 0.13667E+03 0.20167E+03 0.19667E+03 0.26500E+03

W-volume [L] 0.14928E+03 0.60488E+02 0.44712E+02 0.17881E+02 0.26196E+02

In-flow [L/T] 0.22650E+01 0.15791E+00 0.21067E+01 0.00000E+00 0.35524E-03

h Mean [L] -0.20269E+08 -0.81741E-01 -0.34998E+07 -0.47306E+08 -0.23418E+08

Top Flux [L/T] -0.13747E+01

Bot Flux [L/T] 0.35392E-03

WatBalT [L] -0.14430E+04

WatBalR [%] 100.751

 Time [T] 668.8000

Sub-region num. 1 2 3 4

Length [L] 0.80000E+03 0.13667E+03 0.20167E+03 0.19667E+03 0.26500E+03

W-volume [L] 0.14685E+03 0.60688E+02 0.42032E+02 0.17919E+02 0.26207E+02

In-flow [L/T] 0.17081E+01 -0.25826E+00 0.19660E+01 0.00000E+00 0.34332E-03

h Mean [L] -0.19147E+08 -0.71237E-01 -0.48204E+07 -0.41390E+08 -0.23418E+08

Top Flux [L/T] -0.17107E+01

Bot Flux [L/T] 0.34244E-03

WatBalT [L] -0.15094E+04

WatBalR [%] 100.843

Time [T] 699.2000

Sub-region num. 1 2 3 4

Length [L] 0.80000E+03 0.13667E+03 0.20167E+03 0.19667E+03 0.26500E+03

W-volume [L] 0.13791E+03 0.60008E+02 0.33846E+02 0.17844E+02 0.26217E+02

In-flow [L/T] 0.34100E+01 0.69311E+00 0.27165E+01 0.00000E+00 0.33855E-03

h Mean [L] -0.27300E+08 0.24252E+01 -0.22051E+08 -0.56886E+08 -0.23417E+08

Top Flux [L/T] -0.34096E+01

Bot Flux [L/T] 0.33185E-03

WatBalT [L] -0.15778E+04

WatBalR [%] 101.367

Time [T] 729.6000

Sub-region num. 1 2 3 4

Length [L] 0.80000E+03 0.13667E+03 0.20167E+03 0.19667E+03 0.26500E+03

W-volume [L] 0.14928E+03 0.60819E+02 0.44316E+02 0.17919E+02 0.26227E+02

In-flow [L/T] 0.16216E+01 0.68771E+00 0.93359E+00 0.00000E+00 0.32500E-03

h Mean [L] -0.18805E+08 0.49634E+00 -0.40056E+07 -0.40834E+08 -0.23417E+08

Top Flux [L/T] -0.16214E+01

Bot Flux [L/T] 0.32206E-03

WatBalT [L] -0.16533E+04

WatBalR [%] 100.561

Time [T] 760.0000

Sub-region num. 1 2 3 4

Length [L] 0.80000E+03 0.13667E+03 0.20167E+03 0.19667E+03 0.26500E+03

W-volume [L] 0.14747E+03 0.60513E+02 0.42945E+02 0.17777E+02 0.26237E+02

In-flow [L/T] 0.14734E+01 -0.36551E+00 0.18386E+01 0.00000E+00 0.30945E-03

h Mean [L] -0.35671E+08 -0.82140E-01 -0.16923E+08 -0.96195E+08 -0.23417E+08

Top Flux [L/T] -0.14757E+01

Bot Flux [L/T] 0.31297E-03

WatBalT [L] -0.17238E+04

WatBalR [%] 100.531

Time [T] 790.4000

Sub-region num. 1 2 3 4

Length [L] 0.80000E+03 0.13667E+03 0.20167E+03 0.19667E+03 0.26500E+03

W-volume [L] 0.15575E+03 0.60537E+02 0.51131E+02 0.17840E+02 0.26246E+02

In-flow [L/T] 0.33409E+01 0.00000E+00 0.33406E+01 0.00000E+00 0.31153E-03

h Mean [L] -0.25490E+08 0.14980E+01 -0.63792E+07 -0.65593E+08 -0.23417E+08

Top Flux [L/T] -0.13747E+01

Bot Flux [L/T] 0.30451E-03

WatBalT [L] -0.17970E+04

WatBalR [%] 99.913

Time [T] 820.8000

Sub-region num. 1 2 3 4

Length [L] 0.80000E+03 0.13667E+03 0.20167E+03 0.19667E+03 0.26500E+03

W-volume [L] 0.15758E+03 0.60537E+02 0.52950E+02 0.17841E+02 0.26255E+02

In-flow [L/T] 0.33311E+01 0.00000E+00 0.33308E+01 0.00000E+00 0.29882E-03

h Mean [L] -0.25441E+08 0.15352E+01 -0.63682E+07 -0.65406E+08 -0.23417E+08
 Top Flux [L/T] -0.13747E+01
 Bot Flux [L/T] 0.29661E-03
 WatBalT [L] -0.18712E+04
 WatBalR [%] 99.819

 Time [T] 851.2000

Sub-region num. 1 2 3 4

Length [L] 0.80000E+03 0.13667E+03 0.20167E+03 0.19667E+03 0.26500E+03
 W-volume [L] 0.15344E+03 0.60537E+02 0.48876E+02 0.17767E+02 0.26264E+02
 In-flow [L/T] 0.33689E+01 0.00000E+00 0.33686E+01 0.00000E+00 0.28372E-03
 h Mean [L] -0.38070E+08 0.13654E+01 -0.17447E+08 -0.10542E+09 -0.23416E+08
 Top Flux [L/T] -0.13747E+01
 Bot Flux [L/T] 0.28920E-03
 WatBalT [L] -0.19466E+04
 WatBalR [%] 99.953

 Time [T] 881.6000

Sub-region num. 1 2 3 4

Length [L] 0.80000E+03 0.13667E+03 0.20167E+03 0.19667E+03 0.26500E+03
 W-volume [L] 0.15197E+03 0.60662E+02 0.47154E+02 0.17882E+02 0.26273E+02
 In-flow [L/T] 0.34057E+01 -0.20707E-01 0.34261E+01 0.00000E+00 0.28483E-03

h Mean [L] -0.23865E+08 0.11105E+01 -0.36727E+07 -0.61760E+08 -0.23417E+08

Top Flux [L/T] -0.16176E+01

Bot Flux [L/T] 0.28225E-03

WatBalT [L] -0.20230E+04

WatBalR [%] 100.027

Time [T] 912.0000

Sub-region num. 1 2 3 4

Length [L] 0.80000E+03 0.13667E+03 0.20167E+03 0.19667E+03 0.26500E+03

W-volume [L] 0.14663E+03 0.60700E+02 0.41883E+02 0.17765E+02 0.26281E+02

In-flow [L/T] 0.17347E+01 -0.24551E+00 0.19799E+01 0.00000E+00 0.27618E-03

h Mean [L] -0.38942E+08 -0.70363E-01 -0.19488E+08 -0.10687E+09 -0.23417E+08

Top Flux [L/T] -0.17376E+01

Bot Flux [L/T] 0.27571E-03

WatBalT [L] -0.20880E+04

WatBalR [%] 100.283

Calculation time [sec] 0.280000030994415

Excel Calculations and results

Oppervlak (m2)									Layer 1					
Volume (m3)									314045					
Diepte (m)									31404500					
									900					
									Density (g/m3)					
Clean Sandstone									2.65					
Fractured Sandstone									2.3					
Siltstone									2.45					
Shale									2.35					
percent infil									10					
	Dag	rain	Rain m	ET mm	ET m	Response			Layer 1					
Vol total poros									16					
Oppervlak (m2)									314045					
reen oppervlak									314045					
Volume (m3)									31404500					
Dikte (m)									900					
Total pore volume m3		Rain mm		ETo mm					5,150,338	5,150,338			afloop	afloop akt
	1	3.2	0.0032	1.23	0.00123	0.00197	0.00197	619	619	619				0
	2	0	0	1.89	0.00189	-0.00189	-0.00189	-594	25	25				0
	3	0	0	1.67	0.00167	-0.00167	-0.00167	-524	0	0				0
	4	0.2	0.0002	1.26	0.00126	-0.00106	-0.00106	-333	0	0				0
	5	0	0	1.04	0.00104	-0.00104	-0.00104	-327	0	0				0
	6	0	0	1.73	0.00173	-0.00173	-0.00173	-543	0	0				0
	7	0	0	1.97	0.00197	-0.00197	-0.00197	-619	0	0				0
	8	0	0	2.32	0.00232	-0.00232	-0.00232	-729	0	0				0
	9	0	0	1.93	0.00193	-0.00193	-0.00193	-606	0	0				0
	10	0	0	2.13	0.00213	-0.00213	-0.00213	-669	0	0				0
	11	0	0	1.78	0.00178	-0.00178	-0.00178	-559	0	0				0
	12	0	0	5.25	0.00525	-0.00525	-0.00525	-1,649	0	0				0
	13	0	0	5.5	0.0055	-0.0055	-0.0055	-1,727	0	0				0
	14	1.6	0.0016	1.36	0.00136	0.00024	0.00024	75	75	75				0
	15	0	0	2.35	0.00235	-0.00235	-0.00235	-738	0	0				0
	16	0	0	3.85	0.00385	-0.00385	-0.00385	-1,209	0	0				0
	17	4.6	0.0046	0.45	0.00045	0.00415	0.00415	1,303	1,303	1,303				0
	18	2.4	0.0024	1.23	0.00123	0.00117	0.00117	367	1,671	1,671				0
	19	0	0	1.52	0.00152	-0.00152	-0.00152	-477	1,193	1,193				0

Part of Borehole 1 dataset

Serial_number:

2019549

Project ID:

Date	Time	LEVEL	TEMPERATURE
04/06/2013	0:52:45	20.4071	21.140
04/06/2013	1:52:45	20.3999	21.149
04/06/2013	2:52:45	20.3892	21.147
04/06/2013	3:52:45	20.3797	21.152
04/06/2013	4:52:45	20.3714	21.150
04/06/2013	5:52:45	20.3684	21.143
04/06/2013	6:52:45	20.3615	21.153
04/06/2013	7:52:45	20.3623	21.160
04/06/2013	8:52:45	20.3599	21.142
04/06/2013	9:52:45	20.3579	21.153
04/06/2013	10:52:45	20.3534	21.154
04/06/2013	11:52:45	20.3484	21.145
04/06/2013	12:52:45	20.3397	21.153
04/06/2013	13:52:45	20.3305	21.151
04/06/2013	14:52:45	20.3258	21.150
04/06/2013	15:52:45	20.3259	21.158
04/06/2013	16:52:45	20.3267	21.145
04/06/2013	17:52:45	20.3280	21.150
04/06/2013	18:52:45	20.3267	21.148
04/06/2013	19:52:45	20.3322	21.147
04/06/2013	20:52:45	20.3255	21.145
04/06/2013	21:52:45	20.3205	21.146

Part of the Riebeeks River weather station data set

Date	Tave °C	Tmin °C	Tmax °C	SRad mJ/hr	WSAve m/s	Rain mm	LWet%	WDir	RHave %	RHmin %	RHmax %	Sun
25/06/2015	9.1	3.2	12	7.3	1.61	3.2	71	---	80.3	63.3	96	
26/06/2015	9.5	6.1	13.6	10.2	1.77	0	0	---	69.1	53.6	79.4	
27/06/2015	10.5	8.4	13.5	9.4	1.8	0	0	---	72.8	53.5	91.9	
28/06/2015	9.8	8	12.7	7.2	2.38	0.2	42	---	83.7	68.4	99.8	
29/06/2015	10.7	8.9	13.7	5.1	1.83	0	21	---	85.6	74	99.6	
30/06/2015	11.6	9.3	14.8	10	1.21	0	21	---	76.4	63.3	88.1	
01/07/2015	11.3	8.1	15.6	10.3	1.57	0	0	---	71.5	55.4	82	
02/07/2015	13	9.9	17.2	10.3	1.28	0	0	---	54.2	32	68.6	
03/07/2015	12.7	10.1	16.1	9.7	0.89	0	0	---	61.8	51.5	68.6	
04/07/2015	13.8	12.2	17	10	0.9	0	0	---	55	38.2	74.3	

05/07/2015	11.2	9.3	14.5	10.3	1.52	0	0	---	75.3	60.6	93.9
06/07/2015	16.1	9.5	20.7	10.3	5.8	0	0	---	39	19	81.7
07/07/2015	19.6	11.3	25	4.9	6.31	0	25	---	43.4	13.4	99.7
08/07/2015	11.9	10.4	14.9	7.9	2.16	1.6	71	---	91.7	74.6	99.8
09/07/2015	13.9	10.9	18	9.5	2.65	0	0	---	70	53.9	87.1
10/07/2015	18.1	15.3	21.3	9.9	3.54	0	0	---	45.9	37.7	58.8
11/07/2015	11.6	8.6	15.4	1.7	3.23	4.6	67	---	86.1	55	99.8
12/07/2015	7.6	5.7	9.5	8.4	1.89	2.4	75	---	81.5	60.4	99.8
13/07/2015	6.9	5	10	9.8	1.61	0	0	---	73.6	64	79.6
14/07/2015	9.2	5.8	12.6	6.1	2.42	0.2	29	---	47.8	32.3	74
15/07/2015	8.1	5.6	11.1	9.4	1.95	0	0	---	65.3	41.2	88.9
16/07/2015	7.9	5.8	9.9	4.9	3.22	3.2	83	---	93	84.6	99.8
17/07/2015	8.5	7.2	9.3	0.6	8.99	71.4	100	---	99.7	99.1	99.8

Hydrus setup file

Pcp_File_Version=4

*** BLOCK A: BASIC INFORMATION ****

Heading

Welcome to HYDRUS-1D

LUnit TUnit MUnit (indicated units are obligatory for all input data)

m

days

mmol

IWat IChem ITemp ISink IRoot IShort IWDep IScreen IVariabBC IEquil IInverse

t f t f t f t f

ISnow IHP1 IMeteo IVapor IActiveU IFluxes Irrig IDummy

f t f

NMat NLay CosAlpha

3 4 1

*** BLOCK B: WATER FLOW INFORMATION

MaxIt TolTh TolH (maximum number of iterations and tolerances)

11 0.001 1

TopInf WLayer KodTop InitCond

t -1 f

BotInf qGWLf FreeD SeepF KodBot DrainF hSeep

f 1 f 0

hTab1 hTabN

0.001 1000

Model Hysteresis

5 0

thr ths Alfa n Ks l w2 Alfa2 n2

0.07 0.45 0.014 1.56 6 0.5 0.5 3 1.5

0.08 0.5 0.014 1.37 3 0.5 0.5 3 1.5

0.09 0.4 0.014 1.3 1 0.5 0.5 3 1.5

*** BLOCK C: TIME INFORMATION ****

dt dtMin dtMax DMul DMul2 ItMin ItMax MPL

0.1 0.0001 0.5 1.3 0.7 3 10 30

tInit tMax

0 912

lPrintD nPrintSteps tPrintInterval lEnter

t 1 30.42 t

TPrint(1),TPrint(2),...,TPrint(MPL)

30.4 60.8 91.2 121.6 152 182.4

212.8 243.2 273.6 304 334.4 364.8

395.2 425.6 456 486.4 516.8 547.2

577.6 608 638.4 668.8 699.2 729.6

760 790.4 820.8 851.2 881.6 912

*** BLOCK G: ROOT WATER UPTAKE INFORMATION

Model (0 - Feddes, 1 - S shape) cRootMax OmegaC

0 1

P0 P2H P2L P3 r2H r2L

-0.1 -2 -8 -80 0.005 0.001

POptm(1),POptm(2),...,POptm(NMat)

-0.25 -0.25 -0.25

*** END OF INPUT FILE 'SELECTOR.IN' *****

